Microfluidic protein isolation and sample preparation for transmission electron microscopy

Inauguraldissertation

Zur
Erlangung der Würde eines Doktors der Philosophie
vorgelegt der
Philosophisch – Naturwissenschaftlichen Fakultät
der Universität Basel

von

Claudio Schmidli

aus Seewen (SO)

Basel, 2019

Genehmigt von der Philosophisch-Naturwissenschaftlichen Fakultät

auf Antrag von

Prof. Dr. Henning Stahlberg & Prof. Dr. Andreas Engel

Basel, den 17. September 2019

Prof. Dr. Martin Spiess, Dekan

Summary

The knowledge of atomic structures is essential to understand the mechanics and chemistry of proteins in fundamental research and is often the base for drug development. During the last decades, X-ray crystallography has been the primary method for determining atomic models providing an impressive number of molecular structures. Nevertheless, the technique is limited by the fact that the complexes of interest have to be crystallized. Nuclear magnetic resonance (NMR), which is used as an alternative to solve biomolecules in solution, has the drawback of consuming large amounts of protein, being labour intensive and challenging for large molecules.

In recent years, cryogenic electron microscopy (cryo-EM) has evolved as an important tool for protein structure determination. Technical advances in the instrumentation and increased computational power combined with better processing algorithms caused a massive improvement in the resolution of obtained structures. For these achievements Jacques Dubochet, Joachim Frank and Richard Henderson were awarded with a Nobel Prize in 2017. However, sample preparation methods lack behind and did not change a lot. A significant complication is the production of target proteins in sufficient amounts and quality. Although only some thousands to a few million protein particles must be imaged to solve a protein structure, much larger quantities are required to prepare specimens for cryo-EM. Conventional sample preparation methods are very wasteful with proteins and more than 99 % of protein is lost during a paper blotting step. Thus, considerable amounts of purified proteins have to be produced using complex and costly procedures usually including several chromatography steps.

In this thesis, a novel sample preparation and purification system consuming only minute amounts of biological material is presented. The system allows the purification of proteins and the subsequent preparation of isolated targets for negative stain and cryo-EM. We constructed corresponding hardware and software described in Chapters 1 & 2. The application of the system on biological samples is demonstrated in Chapters 3 & 4. As an example, we purified endogenous human 20S proteasome starting with <1 µL HeLa cytosol and determined it's 3D structure at a resolution of 3.5 Å. In Chapter 5, we show the purification of recombinantly expressed proteins by the use of a novel crosslinker that was developed during the course of this thesis.

Contents

1 Introduction

The molecular architecture of biomolecules is the basis for all life forms. Especially proteins are of particular interest since they are the main 'acting' molecules in virtually all biological processes. Proteins are essential for diverse activities, such as the catalysis of chemical reactions, information processing, force generation or energy harvesting. They are the end-product of a tightly controlled translation system, where a genomic nucleotide sequence is translated into a chain of amino acids. In the end, the amino-acid chain folds into a precisely defined three-dimensional (3D) arrangement. This folding is crucial for the proper protein function, and the knowledge of the 3D structure is essential to understand the mechanics and chemistry of the protein. Information about the 3D fold can also be used for practical applications such as drug design. Unfortunately, the folding process is poorly understood, and experimental approaches are required to 'solve' the 3D structure of proteins.

Contents

In the past 60 years the vast majority of macromolecules were determined using X-ray crystallography [Wlodawer *et al.* 2007]. Using this technique proteins are crystallized and exposed to an X-ray beam. The X-rays interacting with the atoms form a unique diffraction pattern, which is used to generate an atomic model. This approach is enormously powerful and provides high resolution information depending on the crystal quality. However, the method is limited by the fact that the artificial growth of 3D-crystrals is a necessity [McPherson & Gavira 2013]. Many proteins cannot be crystallized, e.g. protein filaments must have exactly multiples of the numbers 2, 3, 4 or 6 of subunits to pack into a crystal and even when crystallization

is possible contacts between crystals can lead to local artifacts. Furthermore, the proteins are fixed in a specific conformation depending on the crystal. Thus, for every protein conformation a different crystal form is needed, which explains the rather 'static' picture of proteins that was obtained in the last decades.

In the 1980s nuclear magnetic resonance (NMR) techniques emerged providing an extensive toolset for studying the dynamics, chemistry and kinetics of proteins in solution [Kleckner & Foster 2011]. NMR methods also allow the triangulation of inner distances in macromolecules measured by the *"nuclear Overhauser effect"*. This provides bundles of structures, which reflect in a certain degree the overall structural dynamics of proteins [Markwick *et al.* 2008]. NMR does not need the protein to be crystallized, however, to keep measurement times reasonable, high protein concentrations are required (>20 µM), and the size of the proteins that can be studied is limited (<60 kDa).

In the 1990s cryogenic electron microscopy (cryo-EM) started to be used in many laboratories as a method to study biomolecules. Thereby sample is spread over a thin layer of a holey carbon film. The specimen is then plunged into liquid ethane for vitrification, creating a thin layer of vitreous ice. Later the specimen is exposed to the electron beam in the microscope and 2D projections of the protein particles are recorded. Ideally, the individual copies of protein particles adopt different orientations in the ice layer, which allows for classification and averaging to reconstruct a 3D volume. This is the most commonly used variant of cryo-EM; termed single-particle analysis. Traditionally single-particle EM was used for protein complexes that resisted crystallization because not so long ago, cryo-EM could only provide low resolution structural information. Therefore, X-ray crystallography was the dominating technique for decades. However, during recent years, cryo-EM increasingly gained importance and became the method of choice for many structural studies [Kuhlbrandt 2014]. This development can be attributed two major innovations. Once is the introduction of direct electron detector cameras (DED) for electron microscopes in 2012 [Wu *et al.* 2015]. Direct electron detectors have a much better performance and read out speed compared to traditional recording media, CCD cameras and photographic films. Further, blurring caused by drifting of the stage or beam induced movements can now be compensated with motion correction. The other is improvement of data processing hardware and software. Much more powerful microprocessors allow to use computationally expensive algorithms classifying several thousands of EM images. This technological breakthroughs led to the so called *"resolution revolution"* [Kuhlbrandt 2014]. First sub-3 Å maps were solved in 2015 using the single particle approach [Campbell *et al.* 2015] and transformed the method to a mainstream tool for structure determination. Now cryo-EM provides structures near-atomic resolution, high enough for research e.g. for drug design in pharmaceutical industry.

1.1 Sample preparation for cryogenic electron microscopy

Despite the amazing progress made in the field of cryo-EM in the last years, sample preparation methods did not improve significantly since their invention 30 years ago [Dubochet *et al.* 1987]. Conventional methods consists of pipetting 2 - 3 µL of sample onto a metal mesh (Cu, Ni or Au) covered by a support film (carbon or gold), that is mostly perforated (see Figure 1.1). Then most of the sample is blotted to a thin layer in the order of 10 - 100 nm spanning the micrometer-sized holes of the perforated layer by applying a filter paper to one or both sides of the grid. Immediately after blotting the grid is plunged into liquid ethane or into an ethane/propane mixture for vitrification. Due to the cooling rate greater than $10^4\,\mathrm{K\,s^{-1}}$, a thin sample layer of noncrystalline ice is formed, which is later transferred into an transmission electron microscope (TEM). This procedure allows to conserve proteins near-physiological conditions and preserves structural information, even in the ultrahigh vacuum of the microscopes.

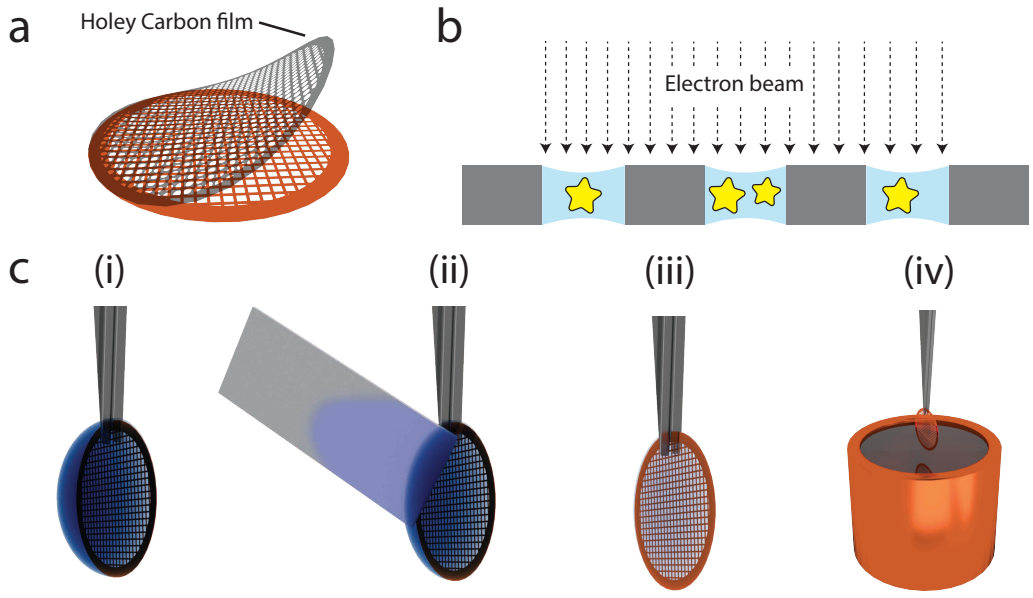

Figure 1.1: Typical structure of a cryo-EM grid and standard cryo-EM sample preparation procedure. **a)** Conventional grid used for cryo-EM, consisting of a metal mesh (commonly copper or gold) covered with a perforated (holey) carbon film [Chester *et al.* 2007]. Alternatively, grids with other supports such as lacey carbon [Baumeister & Seredynski 1976] or perforated gold films are used. **b)** Vitrified grid showing the ice-filled holes of the carbon layer containing the protein (yellow). **c)** Classical cryo-EM grid preparation procedure: i) 2 - 3 µL of sample is pipetted by hand onto the holey carbon film of a cryo-EM grid. ii) Surplus liquid is blotted away with a filter paper to form iii) a thin sample film. iv) Finally, the grid is plunged into liquid ethane for vitrification.

Although this cryo-EM grid preparation method has become well established, it has some major drawbacks. First, most of the 2 - 3 µL sample volume (>99.9 %) is removed by the filter paper and lost during preparation. Often the used proteins were produced in a costly and time-consuming process providing only minimal amounts of a final product. Thus, only a few grids can be prepared with standard sample preparation methods and screening conditions are limited. Apart from this, the filter paper itself leads to various problems. In some cases, inhomogeneous ice thickness can be attributed to the filter paper surface, which is quite rough on a microscopic level. Further, paper blotting can cause protein aggregation, denaturation or deformation. The filter paper consisting out of cellulose contains many trace elements such as calcium or magnesium, so contact might influence pH and properties of the sample. Typically, the blotting process takes 1 - 6 s, which is long enough for contaminats in the filter paper to get to the blotted sample and reach problematic concentrations. Metal-sensitive proteins or certain polymers are unstable in the presence of high levels of divalent ions [Parmar *et al.* 2018, Walker *et al.* 1994]. Also shear rates in the order of $5000\,s^{-1}$ [Lin *et al.* 1992] generated during the blotting process can lead to shear-related changes of proteins that are often not representing the native morphologies in solution.

1.2 Sample preparation for negative stain electron microscopy

For quality control and screening applications, hydrated proteins do not necessarily have to be frozen. Instead, negative staining EM can be used where proteins are embedded into a thin amorphous layer of dried heavy metal salts to increase sample contrast. In this approach, the stain is not applied to the sample but to it's environment. Hence, the electron beam can penetrate the sample easier than the surrounding space and an inverted, "negative" contrast is obtained (see Figure 1.2b). Compared to cryo-EM, the resolution is seriously limited to a maximum resolution of approx. 18 - 20 Å. However, the enhanced contrast allows to analyze relative small proteins. In most cases, samples are first analysed and optimizes using negative staining, since it is a much simpler, faster and more cost-effective method. Thereby, sample properties such as homogeneity/heterogeneity and complex or large assembly formation can be easily assessed without freezing the sample.

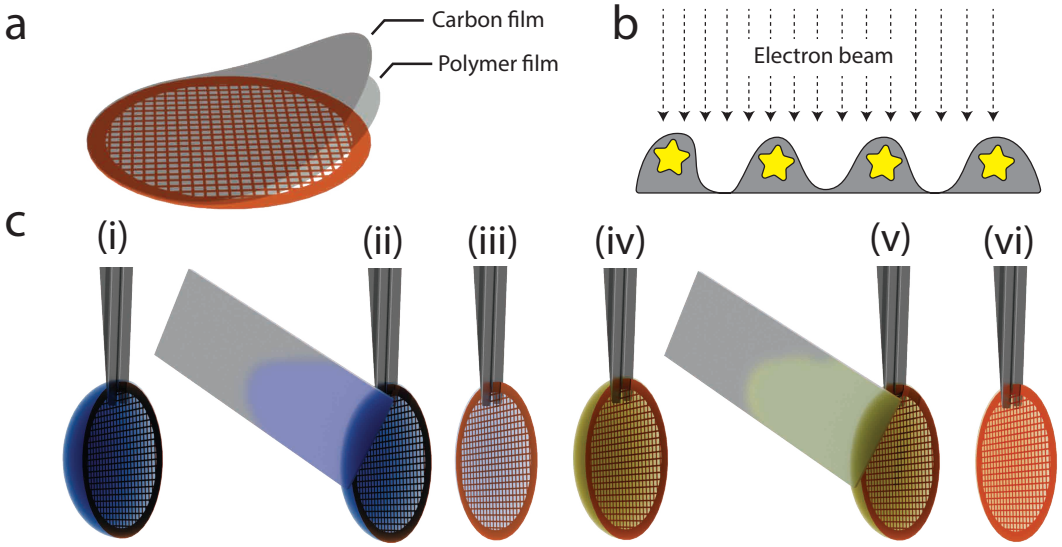

Figure 1.2: Typical structure of a negative stain grid and standard negative stain sample preparation procedure. **a)** Conventional negative stain grid covered with a first layer of an electron transparent polymer (e.g. Parlodion) and a second layer of amorphous carbon. **b)** Negatively stained proteins (yellow) embedded in the electron dense layer of stain (e.g. uranyl acetate). The electron beam mainly interacts with the stain surrounding the proteins. **c)** Classical negative stain grid preparation procedure: 2 - 3 µL of sample is placed on the grid and incubated for typically 1 min. Excess liquid is then blotted away using a filter paper followed by the incubation with a droplet of negative stain solution for a few seconds. Finally, also the stain is wicked away and the sample is dried at room temperature.

In conventional negative staining EM (see Figure 1.2), 2 - 3 µL of sample is deposited on top of an electron transparent two-layer coated grid for around 1 min. During this incubation time, protein particles settle down and adsorb onto the grid coating.

Then the liquid is absorbed by a filter paper and a drop of negative staining solution is applied, which is also blotted away a few seconds later. After drying, the specimen can be introduced into the electron beam for analysis.

1.3 Alternative sample preparation strategies for transmission electron microscopy

There is room to improve many aspects of the classical TEM grid preparation approach. Sample consumption can be reduced using miniaturized setups, for better reproducibility fully automated systems controlling precisely the environment temperature, humidity and the applied sample volume are needed and systems without much user interaction also might improve the overall quality of specimens. Further, the harsh and wasteful paper blotting step involved in traditional grid preparation methods should be avoided. In this section, new grid preparation approaches slowly emerging in the recent years are discussed.

A device termed Spotiton™ was developed in 2012, which dispenses volumes of 2 - 16 nL sample through piezo-electric inkjet technology onto EM grids [Jain *et al.* 2012]. Spotiton™ prepares cryo-EM grids in a highly automated and fast manner using only minimal amounts of sample. Besides sample vitrification for cryo-EM it also allows the deposition of sample onto negative stain grids. However, the staining process itself still has to be done manually with conventional techniques. Although only minimal amounts of sample per grid are needed, the system has to be primed with 1 µL of sample before its use. Further, the well-developed inkjet technology allows controlling the single droplet size very accurately, but the surface tension and low viscosity limit the spreading on the grid. Therefore, the resulting individual droplets are too thick for cryo-EM and custom "self-blotting grids" featuring copper peroxide nanowires on the surface have to be used to wick away surplus liquid. In order to avoid blotting completely, smaller droplet volumes with a diameter of 1 - 30 µm can be used. Such droplets better spread over the grid and result in a film thickness of 100 nm or less. This has been shown using nebulizers, micro-nozzles and electrospray techniques, [Berriman & Unwin 1994, White *et al.* 2003, Lu *et al.* 2009], where the grid is plunged through a sprayed region on its way into the ethane cup. The major advantage of spraying techniques is the precise timing and the possibility of in-flight applications to the sample. This enables mixing two reactant solutions within 10 ms before vitrification for time-resolved studies [Walker *et al.* 1999, Barnard *et al.* 2009, Lu *et al.* 2009]. Unfortunately, such spraying devices entail large death volumes where even more sample is lost than with conventional methods. For this reason, they have not established for mainstream usage so far. Other techniques focus on the deposition of multiple samples onto a single EM grid, which significantly reduces sample consumption and required microscopy time. This has been shown

for negative stain EM, pin-printing three different proteins on a single grid [Castro-Hartmann *et al.* 2013] and also for 96 different inorganic nanoparticle samples that were applied to a single specimen [Mulligan *et al.* 2015]. However, in such approaches problems can arise when treating all the different samples with the same washing and staining procedure, which might need slight adaption in each case. In addition, cross-contamination during washing and staining must be controlled.

1.4 Microfluidic grid preparation for transmission electron microscopy

In this thesis a novel microfluidic based grid preparation was approach used and further developed. For cryo-EM (Figure 1.3a), a glow-discharged grid is placed on a temperature controlled stage kept a few degrees above the dew point and a sample droplet of 3 - 30 nL is applied with a microcapillary. While dispensing the microcapillary moves in a spiral pattern to cover an area of the grid as large as possible. After deposition, excess sample is removed and recovered by re-aspiration and a thin film spreading over the surface of the holey carbon film remains. Subsequently, the grid is plunged into liquid ethane for vitrification using the grid plunge freezing mechanism of the cryoWriter setup. For negative staining (Figure 1.3b), the microcapillary is loaded with 3 - 10 nL of sample and then immersed for 2 - 12 min into negative staining solution. Thereby, a diffusion driven exchange between the salt ions of the sample and the heavy metal salts of the staining solution takes place. Sample loss caused by the diffusion process can be neglected due to the much smaller diffusion coefficients of the proteins compared to the salt ions [Arnold *et al.* 2016]. After the conditioning step, the sample is deposited onto a negative stain grid and dried under controlled conditions. The whole grid preparation procedure for both, negative stain and cryo-EM, is fully automatized using an in-house developed scripting language termed openBEB [Ramakrishnan *et al.* 2014]. In this way, parameters are meticulously controlled providing more reproducible results.

1.5 Microfluidic protein purification for transmission electron microscopy

In single particle cryo-EM thousands of identical protein particles are imaged and computationally averaged together. This requires specimens providing highly concentrated, homogenous particles without a lot of background noise. Thus, proteins must be purified from crude cell lysate and concentrated for data collection. Since, the natural expression level for most proteins is relatively low it is often difficult to achieve sufficient high protein concentrations for cryo-EM studies. Therefore, proteins are commonly recombinant expressed in a host system, which also allows the introduction of affinity tags for purification later. However, several pitfalls can hamper recombinant protein production such as low solubility or toxicity to the

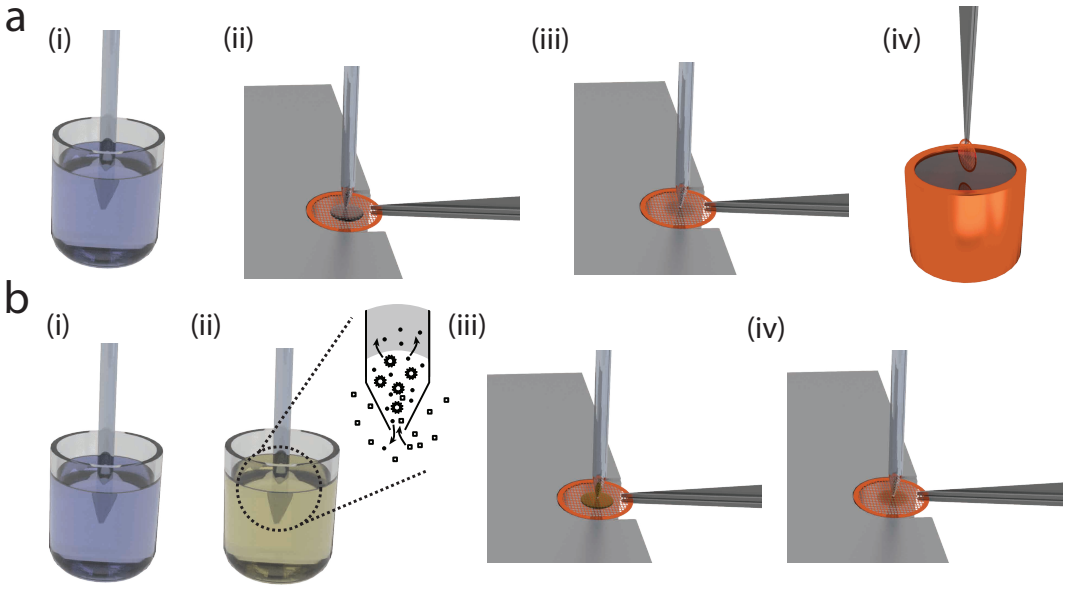

Figure 1.3: Microfluidic cryo-EM and negative stain grid preparation using the cryoWriter setup. **a)** Preparation of a cryo-EM grid: i) Around 3 - 20 nL is aspirated into the microcapillary tip and ii) deposited onto a cryo-EM grid kept at a temperature ~7 °C above the dewpoint. While dispensing the microcapillary is moved relative to the grid in a spiral pattern, covering an area as large as possible. iii) Excess sample is re-aspirated after deposition. Subsequently, the grid is withdrawn from the stage, flipped by 90° into the vertical position, and plunged into a cryogen bath. **b)** Preparation of a negative stain grid: i) 3 - 10 nL sample is aspirated from the sample stock. ii) Then the microcapillary tip is immersed into negative staining solution for a sample conditioning step. Ions and small molecules are exchanged by diffusion, which leads to the introduction of stain and desalting of the sample. iii) Finally, the sample is dispensed on the grid and iv) dried.

host cell. Successful expression is therefore not always possible and endogenous proteins have to be isolated from large amounts of biological starting material. Subsequent methods for protein purification commonly consists of several time-consuming chromatography steps involving cycles of target binding and washing. For each purification step, retention of the biological activity and chemical integrity of the polypeptide must be ensured. Due to the many steps required in such procedures, this can be very challenging. Furthermore, elution steps often involve damaging conditions (e.g. low pH or addition of chemicals) and dilute samples, which results in lower final concentrations. Since only a very small number of individual protein particles (10,000 to a few millions) need to be imaged for high-resolution reconstruction by the single particle approach, miniaturized sample purification become feasible for EM. In this thesis, a microfluidic based approach combined with magnetic separation is presented. The basic principle of the approach is very simple (see Figure 1.4): Magnetic particles having affinity to the target proteins (accomplished e.g. through a

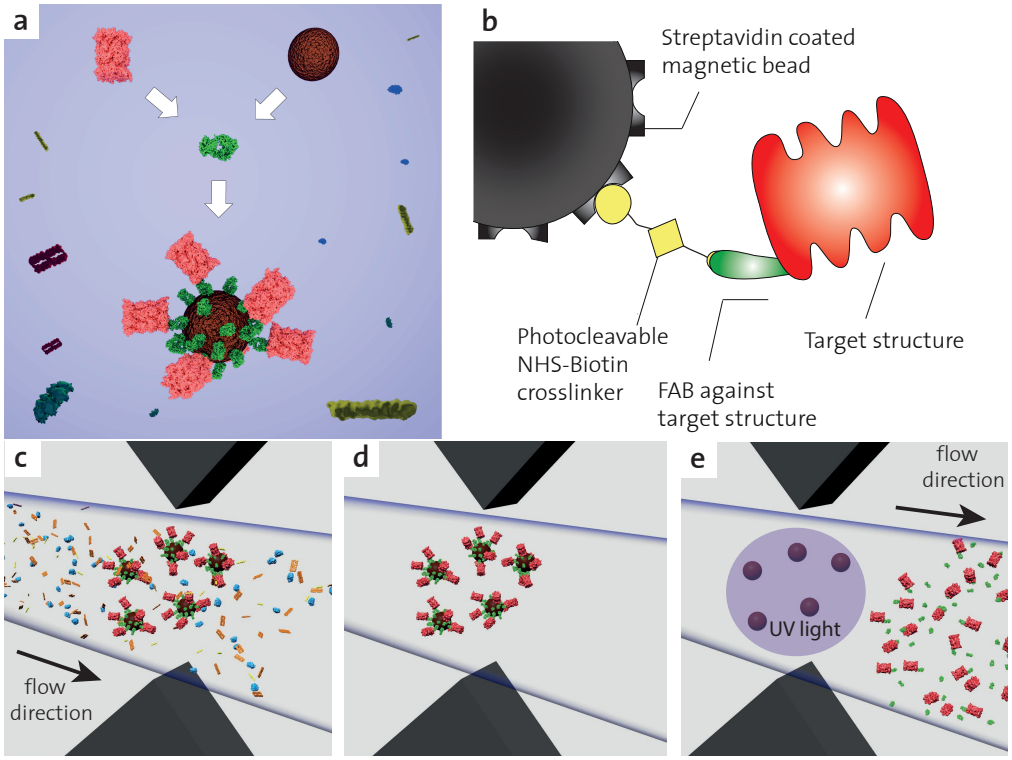

Figure 1.4: Affinity based microfluidic protein isolation using magnetic particles. **a)** Antibody fragments (green) and magnetic nanoparticles (brown) are incubated with the sample and form a complex with the target structure (red). **b)** Scheme of the composite material used for protein extraction: The streptavidin coated magnetic beads are linked via photo cleavable NHS-Biotin cross-linker to an antibody fragment, capturing the target proteins. **c)** Then the sample is passed through a magnetic trap, **d)** where magnetic particles and their cargo are retrained and other components of the sample are flushed away. **e)** Immobilized target proteins are recovered and eluted by photo-cleavage.

primary antibody) are mixed with the sample containing the target compound. The sample can be crude cell lysate, whole blood, plasma, ascites fluid or many others. After a short incubation time, target proteins are immobilized and washed using a magnetic trap. Then the isolated proteins are eluted by cleaving the photo-cleavable crosslinker with UV-light or by removing the magnetic field while the targets are still bound to the magnetic particles. In the second case, the magnetic particles can later be used as electron dense labels for imaging or as fiducials for electron tomography. Microfluidic based approaches comprises many advantages compared to standard purification techniques. The simple low scale procedure consisting of only a few steps makes the protein isolation procedure extremely time and cost effective. Proteins can be purified within only a few hours without the need of expensive chromatography systems, filters, or centrifuges. Pre-processing steps to remove suspended solid and

fouling components present in the sample are not needed; instead, crude sample can be used directly. The use of photo-elution allows gentle protein elution in minute volumes without applying harsh conditions. Only specifically bound proteins are released while unspecific bound proteins remain bound to the immobilized beads. The reduced shearing forces and the higher protein concentrations throughout the isolation process compared to chromatography techniques allows even large protein complexes to remain intact [Giss *et al.* 2014]. And finally techniques involving magnetic particles also have high potential for automatisation e.g. to determine a variety of analytes.

1.6 Magnetic nanoparticles for protein purification

In the recent time, magnetic particles became very popular and were applied in many fields such as magnetic resonance imaging, targeted drug delivery or cancer treatment [Larson *et al.* 2007, Mahon *et al.* 2012, Swain *et al.* 2016]. Particles can be prepared in the laboratory or obtained commercially from a variety of suppliers. The production of particles with uniform shape and narrow size dispersity requires a lot of know-how and finding appropriate high quality magnetic particles for immunoprecipitation is not that easy. Figure 1.5 shows a selection of magnetic particles that were tested in this thesis. In most cases, magnetite (Fe_3O_4) is used as a material because of its interesting magnetic properties [Brullot *et al.* 2012]. Magnetic particles in the size range between 5 and 30 nm exhibit a superparamagnetic behavior, which means that there is no remaining magnetism (remenance) after removal of external fields and particles do not interact with each other anymore (see Figure 1.6) [Bedanta & Kleemann 2008]. This is a highly valuable property, since the particles can be easily resuspended in solution and remain in suspension for a long time. To achieve similar properties for larger particles, polymer-encapsulated shells with magnetic iron oxide pigments are often used. This combines the superparamagnetic behavior of small particles with the easier handling of larger magnetic particles. Typically, all types of magnetic particles designed for biological applications are coated with a polymer, silica or organic ligands [Na *et al.* 2011, Petri-Fink *et al.* 2008, Ji *et al.* 2007]. This stabilizes the particles, improves the colloidal properties and allows to functionalize the surface. For affinity absorption, the surfaces are functionalized with different ligands. In most cases, streptavidin and protein A/G are used. Protein A/G allows binding of antibodies and streptavidin has a high affinity to biotin which can be used to link biotinylated molecules. However, functional groups such as –COOH, −OH or $–NH_2$ present on the coating of the magnetic particles, also allow the immobilization of other ligands.

For immunoprecipitation, specific antibodies have to be coupled to the particle surfaces. Unfortunately, the approach of using the protein A/G interaction entails

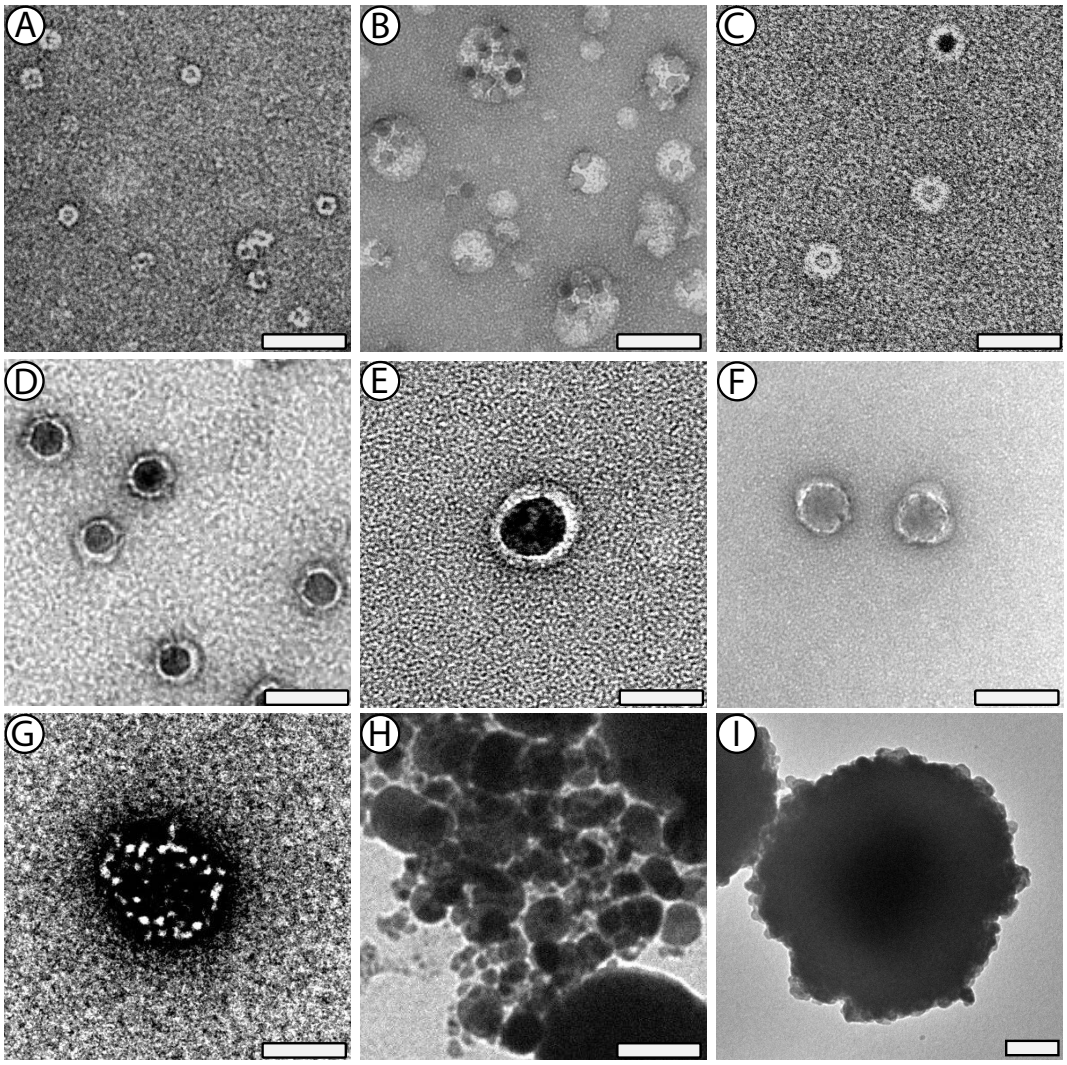

Figure 1.5: Selection of magnetic particles tested in this thesis. **a)** Magnetic ferritin protein particles. **b)** CANdots Series M, 10 nm sized iron oxide particles from CAN GmbH Hamburg. **c)** SHS-10, 10 nm sized iron oxide particles from Ocean NanoTech. **d)** Precision MRX^{TM}, 15 nm sized iron oxide particles from Imagion Biosystems. **e)** SHS-30, 30 nm sized iron oxide particles from Ocean NanoTech. **f)** Precision MRX^{TM}, 25 nm sized iron oxide particles from Imagion Biosystems. **g)** SV0050, 50 nm sized iron oxide particles from Ocean NanoTech. **h)** TurboBeads Amine, 50 nm sized iron oxide particles from TurboBeads Llc. **i)** Dynabeads^{TM} MyOne^{TM} Streptavidin T1, 1 µm sized iron oxide particles from Thermo Fisher Scientific. Scale bars: a-h: 50 nm; i: 200 nm.

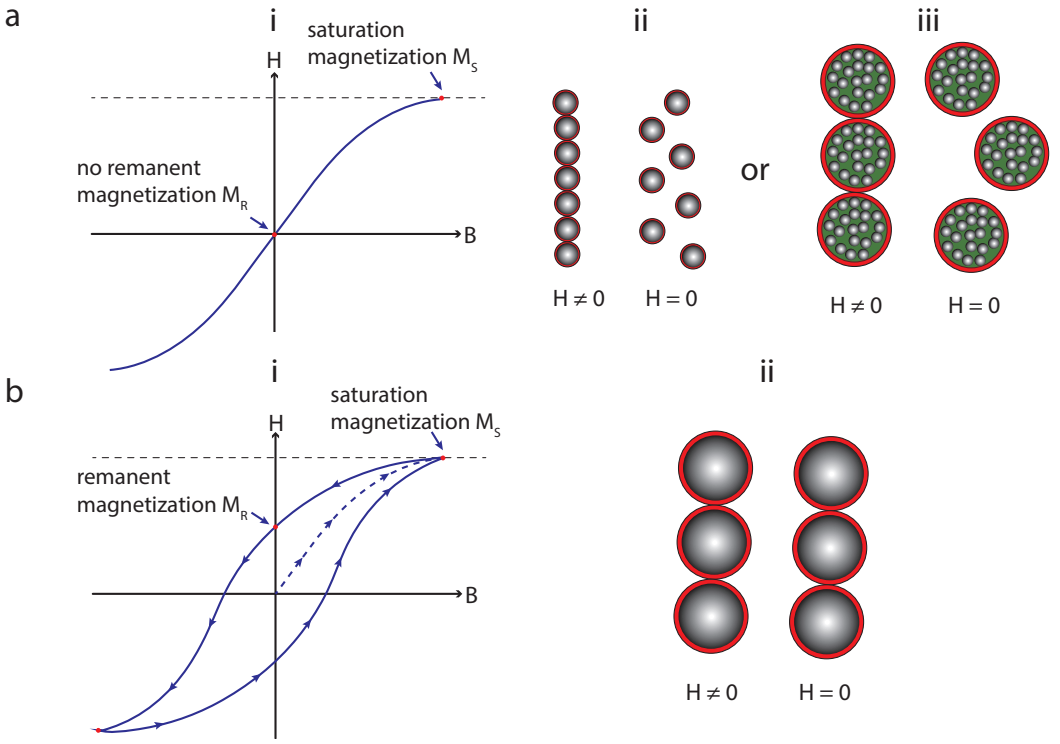

Figure 1.6: Comparison of superparamagnetic and ferromagnetic particles. **a)** i) Typical magnetization curve for superparamagnetic particles, showing zero remanent magnetization after external field removal. Chain-like superstructure of ii) magnetite nanoparticles <30 nm and iii) composite microspheres composed out of magnetite pigments, which exposed to a magnetic field ($H \neq 0$) and the decomposition of the superstructure after field removal ($H = 0$). **b)** i) Typical magnetization curve for ferromagnetic magnetite particles >30 nm, showing non-zero remanent magnetization after external field removal. ii) Here, particle superstructures are still present after external field removal ($H = 0$) due to the dipole-dipole interactions of the still magnetized particles.

some considerable disadvantages: Magnetic particles have to be coated with protein A/G, harsh buffer conditions possibly affecting the protein structure are needed for the elution of isolated targets, and the affinity of protein A/G to antibodies strongly depends on the antibody species and isotype. For this reason an alternative method was developed in this thesis, based on a photo-cleavable crosslinker featuring a biotin moiety on one end (Figure 1.7a&b). Whereas the biotin binds to the streptavidin coated bead surface, the amine reactive ester group on the other site of the crosslinker is linked to an amine group of an antibody such as the α-group of the N-terminus or the ϵ-amine of lysine side chains. Steric hindrance interfering with the bead-antibody coupling reaction is reduced through the polar spacer arm. For protein elution at the end of a purification experiment, two different approaches were used (Figure 1.7d). Either the proteins were eluted together with the still attached magnetic particles

(Figure 1.7d iii), in this case the beads serve as electron dense labels for imaging later; or the photolabile group of the crosslinker was cleaved by UV exposure and the target structures were eluted without beads (Figure 1.7d i). Usually for each approach, different beads were used. For photo-elution, larger beads are more suitable, because of the less dominant scattering effects, which reduce the cleavage efficiency (Figure 1.7c). On the other hand, smaller particles are the best choice when no photo-cleavage is performed to avoid long protein elution steps. If target proteins have more than one antibody binding epitope, they may be cross-connected through the antibodies and aggregation can occur (Figure 1.7d ii). Therefore, fragments having only one antigen binding site instead of full antibodies were often used in this thesis to prevent this problem.

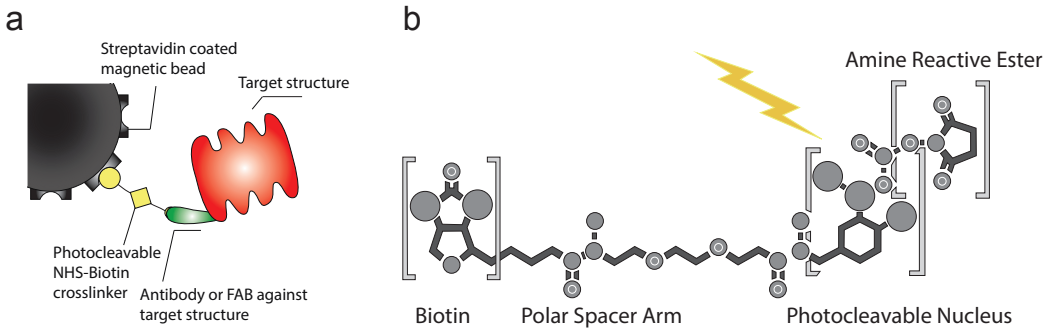

c

Particle Size	Supplier	Transmission
10 nm	OceanNanoTech	2 %
15 nm	MRXPrecision	4 %
20 nm	OceanNanoTech	9 %
25 nm	MrxPrecision	12 %
30 nm	OceanNanoTech	22%
1000 nm	Dynabeads	100%

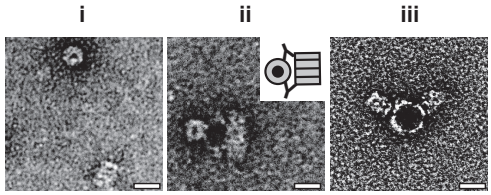

Figure 1.7: Coupling of antibodies to magnetic particles and elution of isolated target structures. **a)** Composite material used for protein extraction. **b)** Crosslinker with photocleavable moiety. **c)** Ratio of a transmitted 365 nm light beam, through a 1 mm light path of 1 mg mL^{-1} iron oxide particle suspensions. Due to scattering effects, the amount transmitted light decreases with the particle size. Hence, for experiments comprising photo-elution, larger beads are more suitable. In contrast, beads can be eluted together with their cargo and be used as electron dense labels in the microscope. In this case smaller particles are more favorable. **d)** i) Isolated 20S proteasomes recovered with photo-elution and purified from cell lysate using 1 µm microspheres with antibody fragments and ii) full antibodies. The application of full antibodies can lead to aggregation. iii) Isolated 20S proteasomes obtained without photo-elution using magnetic iron oxide nanoparticles. Scale bars: 15 nm.

1.7 Development of a magnetic particle trap

For the immobilization of magnetic particles, magnetic separators are needed. Particles > 500 nm can be separated using commercial systems comprising of rare-earth permanent magnets, which are available at reasonable prices. Such systems are commonly designed for standard Eppendorf tubes or titration plates, where volumes from approx. 50 µL up to 10 mL can be applied. Alternatively, more expensive flow-through separators composed of a special column may be used. Particles are pumped through the column matrix made out of fine magnetic grade stainless steel wool or small balls. The matrix magnetized by two external magnets retrains the magnetic particles in the column. After removal of the external magnets, the particles can be eluted by the flow and gentle vibration of the column.

In this thesis, magnetic particles ranging from 10 nm to 2 µm were trapped in a microcapillary of a diameter of 150 µm. Since, there are no commercial systems available applicable to microfluidics and capable to trap nanoparticles in reasonable timeframes, a custom particle trap system was developed and optimized. Therefore, several factors including i) magnetic force, ii) viscous drag, iii) particle/fluid interactions, iv) gravity, v) buoyancy, vi) thermal kinetics and vii) interparticle effects had to be considered. To get a first basic understanding of magnetic particle trapping Newton's equation of motion $\mathbf{F}=\mathbf{m}\cdot\mathbf{a}$ for the magnetic force F_m acting on a saturated magnetic particle was solved:

$$F_m = V \cdot M_S \cdot \mu_0 \cdot \nabla H \tag{1.1}$$

where V is the volume of the particle, M_S the saturation magnetization and H the magnetic field strength. In order to immobilize magnetic particles in a microfluidic system, the magnetic force F_{mag} must be larger than the hydrodynamic drag force F_{drag} acting on a particle given by the Stokes law:

$$F_{drag} = -6\pi\eta r\Delta v \tag{1.2}$$

where η is the viscosity of the medium, r the particle radius, and Δv the velocity difference between the particle.

Equation 1.1 is based on Newton's law and does not consider Brownian motion, which becomes important if the bead diameter D is small enough. The critical diameter can be determined using the condition from Gerber et al [Gerber *et al.* 1983]:

$$|F|D \leq kT \tag{1.3}$$

When the criterion is fulfilled the advection-diffusion equation for the particle concentration c rather than the Newton equation for the trajectory of a single particle has to be solved. The result can be expressed as

$$F_m = \mu_0 V f(H)(H \cdot \nabla)H \tag{1.4}$$

where

$$f(H) = \begin{cases} \frac{3(\chi_p - \chi_f)}{(\chi_p - \chi_f)+3} & H < (\frac{(\chi_p - \chi_f)+3}{3\chi_p})M_S \\ M_S/H & H \geq (\frac{(\chi_p - \chi_f)+3}{3\chi_p})M_S \end{cases}$$

χ_f is the susceptibility of the fluid and χ_p the susceptibility of the particles [Furlani & Sahoo 2006]. For large magnetic field strengths H we obtain the same expression as in Eq. 1.1. Here it is important to mention that all this equations hold true for single magnetic particles in solution. In practice, the dipole-dipole interactions between the particles form aggregates of various shapes (often chains) leading to a larger net size. Therefore, smaller particles can be trapped than predicted by these equations especially when using high particle concentrations.

However, the equations show that high magnetic field gradients are needed to trap magnetic particles. Since, the magnetic force acting on the particles scales with r^2 this becomes particularly difficult for magnetic particles <50 nm. Magnetic field gradients can be generated using permanent magnets or electromagnets, which both have their respective advantages and disadvantages. Permanent magnets don't require a power supply but the magnetic field cannot regulated or switched off. In contrast, the field strength of electromagnets can be adjusted by the applied power. Here, the disadvantage is Joule heating, which is major inconvenient for biological samples.

In this thesis, a magnetic trap consisting of two electromagnets arranged with opposite poles facing one another was developed. Attached iron tips extend the magnet cores and concentrate the magnetic flux to a small area where a high magnetic field gradient is achieved. In this region, magnetic iron oxide nanoparticles down to a size of 10 nm can be immobilized (see Figure 1.8). Joule heating of the trap system is counteracted with an implemented cooling circuit. Depending on the material, also parts of the trap system exhibit remaining magnetism after switching off the electromagnets, similar to the magnetic particles (see Figure 1.6b). We used soft iron, a material known because of it's low remanence for our construction. However, also soft iron has remaining magnetism, which influences the performance of the trap negatively. In order to eliminate the last bit of magnetization, a Degaussing process was implemented employing a decaying alternating current to the electromagnets. Due to the decaying alternating field, the magnetic moments inside the soft iron parts become oriented randomly. The proper implementation allowed a virtual removal of remaining magnetization.

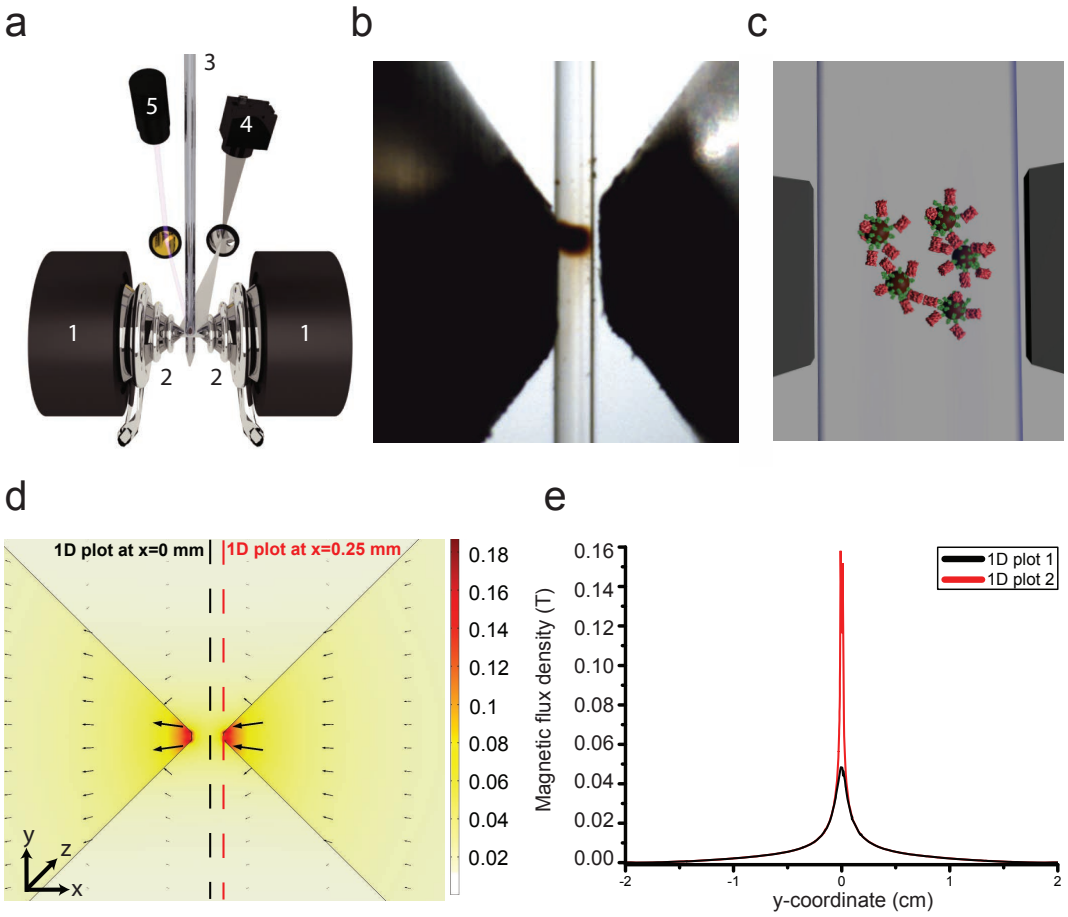

Figure 1.8: Electromagnetic particle trap. **a)** The electromagnetic trap consists of two electromagnets (1) that produce a strong magnetic field gradient via their water-cooled iron tips (2). Sample processing in the capillary (3) is monitored by a camera (4), and a UV LED (5) allows photo-cleavage (see Figure 1.7) of the sample, both via mirrors. **b)** Image of a particle plug and **c)** illustration of it. **d)** Finite element simulation of the magnetic field generated by the electromagnetic trap system. The 2D plot of the magnetic shows the flux density around the iron tips (black solid lines). The direction of the magnetic fields is shown with black arrows. The size of the arrows is proportional to the field strength. The values in the color scale are given in Tesla (T). **e)** Extracted 1D plots of the magnetic flux density from the 2D plot in (a) at the positions indicated with dashed lines. The figure shows that between the tips (x=0) the highest field gradients are observed. This leads to a magnetic force F_m pushing magnetic particles towards this region.

1.8 Surface passivation of a microfluidic system

Nonspecific biomolecule adsorption of internal surfaces in microfluidic devices is a common problem. Highly concentrated samples may cause clogging of the device, whereas in low concentrated samples large proportions are lost. Therefore, surface passivation techniques are widely used. Commonly polymers such as poly(ethylene glycol) (PEG) are bound to the surface of microfluidic channels, which function as a water-binding hydrogel-like brush, with protein-resistant properties [Hellmich *et al.* 2005]. Dependent on the length, flexibility and density of these chains the protein repelling properties can be adjusted. It is assumed that steric repulsion of the polymer brush prevents the contact between the proteins and the underlying surface. Further, a hydration shell around PEG molecules could suppress energetically protein adsorption. However, the molecular protein repulsion mechanisms of PEGylated surfaces is not fully understood [Heuberger *et al.* 2005]. In this thesis, poly(L-lysine)-graft-poly(ethylene glycol) (PLL-g-PEG) was used for surface passivation, which significantly improved the yield of isolated proteins.

1.9 Structure and aim of this thesis

The goal of this thesis is to miniaturize sample preparation and protein purification procedures for TEM. To this end, a robotic system for microfluidic sample handling was constructed in collaboration with other group members. The robot allows preparing minute volumes of sample for TEM in a highly automated manner and the isolation of proteins for high-resolution structure determination from less than 1 µL cytosol. We show first experiments with different samples and present new opportunities, which are opened up through this technology.

Classical TEM sample preparation entails a number of limitations, as discussed in Sections 1.1 & 1.2. This includes problems obtaining reproducible results using manual or only semi-automated procedures and the application of an aggressive paper blotting step. In Chapter 2, we present a novel microfluidic based sample preparation approach where 3 - 20 nL sample is directly deposited on a grid without the need of paper blotting. The whole process is fully automated and performed with an in-house built robotic device. We show typical results of negatively stained and frozen samples and the application of the method to single cells. Using the microcapillary tip of the sample handling system single cells were lysed, aspirated and prepared for the analysis in TEM.

For high-resolution 3D reconstruction of proteins by the single particle approach, samples have to be purified and concentrated. This usually requires several chromatographic steps involving expensive labour equipment and huge amounts of starting material. In Chapter 3, we present a novel microfluidic methodology for the purification of proteins from minute volumes of crude cell lysate. Using magnetic microspheres with linked antibodies to the surface, we were able to isolate endogenous human 20S proteasome from less than 1 µL of HeLa cytosol. We acquired and processed images on one grid resulting in a 3.5 Å resolved map that was then used to build a protein model.

The application of magnetic microspheres requires the separation of isolated proteins from the microsphere surface. Therefore, an additional cleavage step is needed, which entails a certain loss of isolated targets. In Chapter 4, we show how magnetic nanoparticles can be used alternatively. Magnetic nanoparticles in the range of 10 - 30 nm don't have to be cleaved from isolated proteins. Instead, they can be deposited together with the linked sample on a grid and directly be used as electron dense labels in TEM. We isolated a cellular structure involved in malaria from erythrocyte lysate and performed negative stain and cryo-EM analysis. Further, we used the magnetic particles as fiducials to create a 3D tomogram of the isolated sample.

Immunoprecipitation of proteins based on primary antibodies is very specific allowing the purification of proteins at high purity. However, many target proteins are only produced under specific conditions and in minimal amounts. To study such proteins, overexpression systems must be used. In Chapter 5, we propose a novel method for the direct isolation and cryo-EM grid preparation of tagged proteins for atomic structure determination using a novel photo-cleavable NTA crosslinker. The use of magnetic particles linked to this crosslinker allows the isolation of His-tagged proteins from recombinant expression in a very fast and inexpensive manner.

1.10 Publication list

Peer-reviewed and published articles

Schmidli, C., Rima, L., Arnold, S. A., Stohler, T.,Syntychaki A., Bieri, A., Albiez, S., Goldie, K. N., Chami, M., Stahlberg H., Braun, T. 2018. **Miniaturized sample preparation for transmission electron microscopy.** JoVE, e57310

Schmidli, C., Albiez, S., Rima, L., Righetto, R., Mohammed, I., Oliva, P., Kovacik, L., Stahlberg, H., Braun, T. 2019. **Microfluidic protein isolation and sample preparation for high-resolution cryo-EM** PNAS, 116 (30) 15007-15012

Arnold, S. A., Müller, S. A., Schmidli, C, Chami, M., Stahlberg, H., Goldie K. N., Stahlberg, H., Braun, T., 2018. **Miniaturizing EM Sample Preparation: Opportunities, Challenges, and "Visual Proteomics."**
Proteomics 18 (5-6), 1700176

Arnold, S. A., Albiez, S., Opara, N., Chami, M., Schmidli, C., Bieri, A., Padeste, C., Stahlberg, H., Braun, T. 2016. **Total sample conditioning and preparation of nanoliter volumes for electron microscopy.** ACS Nano 10, 981–4988

Syntychaki, A., Rima, L., Schmidli, C., Stohler, T., Bieri, A., Sütterlin R., Stahlberg, H., Castano-Diez, D., Braun, T. 2019. **'Differential visual proteomics': Enabling the proteome-wide comparison of protein structures of single-cells.** Journal of Proteome Research, 18, 9, 1893521-3531

Published Data

Schmidli, C., *et al.* **Endogeneous native human 20S proteasome with bound Fabs isolated from less than 1 µL cell lysate.** The Electron Microscopy Data Bank. http://www.ebi.ac.uk/pdbe/entry/emdb/EMD-4738.
Deposited 28 March 2019.

Schmidli, C., *et al.* **Cryo-EM structure of Tobacco Mossaic Virus from microfluidic grid preparation.** The Electron Microscopy Data Bank.
http://www.ebi.ac.uk/pdbe/entry/emdb/EMD-4628. Deposited 22 February 2019.

Schmidli, C., *et al.* **Endogeneous native human 20S proteasome.** Protein Data Bank. http://www.rcsb.org/structure/6R70. Deposited 28 March 2019.

Schmidli, C., *et al.* **Tobacco Mosaic Virus (TMV)**. Protein Data Bank.
http://www.rcsb.org/structure/6R7M. Deposited 29 March 2019.

Schmidli, C., *et al.* **CryoWriter: 3.5 Å structure of human 20S proteasome with bound Fabs from microfluidic protein isolation, and 1.9 Å TMV structure.** Electron Microscopy Public Image Archive.
https://www.ebi.ac.uk/pdbe/emdb/empiar/entry/10251.
Deposited 21 February 2019.

2 Microfluidic sample preparation for transmission electron microscopy

An instrument and methods for the preparation of nanoliter-sized sample volumes for transmission electron microscopy is presented. No paper-blotting steps are required, thus avoiding the detrimental consequences this can have for proteins, significantly reducing sample loss and enabling the analysis of single cell lysate for visual proteomics.

My own contribution was establishing the improved grid preparation protocols presented here, producing the published movies, paper writing and performing quantitative experiments to demonstrate the loss of protein particles during sample conditioning.

The following section has been published in:

Journal of Visualized Experiments
Issue 137, July 2018, Pages 1-12
http://dx.doi.org/doi:10.3791/57310

Miniaturized Sample Preparation for Transmission Electron Microscopy

Claudio Schmidli[*,1,2], Luca Rima[*,1], Stefan. A. Arnold[*,1,2], Thomas Stohler[1]
Anastasia Syntychaki[1] Andrej Bieri[1],Stefan Albiez[1], Kenneth N. Goldie[1],
Mohamed Chami[3], Henning Stahlberg[1] and Thomas Braun[1]

* These authors contributed equally to this work

1 - Center for Cellular Imaging and NanoAnalytics, Biozentrum, University Basel, Switzerland
2 - Swiss Nanoscience Institute, University of Basel, Switzerland
3 - BioEM lab, Biozentrum, University of Basel, Switzerland

Contents

Abstract

Due to recent technological progress, cryo-electron microscopy (cryo-EM) is rapidly becoming a standard method for the structural analysis of protein complexes to atomic resolution. However, protein isolation techniques and sample preparation methods for EM remain a bottleneck. A relatively small number (100,000 to a few million) of individual protein particles need to be imaged for the high-resolution analysis of proteins by the single particle EM approach, making miniaturized sample handling techniques and microfluidic principles feasible.

A miniaturized, paper-blotting-free EM grid preparation method for sample preconditioning, EM grid priming and post processing that only consumes nanoliter-volumes of sample is presented. The method uses a dispensing system with sub-nanoliter precision to control liquid uptake and EM grid priming, a platform to control the grid temperature thereby determining the relative humidity above the EM grid, and a pick-and-plunge-mechanism for sample vitrification. For cryo-EM, an EM grid is placed on the temperature-controlled stage and the sample is aspirated into a capillary. The capillary tip is positioned in proximity to the grid surface, the grid is loaded with the sample and excess is re-aspirated into the microcapillary. Subsequently, the sample film is stabilized and slightly thinned by controlled water evaporation regulated by the offset of the platform temperature relative to the dew-point. At a given point the pick-and-plunge mechanism is triggered, rapidly transferring the primed EM grid into liquid ethane for sample vitrification. Alternatively, sample-conditioning methods are available to prepare nanoliter-sized sample volumes for negative stain (NS) EM.

The methodologies greatly reduce sample consumption and avoid approaches potentially harmful to proteins, such as the filter paper blotting used in conventional methods. Furthermore, the minuscule amount of sample required allows novel experimental strategies, such as fast sample conditioning, combination with single-cell lysis for "visual proteomics", or "lossless" total sample preparation for quantitative analysis of complex samples.

2.1 Introduction

Hardware and software for the structural analysis of protein complexes by transmission electron microscopy (TEM) has massively advanced during recent years. The improvements made paved the way to a "resolution revolution" [Kuhlbrandt 2014, chen Bai *et al.* 2015] and fundamentally changed structural research. The revolution started with the advent of cryo-electron microscopy (cryo-EM) [Dubochet *et al.* 1988, Lepault *et al.* 1983] allowing the preparation of biological samples under close to phys-

iological conditions while decreasing radiation sensitivity and preventing sample evaporation in the high vacuum of the transmission electron microscope [Baker & Rubinstein 2010]. In the following years, incremental technological progress gradually increased the resolution achievable. Among these innovations were the application of field-emission guns [Crewe *et al.* 1968, Zemlin 1994], and, more recently, improved data analysis algorithms, such as maximum likelihood methods [Scheres 2012, Grigorieff 2007]. Direct electron detector cameras [Li *et al.* 2013a, Milazzo *et al.* 2011, Ruskin *et al.* 2013, Veesler *et al.* 2013], movie-mode imaging and the accompanying software developments [Campbell *et al.* 2012, Ripstein & Rubinstein 2016, Li *et al.* 2013b, McLeod *et al.* 2017], provided the final breakthrough required to achieve atomic resolution for biological samples by single particle analysis (for a review see [Cheng *et al.* 2015]). The importance of cryo-EM was recently recognized by the award of the Nobel prize for chemistry to three of the pioneers.

To image a biological sample by TEM, the method used to load the EM grid with sample (subsequently referred to as "grid preparation") must ensure that the resulting sample layer (i) is thin enough $\leq$100 nm to avoid extensive noise by inelastic or multiply scattered electrons; (ii) withstands the high vacuum of the electron microscope, and, (iii) protects the biomolecules from radiation damage. Two main methods are used to fulfill these perquisites: Negative stain (NS)[BRENNER & HORNE 1959, Carlo & Harris 2011] procedures (Figure 2.1A) adsorb the sample to a thin carbon film, embed the biomolecules in amorphous heavy metal and then allow the assembly to dry in air. This is simple and quick, and the loaded EM grids (subsequently referred to as "sample grids") are easy to store and can be kept for extended periods of time (generally years). In TEM, the preparations exhibit high contrast due to the NS and tolerate higher electron doses than cryo-preparations, but the resolution is limited to approximately 20 Å. Cryo-EM procedures (Figure 2.1B) employ holey carbon supports. A thin film of the sample solution is spanned across the holes and the EM grid is plunged into a cryogen, usually liquefied ethane, to rapidly cool it below −150 °C. The result is an amorphous, vitrified, 50 to 100 nm-thick film of the solution in the support holes. This thin, amorphous film withstands the high vacuum in the electron microscope and, in the ideal case, preserves biological structures in their native state. The procedure allows biological samples to be imaged at high-resolution. However, the sample grid must be kept at temperatures below −150 °C at all times to avoid devitrification. It can be imaged using relatively high electron doses due to the low temperature, but the contrast and signal-to-noise ratio is nevertheless low. Therefore, averaging techniques are employed to increase contrast and, provided the sample is imaged from different angles, a high-resolution three-dimensional (3D) map can be reconstructed. The most commonly used and highly successful method for 3D reconstruction in our days is the single particle approach. For a recent review see [Cheng *et al.* 2015].

Negative stain TEM (NS-EM) is important for screening and quality control, when

high-contrast is needed or when only limited amounts of sample are available (adsorption to the carbon film generally concentrates the sample). Single particle cryo-EM is the gold-standard method if high-resolution 3D reconstructions of the protein structure are aimed for. Unfortunately, the grid preparation methods used for NS and cryo-EM have not improved significantly since they were invented. Current drawbacks are the high sample consumption (approx. 3 µL of 1 mg protein) and the large amount (>99 %) of sample lost (Figure 2.1A,B). Furthermore, the classical method used to prepare grids for cryo-EM is a harsh procedure for proteins: First, it involves an extensive face-on paper-blotting step (Figure 2.1B, ii), and, second, the protein is exposed to the air-water interface for a significant amount of time [Glaeser 2016]. Here, an alternative method for sample pre-conditioning, sample grid preparation and post-processing (grid drying or vitrification) for NS-EM (Figure 2.1C) or cryo-EM (Figure 2.1D is presented. The in-house built setup, called "cryoWriter", uses miniaturized sample handling technology and microfluidic principles to aspirate, condition and dispense sample, avoiding paper blotting completely and providing alternative methods to thin samples for cryo-EM. It significantly reduces sample consumption and improves user-control over sample preparation as a whole. Furthermore, the method allows novel experimental applications; such as the preparation of isolated biological components of individual cells in an approach called "single cell visual proteomics" [Engel 2009, Kemmerling *et al.* 2012, Arnold *et al.* 2016, Kemmerling *et al.* 2013].

2.2 Protocol

A "cryoWriter" (Figure 2.2; for details see [Arnold *et al.* 2016, Arnold *et al.* 2017, Ramakrishnan *et al.* 2014]) or equivalent instrumentation is required for the following protocols. A list of suppliers for the main parts and consumables is given in the **Table of Materials**.

1. Negative Stain (NS) Grid Preparation

1.1. Turn on the instrument and start up the software. Initialize all necessary modules (syringe pump controller, motorized stages, surveillance cameras, and dew point stage).

1.2. Cool the sample support and the dew-point stage. If required, make sure that the dew-point stage temperature is regulated 1-2 °C above the dew point.

Note: The stage is cooled by a commercial Peltier device with a PID controller.

1.3. Prepare NS by filling a 100 or 200 µL PCR tube with 100-150 µL of NS (e.g.,

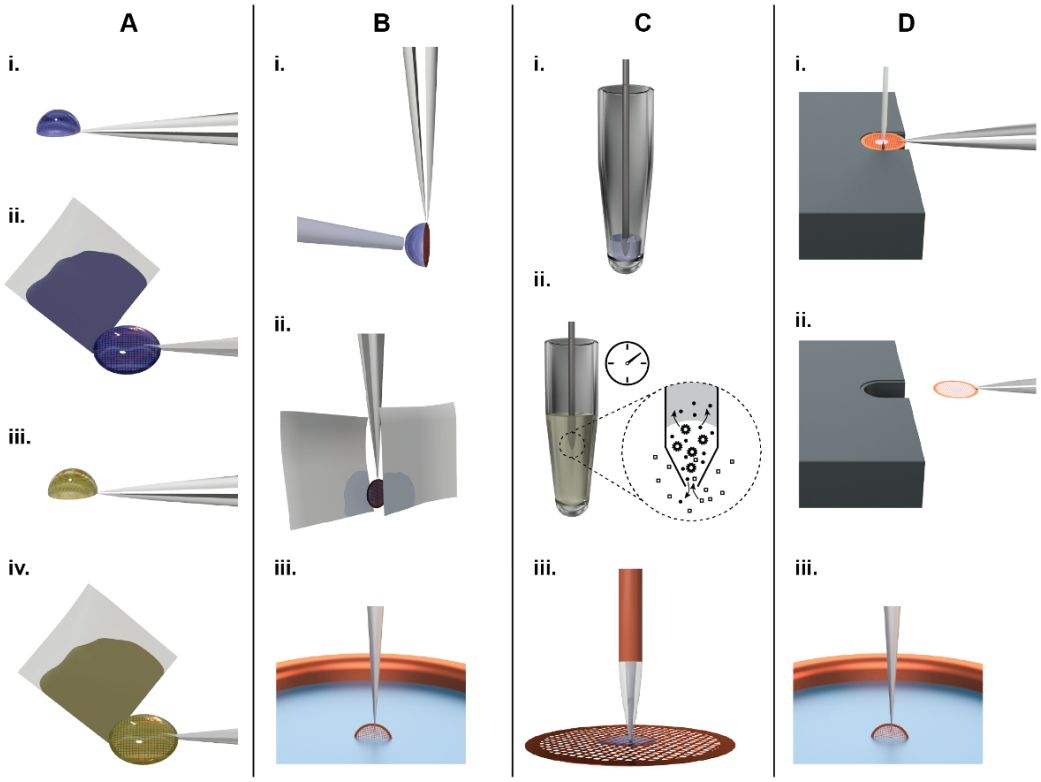

Figure 2.1: Principles of TEM grid preparation and comparison between the classical (panel A, B) and a microfluidic approach (panel C, D). **A)** Classical NS-EM grid preparation: About 3 µL of sample are pipetted by hand onto an EM grid covered with a continuous carbon film (subsequently referred to as an 'NS-EM grid') (i). After incubation for approx. 10 s, filter paper is used to blot away the excess liquid from the side (ii), leaving the adsorbed biomolecules in a thin water film. Subsequently, the protein is incubated in a heavy metal salt solution, e.g., 2 % uranyl acetate, for 20 s (iii), and again the liquid is removed by blotting from the side using filter paper (iv). Finally, the EM-grid is left to dry in air. **B)** Classical cryo-EM grid preparation: About 3 µL of sample are pipetted by a hand onto a holey carbon film. To form a thin sample film, the surplus liquid is removed by paper-blotting face-on from one or both sides (ii). Finally, the grid is rapidly plunged into liquid ethane for vitrification (iii). **C)** NS-EM grid preparation using the cryoWriter setup: A 5 nL volume is aspirated from the sample stock using a microcapillary (i). For sample conditioning, the microcapillary tip is immersed into the conditioning solution, e.g., 2 % ammonium acetate. Ions and small molecules are exchanged by diffusion (ii). Note that the dimensions of the microcapillary ensure that the whole process is diffusion driven. Proteins have much lower diffusion constants than salt ions and are not significantly lost [Arnold *et al.* 2016]. Finally, the sample is dispensed onto the grid and allowed to dry (iii).

(continued)

Figure 2.1: D) Principles of cryo-EM grid preparation using the cryoWriter-based method: An EM grid covered with a holey carbon film is placed on the surface of a temperature-controlled platform and held by tweezers. The temperature of the platform is controlled at an offset from the dew point temperature of the grid environment. The grid is moved relative to the microcapillary containing the sample and the microcapillary is lowered until it is a few micrometers above the grid. Subsequently, a few nanoliters of sample are dispensed from it while the stage is moved in a spiral pattern; excess liquid is re-aspirated (i). After EM grid priming, the microcapillary is withdrawn and the grid remains on the temperature controlled platform (subsequently referred as dew point (DP) stage) for a short time to allow a controlled amount of sample to evaporate. For plunge freezing, the grid is rapidly withdrawn from the stage using the tweezers (ii), flipped by 90° into the vertical position, and plunged into a cryogen bath (iii) (subsequently referred to as 'pick-and-plunge' mechanism).

2 % methylamine tungstate). Place the tube on the cooled sample support of the instrument.

1.4. Position the sample

1.4.1. Put the sample 0.5-1 µM into a 100 or 200 µL PCR tube. If less than 50 µL of sample is available, cut off the bottom of a PCR tube with a razor blade and use it as a sample well. This will ensure that the microcapillary can easily reach the sample.

Note: It is easiest to aspirate samples from 100 or 200 µL PCR tubes, because the microcapillary used later to aspirate the sample is slightly tilted and the travel-height z-axis direction is limited.

1.4.2. Place the PCR tube/container on the cooled sample support in the instrument to prevent evaporation. Alternatively, samples can be aspirated from well plates in the microscope stage top incubator at room temperature; cooling is not implemented for well plates.

1.5. Define positions. Use the cryoWriter joystick that controls the motorized xy-stage and software control buttons for the linear x-, y-, and z-axis stages to position the microcapillary. Use the camera to check the position of the capillary.

1.5.1. Move the microcapillary to the sample reservoir. Immerse the tip into the sample liquid and save this position as "sample".

1.5.2. Move the microcapillary to the NS PCR tube, immerse the tip into the NS solution and save this position as "stain".

1.5.3. Place the microcapillary roughly 100 µm above the center of the slot where

the EM grid will be positioned and save this position as "grid_save".

1.6. Aspirate sample and condition it for NS-EM.

1.6.1. If not already installed, mount a 10 µL syringe (0.46 mL inner diameter) on a precision syringe pump.

1.6.2. Glue one end of a 30 cm long fused silica microcapillary (outer diameter 360 µm, inner diameter 150 µm) to the syringe outlet.

1.6.3. Connect the other end of the microcapillary to a short (5 cm) long tapered microcapillary via press fit connector. The tapered tip of the short microcapillary forms the dispensing tip.

1.6.4. Fill the syringe with degassed double-distilled water (ddH_2O; system liquid) and avoid the formation of air bubbles.

1.6.5. Dispense a few tens of nanoliters of system liquid and remove any drops from the microcapillary with a lint-free tissue.

1.6.6. Double-click on the saved sample position. This positions the microcapillary in the sample well. While the capillary is moving, dispense 3 x 0.5 nL of system liquid just before the microcapillary tip is immersed into the sample to prevent air bubble from being trapped there (see note 2 below).

IMPORTANT NOTE: (1) When switching from aspiration to dispensing mode or vice versa, there is a small loss in piston stroke due to backlash in the gears of the syringe pump. According to the manufacturer, the backlash of a new unit lies between 7 and 10 nL. For our syringe with a barrel diameter of 0.46 mm, this translates to 1-2 nL. Therefore, 1-2 nL can be "dispensed", before sample is actually dispensed. Usually, a tiny droplet starts to exit the microcapillary tip after the third 0.5 nL dispense step. (2) An air bubble trapped above/below the sample would make dispensing less accurate and prevent sample conditioning by diffusion.

1.6.7. Leave the microcapillary immersed for 3-12 min, depending on the sample buffer and nozzle geometry.

Note: The higher the salt and/or phosphate concentration in the buffer, the longer the required immersion time. NS (relatively quick) diffuses into the sample plug while buffer salts (relatively fast) and protein (much slower) diffuse out. This lowers the concentration of buffer salts in the sample preventing them from crystallizing when the loaded grid dries.

Further, phosphate tends to form a precipitate in combination with NS.

1.7. Prepare a grid and deposit a spot of the conditioned sample.

1.7.1. While the sample is being conditioned, take a piece of adhesive tape and a PDMS block and clean the top side of the PDMS by applying and removing the adhesive tape to ensure that there is no dust. Put the PDMS block in a Petri dish.

Note: New PDMS blocks are taken from the clean room.

1.7.2. Carefully pick up a grid (e.g., Cu, 200 or 400 mesh coated with Parlodion/C film). Make sure to touch only the edge of the grid with the tweezers. Place it on the clean PDMS block with the carbon film facing upwards.

1.7.3. Place the PDMS block with the grid in an air glow-discharge unit and glow discharge it for 20 s with 100 W power at 0.4 mbar. Store the grid in a closed Petri dish. Longer glow discharge times generally lead to a larger spreading of the deposited sample volume on the grid. As a result, the stain layer becomes thinner (weaker stain).

1.7.4. 1 min before the immersion time is up, grasp the glow-discharged grid with the cryoWriter tweezers. Make sure the electromagnet is turned ON; otherwise turn it on in the software. Mount the tweezers on the electromagnet and use the manual micromanipulator screw to align the grid flat on the dew-point stage, carbon film side up. Make sure that the dew-point stage temperature is regulated 1-2 °C above the dew point to reduce the rate of evaporation after sample is loaded.

1.7.5. When the immersion time is up, double-click on "grid_save". The microcapillary tip will be placed safely above the grid surface. Manually bring the microcapillary tip into contact with the grid. Lift the nozzle by 10 µm and position it above the center.

CAUTION: Some samples containing detergents tend to move up along the outer surface of the microcapillary when liquid is dispensed due to the lower surface tension. It is important to be very close to the grid surface to prevent such losses.

1.7.6. Dispense 5 nL of sample onto the grid. On a dry day, when rapid evaporation takes place at the microcapillary tip, one can also slowly dispense until the sample is at the very tip, and then quickly dispense 5 nL.

1.7.7. Withdraw the microcapillary and let the conditioned sample dry slowly on the dew point stage (DP-stage).

1.7.8. Once the sample spot has dried, remove the grid and store it at room temperature in a grid box or Petri dish.

1.7.9. Dispense 500 nL of system liquid from the microcapillary and remove it with a lint-free tissue. Flush the capillary 5 times with either ethanol, detergent or 1 M NaOH. This cleans the microcapillary allowing it to be used with a different sample.

2. Cryo Grid Preparation

2.1. To prepare the instrument and sample, follow steps 1.1 to 1.5 described above. If NS is not required omit steps 1.3 and 1.5.2. To exchange the sample buffer or condition the sample for cryo-EM by dialysis, e.g., to reduce the concentration of buffer salts or to introduce additives (e.g., trehalose, detergents) use the desired buffer instead of NS in steps 1.3 and 1.5.2.

2.2. Prepare liquid ethane in a standard cryo container.

2.2.1. Assemble the ethane cup, cryo box holder, and spider and fill the cryogen container to the brim with liquid nitrogen; usually requires about 200 mL. Wait a few minutes until the ethane cup has cooled down and is free of liquid nitrogen.

2.2.2. Open the ethane gas bottle and slowly let the gas stream into the ethane cup. Let it fill with liquid ethane until the level is 2-3 mm below the top; this takes a few minutes and requires about 5 mL of liquid ethane.

2.2.3. Take a cryo box and place it in a free slot in the cryogen container.

2.2.4. Remove the spider, place the polystyrol lid on top, and place the cryogen container on the mounting in the cryoWriter.

2.3. Glow discharge an EM grid.

2.3.1. Take a piece of adhesive tape and a polydimethylsiloxane (PDMS) block and clean the top side PDMS by applying and removing the adhesive tape (removes any dust). Put the PDMS block in a Petri dish.

2.3.2. Carefully pick a grid from the grid box. Make sure to touch only the edge of the grid with the tweezers. Place it on a clean PDMS block with the holey carbon film facing upwards.

2.3.3. Place the PDMS block with the grid in a plasma cleaner and plasma-

clean the grid surface (e.g. use 75 % Ar/25 % H_2, power 50 W, pressure 25 mTorr). Place the PDMS block with the glow-discharged grid in a Petri dish.

2.4. Position the grid in the instrument

2.4.1. Grasp the glow-discharged grid with the cryoWriter tweezers. Make sure the electromagnet is turned ON; otherwise turn it on in the software. Mount the tweezers on the electromagnet and use the manual micromanipulator screw to align the grid flat on the stage, carbon film side up.

2.4.2. Double-click on "grid_save". Adjust the microcapillary position so that the tip is approx. 10 µm above the grid surface. Make sure that the microcapillary can move freely across the grid without touching it anywhere, if necessary withdraw the microcapillary a few micrometers.

2.4.3. Go back to the center of the grid and save the new position as "grid".

CAUTION: Correct naming is mandatory for the macro script to work.

2.5. Write sample and plunge-freeze grid.

2.5.1. Initialize the transistor to transistor logic (TTL) module in the control program, which is required to trigger the plunge mechanism.

2.5.2. Flush the microcapillary with a few tens of nanoliters of system liquid and remove any drops from the microcapillary with a lint-free tissue.

2.5.3. Start macro script. The macro will perform the following steps:

2.5.3.1. Dispense 5 nL (to remove any air bubbles at the tip) and go to sample position.

2.5.3.2. Aspirate 65 nL of sample. Infuse 5 nL back into the sample tube. This accounts for system backlash and allow synchronized writing, i.e., to ensure that dispensing and stage movement start at the same time.

2.5.3.3. Move to "grid" position.

2.5.3.4. Initiate 'writing pattern', which will cause the microcapillary to move across the grid, simultaneously dispensing 45 nL of sample.

2.5.3.5. Afterwards, move the microcapillary back to the center of the grid,

lower it another 10 µL, and withdraw excess sample liquid.

2.5.3.6. Withdraw the microcapillary and turn off the electromagnet. This releases the tweezers and initiates plunge freezing.

2.6. Grip the tweezers and carefully release the magnetic adapter from the plunger. Quickly transfer the grid from the ethane cup into the cryogen container containing the cryo box and place the grid in a free slot.

3. Single-cell Lysate Preparation

3.1. Prepare the microcapillaries for electroporation.

Note: The tapered (laser-pulled and inspected) fused silica microcapillaries have a protecting polyimide coating on the outside, except for the tip, where the coating is burnt off during the tapering process.

3.1.1. To coat the microcapillaries with a conductive layer, mount them at an angle of 45° on a metal rail, with the tips pointing upwards. Use an aluminum foil to shield the lower end (2 cm) of the tips, as uncoated polyimide forms the best seal with the press-fit connectors employed later.

3.1.2. Sputter deposit a sticky layer of 20 nm Ti/W, and then a 200 nm-thick layer of Pt.

3.2. Make the microcapillary tip hydrophobic.

3.2.1. Prepare a 1 M solution of 1-dodecanethiol in EtOH.

3.2.2. Glow-discharge the microcapillary in air for 1 min with 100 W power at 0.4 mbar.

3.2.3. Immerse the tip of the microcapillary in the 1 M solution of 1-dodecanethiol for a few hours (ideally overnight). It is best to prepare tips freshly one day before use.

3.3. Install a new microcapillary.

3.3.1. Remove the microcapillary from the 1-dodecanethiol solution, rinse the outside with ethanol and flush the inside with ethanol using a syringe.

Note: If no functionalized microcapillaries are available, quickly glow discharge the tip of a microcapillary and dip it in a drop of commercial car window treatment, which is a mixture of PDMS and sulphuric acid. The resulting hydrophobic functionalization is not as good as with

1-dodecanethiol, but generally sufficient.

3.3.2. Cleave its uncoated end with a capillary cutter.

Note: A clean cut is important for a good seal with the press-fit connector.

3.3.3. Use a toothpick to apply silver paste to the sharp boarder formed between glass and the polyimide coating when the polyimide coating was burnt off by the laser during capillary pulling.

Note: This reinforcement is necessary as the Pt coating is very weak in this region, and electrical conduction can easily break down.

3.3.4. Wash the polyimide end of the microcapillary with acetone. Leave a small drop of acetone at the end and insert it into the orifice of the press-fit connector. Apply light pressure to form a good seal.

3.4. Calibrate the microcapillary position.

3.4.1. Turn on the instrument and start the software as described in step 1.1. Additionally, initialize the microscope camera and the function generator.

3.4.2. Place a glass microscope slide into the slide holder on the microscope.

3.4.3. Lower the microcapillary close to the glass slide and center it over the microscope objective until it appears in the microscope camera view. Use the x- and y- axis linear stages to position the tip of the microcapillary at the center of the image. Then slowly lower the tip until it slightly touches the glass slide.

CAUTION: Choose very small steps (5 µm) towards the final approach. Otherwise, the tip can be damaged.

3.4.4. Press the "Calibrate Nozzle" button. This retracts the microcapillary 40 mm, and sets this position as home position.

3.5. Preparation of stamped PDMS pieces and ITO slides.

3.5.1. Mix PDMS and crosslinker in 10:1 ratio, pour into a large Petri dish to a depth of about 2-3 mm. Bake at 60 °C for a few hours in a hybridization incubator or similar device.

3.5.2. With a hammer and a stamp (12 mm diameter), cut holes in the PDMS layer. Afterwards, use a scalpel to cut out 2 cm long squares or rectangles

including the holes to obtain stamped pieces that fit on a microscope slide. Usually, two stamped pieces are mounted on one microscope slide.

3.5.3. Wash the PDMS pieces and the ITO slides first with detergent and then with 70 % ethanol. Place them, wet, in a Petri dish and let the ethanol fully evaporate in an oven at 60 °C.

3.5.4. Glow-discharge the ITO slides for 1 min with 100 W power at 0.4 mbar and then apply 1 mL of coating solution (e.g., poly-L-lysine (PLL)). Incubate for 5 min, remove the solution with a pipette, and apply 1 mL of ddH_2O. Slightly agitate for 1 min, and then remove the ddH_2O using a pipette. Let the slides dry at 60 °C.

3.6. Prepare the cell culture. Follow standard adherent-cell culturing protocol (e.g., [Arnold *et al.* 2016, Kemmerling *et al.* 2013]). Seed cells on ITO during normal splitting/passaging runs.

3.6.1. Take a freshly PLL-coated ITO slide and add a PDMS piece. Apply some pressure to form a watertight seal. This produces small wells with the slide as their base.

3.6.2. Add about 300 µL of cells suspended in fresh medium to the PDMS wells. The seeding density should be around 75,000 cells per well.

3.6.3. Incubate the ITO slides for 1-2 d days under standard conditions.

3.7. Prepare for cell lysis experiment:

3.7.1. Pre-warm a few milliliters of the electroporation buffer (e.g., phosphate buffered saline (PBS)).

3.7.2. Set up the instrument according to steps 1.1-1.5 (for NS) or step 2.1 (for cryo).

3.7.3. Load the standard lysis parameters, e.g., the lysis voltage.

3.7.4. This is a good moment to prepare the cryogen for cryo (steps 2.2).

3.7.5. Take the ITO slide from the incubator, and mount it on the microscope insert. Use two screws to fix the slide on the aluminum insert and to ensure electrical contact between the ITO coating of the slide and the electrically grounded aluminum frame.

3.7.6. Remove the cell culture medium and wash twice with 300 µL of electroporation buffer. Keep the cells in electroporation buffer.

3.7.7. Place the aluminum insert holding the ITO slide in the live-cell incubator stage on the setup.

3.7.8. Locate the cell culture in the microscope view and choose an area with no cells. Approach the tip to the ITO surface and gently touch it, then withdraw the tip 100 µm and save the position as "cells".

3.7.9. Quickly leave the cell culture and flush the microcapillary tip with a few tens of nanoliters of system liquid then put it into the cell culture again. Dispense a few nanoliters during immersion into the PDMS well to ensure that no air bubbles are trapped at the tip.

3.7.10. Gently approach the ITO surface (initially, you must be at position "cells", i.e., 100 µm above the surface). Upon contact, retract the tip 10 µm.

3.7.11. Select a nearby cell for lysis. Place the tip of the microcapillary above the targeted cell.

3.8. Start the macro script for single-cell lysis.

3.8.1. Name the position the microcapillary should be moved to after a cell has been successfully lysed. This will be the NS reservoir (NS-EM), a desalting buffer (cryo-EM) or the EM grid (cryo-EM). Avoid spelling errors and press "ok".

3.8.2. The macro proceeds without user intervention:

(i) The microscope stage and cell culture 100 µm are moved to the left, a snapshot of the targeted cell is taken, and 50 nL of ddH_2O system liquid are dispensed from the microcapillary. This displaces and dilutes the high salt buffer and applies osmotic pressure to the cell.

(ii) The stage is moved back to position the tip above the targeted cell again. The predefined voltage burst is applied, and after 500 ms the pump system starts to aspirate 3 nL of sample at a flow rate of 2 µL min^{-1}.

(iii) The stage is moved to the left again, allowing the cell to be inspected. A window appears, asking for user input.

3.8.3. Say whether the lysis step was successful or not.

3.8.3.1. If the answer is no, take over, flush the microcapillary and target a new cell.

3.8.3.2. If the answer is yes, a snapshot of the removed (lysed) cell is taken, and afterwards the microcapillary is moved to the location specified in 3.8.1. If this is NS or a buffer reservoir, use the standard user interface to dispense 3 x 0.5 nL of liquid while the microcapillary is moving to ensure that there are no air bubbles. The tip is immersed in the reservoir liquid by the macro.

3.9. Continue to condition the sample and/or prepare grids as explained in sections 1.6.9 – 1.7.9 for NS-EM or section 2.2 – 2.6 for cryo-EM.

2.3 Representative results

The "cryoWriter" setup was developed (depicted in Figure 2.2) in order to test the miniaturized EM grid preparation procedures proposed in Figure 2.1C,D. Figure 2.2A shows an overview of the various components mounted to an inverse fluorescence microscope. A cell-culturing module is installed on the left side of the microscope; a module for EM grid preparation is located on the right. The cell-culturing module (Figure 2.2B) allows the growth of adherent eukaryotic cells and live-cell imaging of the cell culture by the light microscope. Individual cells are lysed by the combined action of osmotic shock, electroporation and aspiration of the cell content into a microcapillary (Figure 2.2B, Figure 2.6A) [Arnold *et al.* 2016, Kemmerling *et al.* 2013]. The aspirated lysate sample can then be used to prepare grids for NS- or cryo-EM. Alternatively, a stock protein solution in a PCR tube can be the sample source. The microcapillary (Figure 2.2B) employed is connected to a high-precision pump system allowing sample volumes to be aspirated and dispensed with sub-nL precision. As detailed in the protocols, all sample processing is performed within this microcapillary or on the EM grid itself without significant sample transport. For example, the same microcapillary is used to lyse individual eukaryotic cells, aspirate the lysate, condition it, and finally dispense aliquots onto EM grids. The grid preparation module consists of a movable DP-stage that allows the temperature of the EM grid placed on it to be precisely controlled (Figure 2.2C). For NS-TEM, the prepared sample grid can then simply be removed from the cold stage and allowed to dry in air at room temperature. However, the so-called coffee-ring effects that can then result need to be avoided for quantitative TEM where protein 'particles' are counted. To do so, grids are dried slowly on the DP-stage using a gradually increasing temperature gradient to slow down liquid evaporation. For cryo-EM, the temperature of the grid is kept close to the dew point; a positive offset of approx. 8 °C is chosen, allowing the controlled evaporation of sample liquid for thin film stabilization and thinning, which can be monitored by a sensor if necessary [Arnold *et al.* 2017]. After the selected thinning time, a pick-and-plunge mechanism is activated and the sample is vitrified (Figure 2.2C). Note that this plunging mechanism is not needed for NS-EM

grids, which are stored at room temperature. Figure 2.3 shows representative results obtained for NS-EM grids prepared using the cryoWriter setup. The tip of the microcapillary was loaded with 5 nL of sample from a stock solution and dipped into a reservoir of NS solution (2 % methylamine tungstate) for several minutes to allow diffusive exchange of NS and salt ions (for a theoretical discussion see [Arnold *et al.* 2016]). Afterwards, the conditioned sample was dispensed onto the thin carbon film of a NS-EM grid and dried. Figure 2.3A shows the use of a slot grid in the same way to visualize the complete droplet, as required for quantitative TEM. In order to avoid the coffee ring effect, the freshly glow-discharged grid was initially held at the dew-point temperature (no water evaporation) and then slowly warmed up on the DP-stage. Note, that for most applications (e.g., quality control of the sample or structural analysis) this slow-drying process is not needed. High-quality NS-preparations are obtained without it, as shown in Figure 2.3B,C. Conditioning times for phosphate-free low salt buffers are around 3 min, e.g., with low-salt Tris-buffer (20 mM Tris-HCl pH 7.4 with 50 mM NaCl), as shown in Figure 2.3B using tobacco mosaic virus (TMV) as sample. Figure 2.3C presents a worst-case scenario as the TMV was in PBS buffer (2.7 mM KCl, 1.5 mM KH_2PO_4, 136.9 mM NaCl, 8.9 mM $Na_2HPO_4 \cdot 7\,H_2O$, pH 7.4). Phosphate ions form transient crystals with the heavy-metal ions of NS (see Figure 2.5C), lengthening the conditioning time required (7 min). Other heavy metal salts can also be used with the grid preparation module, e.g., 2 % methylamine vanadate or ammonium molybdate (see also [Arnold *et al.* 2016]). However, uranyl acetate is not suitable; the crosslinking effect of this stain leads to aggregates if the protein sample is conditioned in solution, before adsorption to a carbon film (see Figure 2.5E) [Kemmerling *et al.* 2012]. Typical results obtained for cryo-EM grids prepared using the cryoWriter setup are depicted in Figure 2.4. Panel 4A shows a grid atlas of the area covered by vitrified sample. Panel 4B shows the homogeneity of the vitreous ice in a selected grid slot. In both cases, the sample was in 25 mM HEPES-KOH pH 7.5, 50 mM NaCl buffer containing 0.05 % Fos 14 detergent. Many samples and buffers were tested and a comparable high quality vitreous ice was obtained, but the conditions required are buffer dependent (see also discussion of Figure 2.5). Panel 4C shows apoferritin particles and a bacteriophage in Tris-HCl buffer (20 mM Tris-HCl, 50 mM NaCl; pH 7.4) imaged at high defocus to increase contrast. Panel 4D shows a 200 kDa membrane protein stabilized by amphipoles. The cryoWriter setup allows systematic screening for optimal EM-grid preparation conditions; an example is shown in Figure 2.5A (apoferritin in 25 mM HEPES-KOH pH 7.5, 50 mM NaCl, 0.05 % Fos 14). In this experiment, the vitreous ice "thinning" temperature was varied, but the thinning time (i.e., the time gap between sample application and plunge freezing) remained constant (1 s). At low offset temperatures (e.g., 8 K), the sample layer was too thick. At higher offset temperatures, the vitreous ice in the holes was thinner (10 K, 12 K), until at some stage (above 18 K) the grid became completely dry (not shown). In the results presented here, an offset of 12 K lead to a large homogeneous area of vitreous ice as indicated by the black arrows.

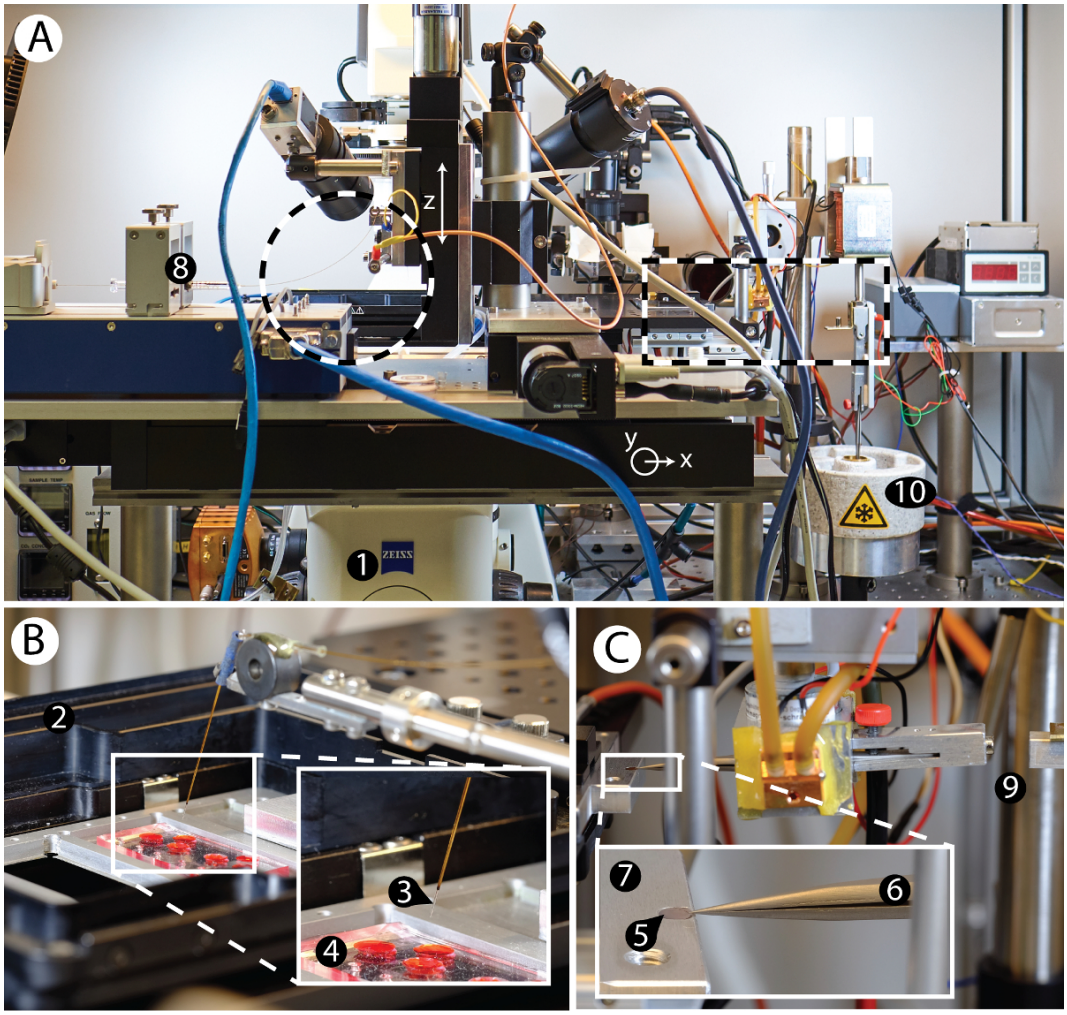

Figure 2.2: Overview of the cryoWriter setup. **A)** Overview of the cryoWriter setup mounted on an inverse light-microscope (1). **B)** Inset of area indicated on the left side in panel A. Cell culturing compartment (2), with a microcapillary (3) for sample manipulation and cell lysis positioned above a miniaturized PDMS-based cell culture plate (4). **C)** Inset of area indicated on the right side in panel A. 'Pick-and-plunge' mechanism. A holey carbon film EM grid (5) is mounted between the tips of tweezers (6) and positioned horizontally in direct contact with the temperature-controlled stage (7), referred as the dew-point stage (DP-stage) in the main text. The stage temperature is tightly controlled via a PID controller and a water-cooled Peltier element, keeping it at or close to the dew point temperature, depending on the ambient environment. The DP-stage (7) is mounted on a motorized xy axis to move the grid relative to the microcapillary. The microcapillary itself is mounted on a z-stage, and can be lowered until it is very close to the surface of the EM grid and used to dispense nanoliter-sized volumes onto the sample support covering it (a continuous thin carbon layer for NS-EM or a holey carbon film for cryo-EM). Note, liquid uptake and dispensing is performed using a high-precision pump system (8). The dispensed liquid can be distributed by moving the grid relative to the microcapillary in a spiral pattern. For cryo-EM preparation, the pick-and-plunge freezing mechanism (9) rapidly transfers the sample-loaded grid into liquid ethane (10) for rapid cooling and sample vitrification.

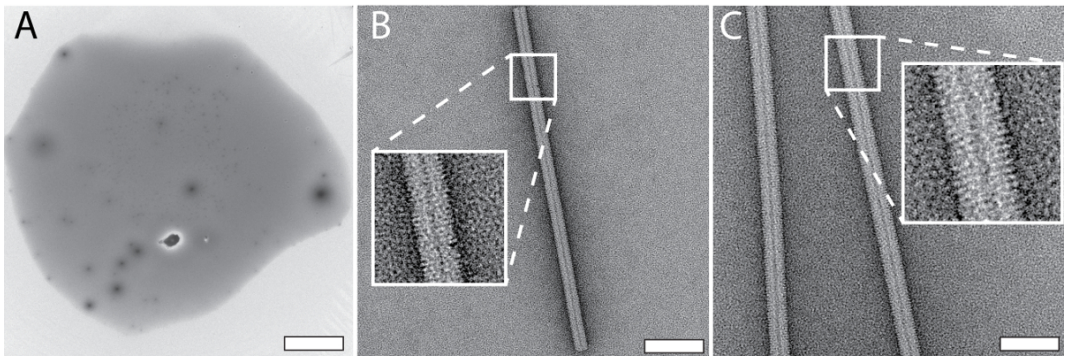

Figure 2.3: Typical results for NS grids prepared using the cryoWriter setup as indicated in Figure 2.1C. **A)** Overview image of a 3 nL droplet dispensed on a slot grid after conditioning with 2 % methylamine tungstate. **B)** TMV in 20 mM TRIS buffer. The inset shows a 3x enlargement of the indicated region. Adapted from [Arnold *et al.* 2016] (further permissions related to the material excerpted should be directed to the ACS). **C)** Tobacco mosaic virus (TMV) in PBS buffer. The inset shows a 3x enlargement of the indicated region. Adapted from [Arnold *et al.* 2016] (further permissions related to the material excerpted should be directed to the ACS). Scale bars: A, 100 µm; B, 50 nm; C, 80 nm.

Such optimization experiments can be performed with the buffer of the target sample using "test" proteins (such as apoferritin). The best conditions found are then applied to the target sample. Furthermore, grids with parameters far from the optimum can often be recognized during the preparation procedure and do not need to be screened in the electron microscope, saving significant time. Figure 2.5 also shows a gallery of typical cryo-EM (Panel B) and NS-EM (Panels C to E) artifacts specific to the cryoWriter setup. The cryo-EM grid shown in Panel 5B with TMV in PBS containing 0.1 % decyl-β-D-maltopyranoside (2.7 mM KCl, 1.5 mM KH_2PO_4, 136.9 mM NaCl, 8.9 mM $Na_2HPO_4 \cdot 7\,H_2O$, pH 7.4, 0.1 %) was excessively thinned. The background of the image is grainy because the salt concentration became too high. In general, the visual appearance of a sample does not seem to be a linear function of the salt concentration; grains suddenly become prominent when a threshold concentration is reached during the thinning process. Note, that unwanted substances can be removed by a conditioning step prior to grid preparation, as described for NS-EM in protocol section 1.6. NS can cause other artifacts. In the example shown in Panel 5C, PBS buffer (2.7 mM KCl, 1.5 mM KH_2PO_4, 136.9 mM NaCl, 8.9 mM $Na_2HPO_4 \cdot 7\,H_2O$, pH 7.4) without sample was conditioned in 2 % methylamine tungstate for 3 min. Precipitates and crystals are evident and exert extensive forces on the carbon surface leading to cracks. The precipitates only form in a certain PBS and NS concentration range and can be avoided by conditioning the sample for longer (compare Figure 2.3C). Panel 5D shows the periphery of a dispensed NS sample droplet exhibiting a "coffee ring". This would disturb quantitative, total sample analysis and can be avoided by slowing down the drying process, i.e., by keeping the

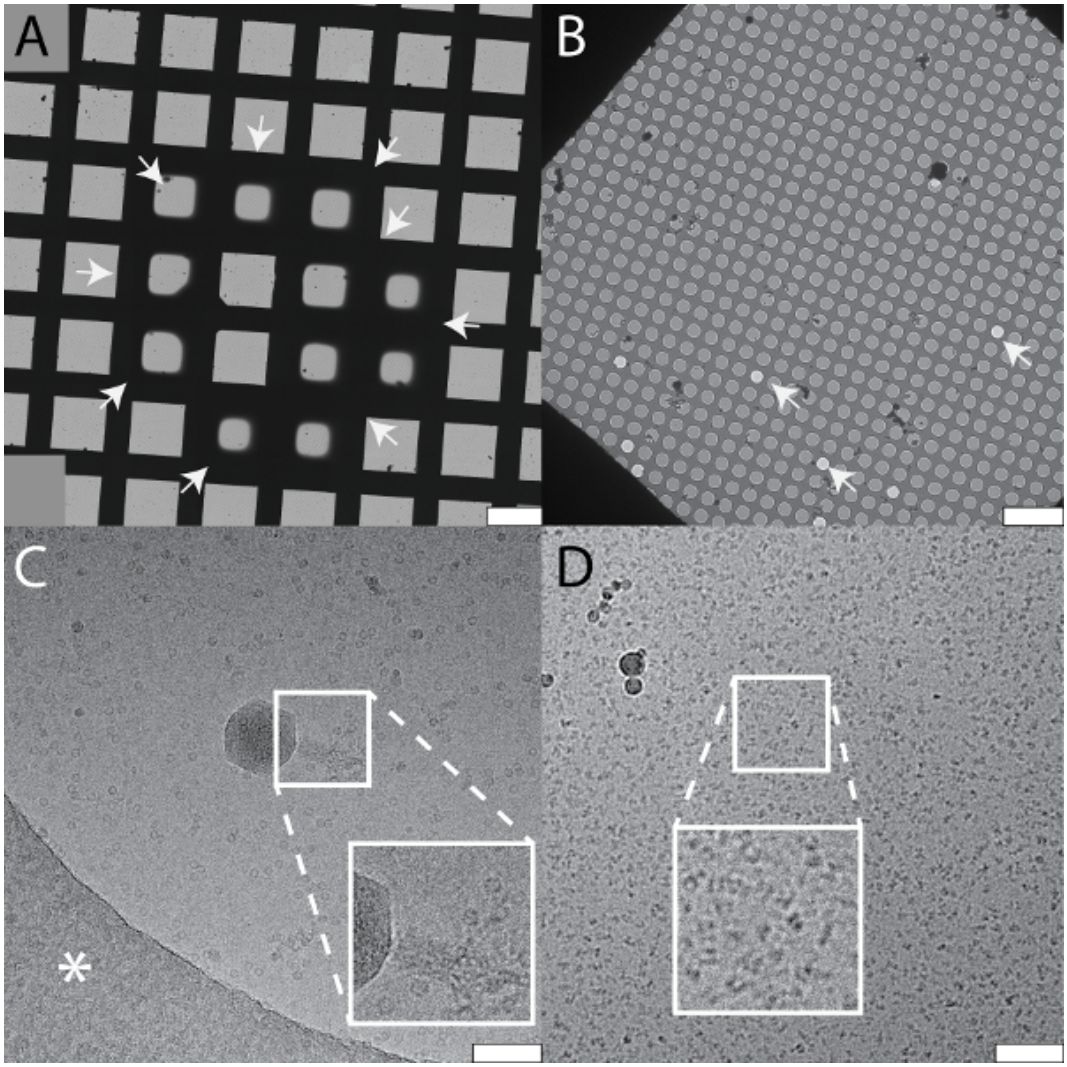

Figure 2.4: Typical results for cryo-EM grids prepared using the cryoWriter setup as indicated in Figure 2.1D. The samples and the buffers vary in the examples shown. All samples were loaded on holey carbon films. **A)** Collage of overview images ("grid atlas") of a sample containing a 150 kDa membrane protein, the periphery of the vitreous ice is indicated by white arrows. **B)** Enlarged grid slot from a grid prepared with the same buffer, showing the holey carbon film with vitreous ice. Some holes are not filled with sample buffer as indicated by white arrows. **C)** Carbon hole with vitrified sample containing apoferritin protein complexes and bacteriophages. Inset: twofold enlargement showing the tail of a bacteriophage. The white asterisk indicates the carbon film. Note that the image was recorded with high defocus to increase contrast. **D)** A 200 kDa membrane protein reconstituted in amphipols. Inset: a 2x enlargement of the indicated region shown with increased contrast. Scale bars: A, 100 µm; B, 10 µm; C and D, 80 nm.

EM grid at the dew point temperature during sample application, and then gradually increasing the temperature to dry it (see Figure 2.3A). Panel 5E (apoferritin in 20 mM HEPES, pH 7.0, conditioned 3 min) shows the crosslinking activity of 2 % uranyl acetate stain, which cannot be used to condition protein samples before they are adsorbed to carbon film supports. The small amount and volume required for EM grid preparation using the cryoWriter setup enables new types of experiments. For example, the total contents of a single cell can be collected and prepared for NS- and cryo-EM. The procedure is indicated in Figure 6A. An adherent, eukaryotic cell (HEK 293) is lysed by simultaneous electroporation and sample aspiration (Panel 6A)[Kemmerling *et al.* 2013]. A total volume of 3 nL is aspirated, which contains the cell lysate, and is retained in the microcapillary for further processing. For the NS-EM shown in Panel 6B, the cell-culturing medium was exchanged with PBS buffer (2.7 mM KCl, 1.5 mM KH_2PO_4, 136.9 mM NaCl, 8.9 mM $Na_2HPO_4 \cdot 7\,H_2O$, pH 7.4) prior to cell lysis. The cell contents were aspirated in 3 nL of buffer and conditioned in a reservoir of NS as indicated in Figure 2.1C for 10 min. Afterwards, a 5 nL volume was dispensed onto the continuous carbon film of a NS-EM grid. Individual proteins, e.g., filamentous actin, and membrane patches with attached proteins can be recognized in the image. For the cryo-EM, shown in Figure 2.6C, a volume of 3 nL was dispensed on a holey carbon EM grid without re-aspiration to remove liquid. The relatively thick film of sample formed was extensively thinned before vitrification. To do this, the DP-stage temperature was gradually increased, starting at the dew-point temperature. The thinning process was monitored by a real-time sensor-system until a pre-specified threshold was reached triggering the 'pick-and-plunge' mechanism and sample vitrification (for details see [Arnold *et al.* 2017]). Membrane structures and proteins can be recognized in the image.

2.4 Discussion

The 'cryoWriter' instrument and the protocols required to prepare sample grids for NS- and cryo-EM from nL sized total sample volumes and completely avoid the classical paper-blotting step are presented. Microfluidic principles and a micromechanical system are combined in the cryoWriter to make this possible.

Our experience shows that when the miniaturized methods presented in this manuscript are used the parameter space for EM-grid preparation is larger than for classical methods, and under tighter user control. Importantly, the increased reproducibility achieved makes it possible to pre-screen with sample buffer system, complemented with a readily available test protein, to determine the optimum parameters before the actual experiment is performed. This keeps consumption of the sample of interest to the absolute minimum and is highly recommended. Critical steps for both NS- and cryo-EM grid preparation are: (i) Priming of the pump system; for sub-nanoliter

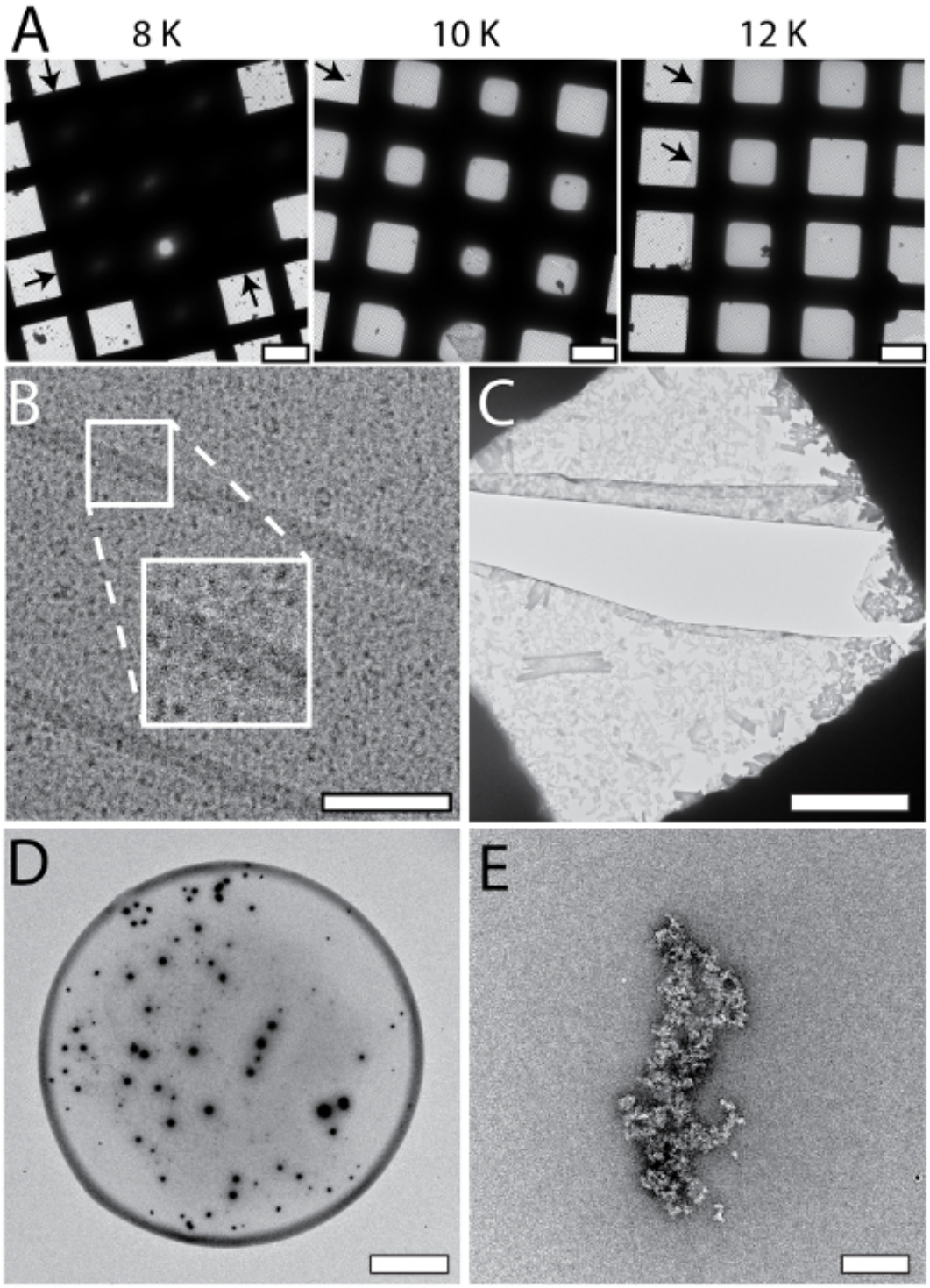

Figure 2.5: Systematic changes and artifacts observed when the cryoWriter set-up was used to prepare grids for NS- and cryo-EM. **A)** Systematic vitreous ice thickness variation; optimization of grid preparation for cryo-EM. The offset temperature of the DP-stage was varied (8 K to 12 K) keeping the thinning time constant (1 s). The arrows indicate the periphery of the sample layer.

(continued)

Figure 2.5: B) Salt effects; too highly concentrated, i.e., the thinning step was too long. The inset depicts a 2x enlargement of the indicated region. **C)** Salt precipitates formed by PBS buffer in the presence of heavy metal salts. Samples containing PBS buffer must be conditioned longer than samples in other buffers. Here, PBS buffer without sample was conditioned in 2 % methylamine tungstate for 3 min, a typical time for other sample buffers. Note the crack in the carbon film most probably due to the strong forces from the precipitates acting on the thin support during the drying process. **D)** 'Coffee ring' effect. **E)** Apoferritin conditioned in 2 % uranyl acetate for 3 min. Uranyl ions exhibit significant crosslinking activity and the apoferritin clusters form large aggregates. Scale bars: A, 80 µm; B, 80 nm C, 12 nm; D, 80 µm; E, 200 nm.

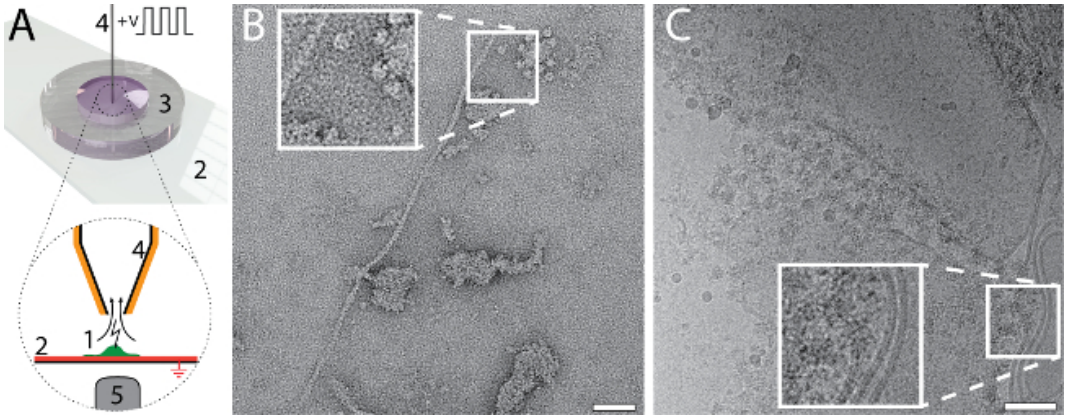

Figure 2.6: Single cell visual proteomics using the cryoWriter set-up. **A)** Lysis of a single adherent eukaryotic cell. The cell is grown (1, green) on an functionalized, ITO coated (red) glass-slide (2) in a miniaturized petri-dish (3) [Kemmerling *et al.* 2013]. The ITO layer is electrically grounded. The cell is approached by the microcapillary (4), which is coated with platinum. An initial osmotic shock (not indicated) is given to facilitate lysis, which is performed by a series of electric pulses and by the shear forces exerted during the aspiration of the cell lysate. The process can be monitored by light microscopy; the objective lens of the microscope is indicated (5). For details, see our previous work [Arnold *et al.* 2016, Kemmerling *et al.* 2013]. **B)** NS-EM image of lysate from an individual HEK 293 cell. Filamentous actin and membrane patches with attached proteins are visible. Panel adapted from [Arnold *et al.* 2016] (further permissions related to the material excerpted should be directed to the ACS). **C)** Cryo-EM image of lysate from an individual HEK 293 cell. The inset shows a 2x enlargement of the indicated region where typical membrane structures with associated proteins are visible. Panel C adapted from [Arnold *et al.* 2017]. Scale bars: B, 50 nm; C, 80 nm.

volume dispensing, the system liquid (water) must be degassed and bubble free. (ii) Precise control of the glow discharge or plasma cleaning step; the surface characteristics of the EM grid are crucial for reproducible results. (iii) Sample conditioning; the time required for conditioning, e.g., with NS, depends on the buffer type, salt content and concentration Figure 2.3, as well as on the nozzle geometry of the microcapillary [Arnold *et al.* 2016]. (iv) Evaporation rates for NS-EM preparations for quantitative EM; the coffee-ring effect can prohibit the quantitative analysis of NS-EM preparations, and must be suppressed by slow evaporation rates controlled by the DP-stage.

Different aspects of the presented grid preparation methods can be freely combined allowing the development of versatile protocols for specific samples. Typical examples would be the removal of a substance that prevents high-resolution EM, e.g., glycerol, by a conditioning step prior to grid preparation for cryo-EM; the introduction of mediator molecules, such as ligands, by conditioning before the grids are prepared; or the examination of single cell lysate by NS- or cryo-EM Figure 2.6.

The use of microfluidics and minimal sample amounts in the presented methods completely removes the need for paper-blotting steps. This is a great advantage, because paper blotting is a harsh treatment for proteins, potentially contaminating the sample with unwanted ions and inherently leading to massive sample loss. On the other hand, effects potentially caused by the air-water interface of the thin sample film formed when cryo-EM samples are prepared in the classical manner, are not avoided when the cryoWriter is used. Grids suitable for cryo-EM can be prepared with less than 0.2 s wait time between sample application and vitrification (data not shown). However, as proteins travel a few tenths of a nanometer in a few nanoseconds by diffusion, there is still enough time for them to collide with the air-water interface of a 100 nm thick sample film several times. However, the amount of proteins sticking to the air-water interface might be significantly reduced by these short time gaps and might prevent protein denaturation or restricted particle orientation. Another promising approach that might protect sensitive proteins from the air-water interface is to cover the sample film by low molecular weight surface-active substances. These compounds could be rapidly introduced by a conditioning step in the cryoWriter before grid preparation. The high surface-to-volume ratio of microfluidic systems is a further limitation of the cryoWriter, as sample can potentially be lost by unspecific adsorption to the microcapillary surface and disturb quantitative analysis by particle counting. The problem is addressed in two ways: First, the sample does not travel long distances within the microcapillary. Indeed, the nanoliter sample volume remains at the capillary tip throughout the processing. Second, the surface to volume ratio is further reduced by using microcapillaries with relatively large inner diameters, e.g., 180 µm. Third, the surfaces of the microcapillaries can be easily passivated if necessary, e.g., by treating them with commercially available polylysine ethanol glycols (PLL-PEG).

The high-resolution analysis of proteins by the single particle approach used in EM only requires 100,000 to a few million images of individual protein particles. This means that microfluidic techniques can provide enough protein complexes for the structural investigation. A miniaturized immuno-precipitation method for the fast isolation of protein-complexes (around 1 hour) from minimal cell amounts (approx. 40,000 cells) was developed earlier [Giss *et al.* 2014]. This method will now be directly linked to the miniaturized sample preparation stage of the cryoWriter. The final goal is to develop an integrated microfluidic pipeline for ultra-fast protein isolation and cryo-EM grid preparation that requires less than two hours in all. Furthermore, as demonstrated by Figure 2.6, the minute amount and volume of material needed for sample preparation and the almost lossless conditioning and grid preparation procedure achieved using the cryoWriter, make it possible to study the protein complexes of individual cells. Together, the miniaturized immuno-precipitation method and the cryoWriter lay the foundation of a new proteomics method called "single cell visual proteomics", as we recently demonstrated for heat-shock experiments [Giss *et al.* 2014]. Data analysis algorithms geared to the analysis of "visual proteomics" images are currently being tested.

2.5 Acknowledgments

The authors would like to thank the workshop of the Biozentrum of the University Basel for their support, S. A. Müller for critical discussions and for carefully reading the manuscript, A. Fecteau-LeFebvre for technical assistance with EM, Ricardo Adaixo, Frank Lehmann for membrane protein test samples (all from the C-CINA, Biozentrum, University of Basel) and A. Engel, emeritus University Basel for his inspiring conversations. Test samples were kindly provided by P. Ringler, M.-A. Mahi, and T. Schwede (Biozentrum, University of Basel), P. Leiman (Laboratory of Structural Biology and Biophysics, EPFL) and R. Diaz- Avalos (New York Structural Biology Center, USA). The project was supported by the Swiss Nanoscience Institute (SNI, project P1401, ARGOVIA project MiPIS) and the Swiss National Science Foundation (SNF, project 200021_162521).

Disclosures

The authors Stefan A. Arnold, Henning Stahlberg and Thomas Braun declare the following competing financial interest: The cryoWriter concept is part of patent application PCT/ EP2015/065398 and EP16194230.

3 Microfluidic sample purification for transmission electron microscopy using magnetic microspheres

In this section, a new microfluidic sample purification methodology for TEM using 1 µm sized magnetic microspheres is presented. An additional module was constructed and integrated into the *cryoWriter* setup allowing the isolation and preparation of proteins from less than 1 µL crude cell lysate.

My contribution was developing the protein isolation methodology, producing the corresponding hardware and software, performing the presented purification experiments, paper writing, creating the shown figures and building and refinement of the shown protein models.

The following section has been published in:

PNAS
Volume 116, Issue 30, July 2019, Pages 15007-15012
https://doi.org/10.1073/pnas.1907214116

Microfluidic protein isolation and sample preparation for high-resolution cryo-EM

Claudio Schmidli[1,2], Stefan Albiez[1], Luca Rima[1], Ricardo Righetto[1], Inayatulla Mohammed[1], Paolo Oliva[1,2], Lubomir Kovacik[1], Henning Stahlberg[1] and Thomas Braun[1]

1 - Center for Cellular Imaging and NanoAnalytics, Biozentrum, University Basel, Switzerland
2 - Swiss Nanoscience Institute, University of Basel, Switzerland

Contents

Abstract

High-resolution structural information is essential to understand protein function. Protein-structure determination needs a considerable amount of protein, which can be challenging to produce, often involving harsh and lengthy procedures. In contrast, the several thousands to a few million protein particles required for structure-determination by cryogenic electron microscopy (cryo-EM) can be provided by miniaturized systems. Here, we present a microfluidic method for the rapid isolation of a target protein and its direct preparation for cryo-EM. Less than 1 µL of cell lysate is required as starting material to solve the atomic structure of the untagged, endogenous *human* 20S proteasome. Our work paves the way for high-throughput structure determination of proteins from minimal amounts of cell lysate and opens new opportunities for the isolation of sensitive, endogenous protein complexes.

3.1 Significance statement

The recent improvements in cryogenic electron microscopy (cryo-EM) caused a revolution in structural biology. However, (i) protein isolation and (ii) sample preparation methods lag behind, and cryo-EM is performed at far from full efficiency. Here, we present a microfluidic method for the rapid isolation of a target protein from minimal amounts of cell lysate and for its direct preparation for high-resolution cryo-EM.

Our technology opens new avenues for structural biology: high-throughput structure determination of proteins in a multitude of conditions, ultrafast isolation and structure determination of sensitive proteins, and the analysis of proteins that cannot be produced in sufficient amounts using conventional approaches.

3.2 Introduction

Knowledge of a protein's architecture at high resolution is vital to understand its mechanics and chemistry. In recent years, cryogenic electron microscopy (cryo-EM) [Dubochet *et al.* 1988] has matured into a powerful method that can determine the architecture of biological macromolecules at the resolutions required to interpret the atomic fold of proteins [Kuhlbrandt 2014, Cheng 2018]. In the single-particle cryo-EM approach [Frank 1975, Heel & Frank 1981], an unsupported, thin layer of isolated protein complexes in amorphous (vitrified) ice is visualized at close to physiological conditions. Only several thousand to a few million imaged particles are needed to calculate a high-resolution, three-dimensional (3D) structure. Nevertheless, protein production, purification, and sample preparation for cryo-EM are nowadays considered the bottleneck for structure determination [Glaeser 2016, Thompson *et al.* 2016, Stark

& Chari 2015]. We have identified two dominating reasons for this: Firstly, significant amounts of protein must be produced. Conventional sample preparation for cryo-EM requires several microliters of a purified protein solution at a concentration of approx. $1\,\mathrm{mg\,mL^{-1}}$ per grid, from which extensive filter-paper blotting later removes the vast majority of protein particles [Taylor & Glaeser 1976, Dubochet *et al.* 1988, Kemmerling *et al.* 2012, Arnold *et al.* 2018]. Secondly, both, protein purification and cryo-EM sample preparation are lengthy and harsh procedures. Mostly, high-yield expression systems are employed, and one or two chromatographic steps are needed to purify the protein particles. In addition, the classical cryo-EM sample preparation process that follows is a rough procedure [Glaeser & Han 2016], primarily because of the blotting step, and many proteins denature.

We recently developed a microfluidic cryo-EM grid preparation system termed *cryo Writer*, allowing the preparation of cryo-EM specimens from nanoliters of sample-solution [Arnold *et al.* 2016, Arnold *et al.* 2017, Schmidli *et al.* 2018]. Since the *cryo Writer* does not use paper blotting, it ensures that grid preparation is gentle and virtually lossless. Here, we report the combination of sample grid preparation using the *cryo Writer* with microfluidic protein purification [Giss *et al.* 2014], to determine the 3.5 Å cryo-EM structure of the untagged *human* 20S proteasome complex, which is the 'catalytic core' of the ubiquitin-proteasome system involved in 80 % of protein degradation [Bhardwaj *et al.* 2009] and an important drug target [Cromm & Crews 2017].

3.3 Results

The microfluidic toolchain developed (Figure 3.1a) consists of a module for affinity-isolation of the untagged protein from small quantities of cell lysate, followed by modules to write the purified protein onto a cryo-EM grid and vitrify the sample [Giss *et al.* 2014, Arnold *et al.* 2017, Schmidli *et al.* 2018]. Briefly, antibody 'fragment antigen binders' (Fabs) are used to recognize and extract untagged target proteins from cell lysate. These Fabs are biotinylated with a photo-cleavable cross-linker, which binds with high affinity to the streptavidin functionalization of super-paramagnetic beads (Figure 3.1b). First, the cell lysate is incubated with Fabs and super-paramagnetic beads. A $<1\,\mu\mathrm{L}$ volume of this solution is then aspirated into the microcapillary of the *cryo Writer* system (Figure 3.1c). The super-paramagnetic particles are immobilized in a 'magnetic trap,' (see Figure 3.4) isolating bound Fabs and their target proteins, while other cellular components are washed out. Ultra-violet (UV) light is used to break the photo-cleavable biotin cross-linker and the target proteins with the bound Fabs are eluted [Giss *et al.* 2014]. This procedure results in a 25 nL eluate, which is directly used to prepare one or more cryo-EM grids, while the magnetic particles are retained in the microcapillary.

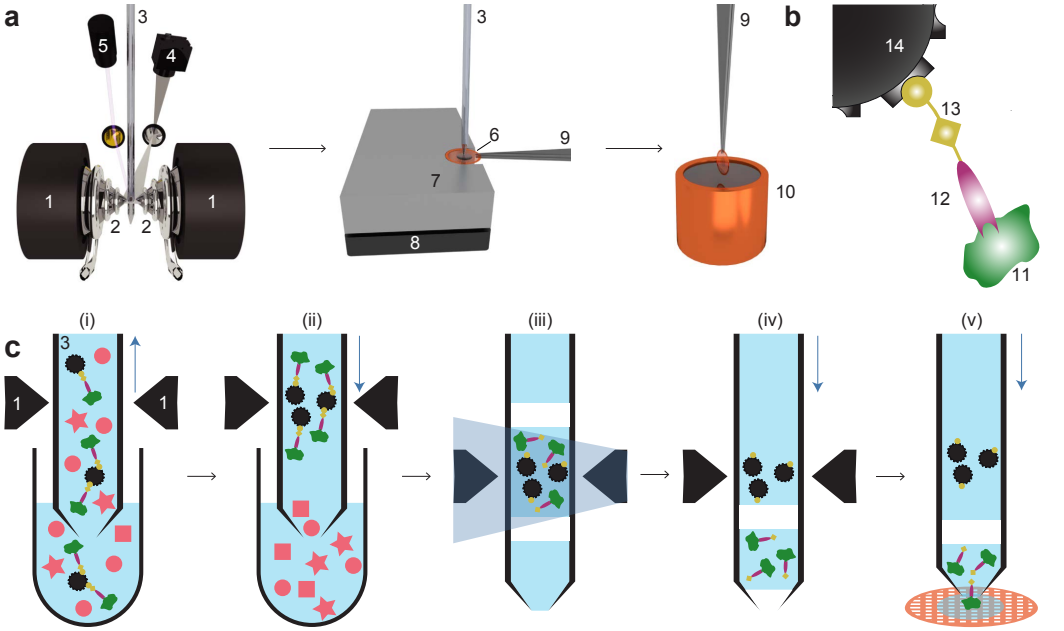

Figure 3.1: Schematic work-flow for microfluidic protein isolation and cryo-EM grid preparation. **(a)** Hardware for protein-isolation and cryo-EM grid preparation. The electromagnetic trap consists of two electromagnets (1) that produce a strong magnetic field gradient via their water-cooled iron tips (2). Sample processing in the capillary (3) is monitored by a camera (4), and a UV LED (5) allows photo-cleavage (see panel b) of the sample, both via mirrors. After protein isolation, the capillary nozzle is moved above a cryo-EM grid covered with a holey carbon film (6). The cryo-EM grid is positioned on a stage (7) that is temperature controlled by a Peltier element (8) and held with a Peltier-cooled tweezer (9). The isolated protein is directly written onto the grid and plunge-frozen in liquid ethane (10). **(b)** Composite material for 'protein fishing.' The target protein (11) is recognized by a Fab (12) that is covalently modified by a photo-cleavable cross-linker (13). The linker molecule ends with a biotin moiety, which strongly binds to the streptavidin coated bead (14). **(c)** Protein isolation work-flow. (i) Magnetic beads are incubated with biotinylated Fabs and cell lysate to capture the target structures (green). Less than 900 nL of sample is aspirated into the microcapillary for the protein isolation. (ii) The magnetic beads are immobilized in the magnetic trap (1). Non-bound lysate components (red) are flushed out. (iii) Illumination with UV light breaks the cross-linker. Before photoelution, two air bubbles are introduced and serve as boundaries to avoid dilution of the released proteins by diffusion (see Supplementary Figures 3.4 & 3.6 for details). (iv) Separation of the capturing magnetic beads and the eluted proteins. (v) The isolated target proteins are directly deposited on a cryo-EM grid for vitrification. The blue vertical arrows indicate the pump direction.

We used Fabs instead of full-length antibodies to avoid the cross-linking and aggregation that occurs when target proteins display more than one epitope. A linear cross-linker with three functional groups is used to connect the Fab to the super-paramagnetic beads. One end of the linker covalently attaches to the Fab while the biotin at the other end binds to the streptavidin-coated bead. A nitrobenzene moiety in between allows photo-cleavage of the linker upon illumination with UV light at 365 nm (Figure 3.1b). Preparation of Fab fragments from antibodies and biotinylation with the cross-linker took ≈7 h; the biotintilated Fabs could be stored in the dark for several weeks at 4 °C.

The cell lysate was incubated with the Fabs and beads outside of the microcapillary in a 5 µL well. The cytosol/Fab mixture was incubated for 5 h, and then for an additional 1 h together with the super-paramagnetic beads. The use of miniaturized sample wells rather than the microcapillary, allowed several of these time consuming incubations to be carried out in parallel.

After incubation, a volume of 900 nL was aspirated from the well into the microcapillary, which was precisely positioned between the iron tips of the particle trap system. In this setup, the trap is formed by electromagnets with water-cooled (4 °C) iron tips that concentrate the magnetic flux between the opposite poles and generate the field gradients required to trap the super-paramagnetic particles (see also Figure 3.4). The cooling system prevents heating and denaturation of the sample. A camera and magnifying lens system allow the procedure to be monitored. The 1 µm super-paramagnetic beads employed, can be easily immobilized in the magnetic trap and only marginally scatter photons with 365 nm wavelength, allowing efficient photoelution in 15 min [Giss *et al.* 2014]. Photoelution releases less non-specifically bound protein than the competitive elution typically used in other methods, because it does not change the buffer composition [Giss *et al.* 2013]. Just before elution, the beads were enclosed by two 6 nL air bubbles in a 25 nL buffer-plug, to prevent diffusion and Taylor dispersion [Squires & Quake 2005]. After photoelution, the eluate was separated from the immobilized beads by the pump system and moved towards the apex of the microcapillary.

For cryo-EM specimen preparation, a sample carrier (grid) covered by a holey carbon film was placed on a temperature-controlled stage regulated to a temperature 7 °C above the environmental dew-point. This temperature offset builds a micro-environment on the grid surface, allowing controlled evaporation of the sample liquid. In a first step, 20 nL of the eluate containing the purified protein was written onto the grid, covering an area of ≈0.75 mm^2. Excess sample was re-aspirated into the microcapillary, leaving a thin layer of the protein on the holey carbon film. This

layer was left to settle for ≈50 ms with the grid still on the dew-point stage. The gentle evaporation that occurs during this time stabilizes [Padmakar *et al.* 1999] and thins the sample film. Finally, the written grid was rapidly removed from the stage and plunge-frozen, resulting in a vitrified ice layer [Arnold *et al.* 2017, Schmidli *et al.* 2018]. In principle, several cryo-EM grids can be written with one 25 nL eluate. Interestingly, when this was done the first cryo-EM grid contained more protein particles than later grids. For the analysis presented here, we only used one cryo-EM grid, and this was the first grid prepared from the eluate. The whole *cryoWriter* process starting from protein isolation and ending with cryo-EM grid preparation could be performed in less than 1 h.

We employed the *cryoWriter* toolchain to isolate endogenous and untagged *human* 20S proteasome from commercially obtained HeLa cell lysate using Fabs generated from an antibody against the α4 subunit of the protein complex. As a positive control for the cryo-EM grid preparation, tobacco mosaic virus (TMV) particles were added to the elution buffer. The cryo-EM grid showed homogeneous ice layers (Figure 3.2a,b) with the protein embedded in thin, vitreous ice. TMV particles and randomly oriented 20S proteasomes are visible, as well as smaller protein particles that are most probably unbound Fabs.

From only one grid, 523 dose-fractionated image stacks (movies) were recorded, yielding a total of 55 135 particles, which were processed with cryoSPARC v2 (Structura Biotechnology Inc.) [Punjani *et al.* 2017] and RELION 3 [Zivanov *et al.* 2018] for structure determination. Figure 3.2c shows typical projection class averages obtained from the 20S proteasome. A seven-fold pseudo symmetry is observed in the top view, with weakly visible Fab fragments attached to the two α4 subunits. The side-view exhibits the distinctive stack of α-β-β-α rings. Figure 3.2d shows a projection class average of TMV. The secondary structure was visible in all projection-averages, demonstrating the excellent quality of the cryo-EM grid.

The 3D reconstruction of the human 20S proteasome shown in Figure 3.3 has a resolution of 3.5 Å (for details see Figure 3.7). The structure exhibits the typical dimeric, C2-symmetric arrangement of an α-β and a β-α ring-pair, each ring with a pseudo-7-fold arrangement of the respective subunits. We refined the X-ray structure [Schrader *et al.* 2016] into our density map. The two Fabs against the α4-subunits aided the assignment of the individual components. Figure 3.3b shows the α and β rings with all 14 models fitting the experimental densities in good agreement (see also Figure 3.3c,d, and Table 3.5). The densities of subunits β4, β5 and β6, are less well resolved (see also Figure 3.8), which can be attributed to their catalytic activity [da Fonseca & Morris 2015]; we assume that the lower resolution reflects the greater flexibility they require to perform their biological function.

The reconstruction of the added TMV particles has a resolution of 1.9 Å (see Fig-

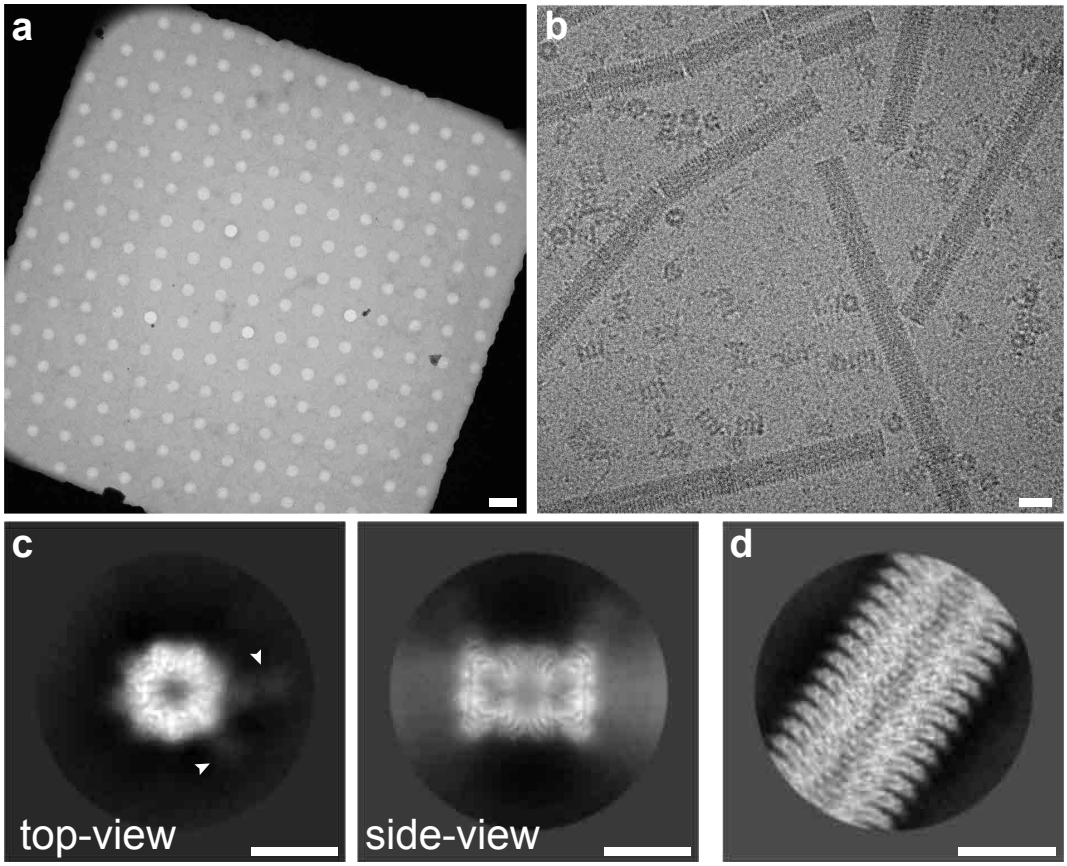

Figure 3.2: Sample quality and data-collection. **(a)** Overview image of a grid square and the holey carbon film, showing a thin film of vitreous ice. Scale bar: 4 µm. **(b)** High magnification image of the isolated 20S proteasome sample. Arrows indicate 20S proteasome as top and side views; asterisks denote TMV. Furthermore, small particles are visible in the background, most probably unbound Fabs. Scale bar: 20 nm. TMV was added to the elution buffer as positive control for the cryo-EM grid quality (see Figure 3.7). The contrast of the image was increased using a Gaussian blur and subsequent histogram adjustment. **(c)** Selected projection averages of the 20S proteasome. Arrows indicate two bound Fabs recognizing the α4 subunit. Scale bar: 10 nm. **(d)** Typical projection average of TMV from the same cryo-EM grid as the 20S proteasome. Scale bar: 10 nm.

ures 3.7 & 3.10), indicating that the microfluidic sample preparation did not limit the resolution of the *human* 20S proteasome. Unlike the archaeal T20S proteasome, which is often used as a cryo-EM test-sample thanks to its 14-fold D7 symmetry, the *human* 20S proteasome is only two-fold symmetric. The lower symmetry reduces the internal averaging by a factor of 7. Moreover, the similar subunits around the 'pseudo-sevenfold' axis can lead to misalignments of the particle projections. Together, these factors explain why existing cryo-EM maps are at the lower resolution

of 3.5 Å [da Fonseca & Morris 2015, Morris & da Fonseca 2017].

3.4 Conclusion

Several methods have been presented to improve sample preparation for cryo-EM, all having their own specific purpose. Examples include high-throughput grid preparation [Dandey *et al.* 2018, Razinkov *et al.* 2016, Noble *et al.* 2018], time-resolved EM [Feng *et al.* 2017], and single-cell visual proteomics [Arnold *et al.* 2017, Arnold *et al.* 2016]. Furthermore, antibody-functionalized EM-grids were proposed to 'fish' target proteins [Derrick 1973, Yu *et al.* 2016], and affinity grids designed to capture proteins with engineered his-tags [Kelly *et al.* 2008]. In both cases, the vitrified protein is supported by a continuous carbon film, which can limit the resolution obtained. Here, we combined microfluidics for protein isolation and purification with cryo-EM grid preparation, resulting in free-standing layers of vitrified protein samples that allow high-resolution cryo-EM.

Microfluidic methods could potentially overcome the current bottleneck in cryo-EM, resulting from the large amount of protein used for sample preparation and the long and harsh conditions used for protein purification. We demonstrated that microfluidics (i) can deliver cryo-EM grids of high quality allowing <2 Å resolution from 20 nL of a sample and (ii) allows the isolation of endogenous proteins from less than 1 µL cell-lysate with subsequent structure determination at 3.5 Å. In addition, the method presented here significantly reduces both the amount of starting material and the time needed for the structural analysis of proteins, avoids harsh protein purification conditions, and eliminates the stringent and wasteful blotting steps otherwise employed on cryo-EM grid preparation.

The high efficiency of cryo-EM combined with the microfluidic approach will allow the structure of proteins that cannot be produced in large quantities to be studied. Up to now, structural studies were only possible if the protein could be over-expressed or produced in a large numbers of cells. The small sample volumes used during the microfluidic purification process allow a high protein concentration to be maintained, which is helpful if protein complexes fall apart upon dilution. Furthermore, the small sample volume also allows for 'buffer conditioning' [Arnold *et al.* 2016], e.g., for the introduction of small ligands before sample vitrification. In addition, further optimization of the purification step and use of the *cryoWriter*, will almost certainly make it possible to perform the whole preparation in less than 1 h, facilitating the investigation of sensitive proteins targets. Finally, the toolchain presented here can also be combined with *in vitro* translation systems, which would enable high-throughput structure determination, or with a single cell lysis device [Kemmerling *et al.* 2013, Arnold *et al.* 2016, Arnold *et al.* 2017], which would bring the structural analysis of proteins originating from a single cell within reach.

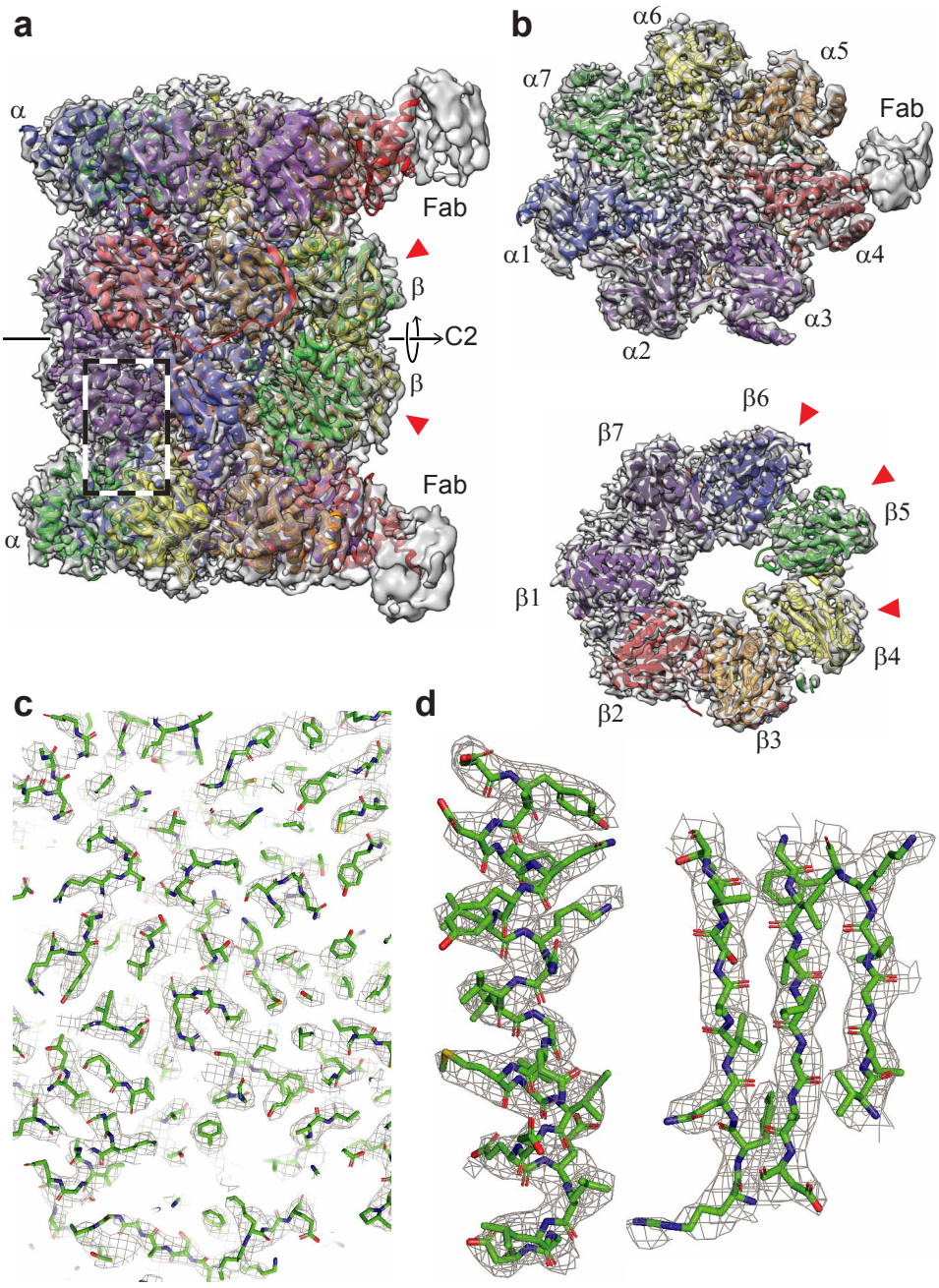

Figure 3.3: 3D reconstruction of the human 20S proteasome. The red arrowheads indicate the catalytically active subunits. **(a)** Side view showing the two α and two β rings, all 14 subunits are fit into the mass-densities. Parts of the two bound Fabs are visible at lower resolution, due to the high flexibility of the attached Fabs. The C2 symmetry-axis is indicated. **(b)** Top view of an α and a β ring, both have a pseudo 7-fold symmetry. Different subunits are indicated by different colors. **(c)** A zoom into the side-view region indicated by the dashed box in panel a, documenting the quality of the data and model fitting. An enlarged view of one α helix and three strands of a β-sheet are shown in **(d)** as an example.

3.5 Material and methods

Generation of Fabs

Fabs were generated from an antibody against the α4-subunit of the human 20S proteasome (Enzo Life Sciences, BML-PW8120, Switzerland), using a commercial kit (Thermo Fisher Scientific Inc., # 44685, Switzerland) and following the provided protocol. After generation of Fabs, the buffer was changed to phosphate-buffered saline (PBS, pH 7.4, 150 mM NaCl, 1.5 mM KH_2PO_4, 8.1 mM Na_2HPO_4, 2.6 mM KCl; Sigma, # D8537, Switzerland), and the Fabs were concentrated to a concentration of 0.28 mg mL^{-1} using a centrifugal filter unit (Sigma, # UFC501024, Switzerland).

Biotinylation of Fabs

To biotinylatilate the Fabs, a six-fold molar excess of photo-cleavable NHS-biotin cross-linker (Fisher Scientific, # NC1042-383, USA) was added to the Fabs (0.28 mg mL^{-1}, 5.6 mM) and incubated at room temperature for 1 h. Excess, unbound cross-linker was removed using a spin desalting-column (Thermo Fisher Inc., # 87764, Switzerland) following the instructions from the kit-protocol.

Binding of the 20S proteasome to magnetic particles

To 'fish' the human 20S proteasome, HeLa cell lysate (human origin, Enzo Life Sciences, BML-SW8750, Switzerland) was incubated in the presence of 0.7 mM of biotinylated Fabs at 4 °C for 5 h. Subsequently, super-paramagnetic Dynabeads^{TM} (Thermo Fisher Scientific Inc., # 65602, Switzerland) were added to achieve a final concentration of 5 pM and incubated additionally for 1 h at 4 °C. Glycerol and ATP which maintain proteasome stability were intentionally not added to the buffers to ensure that the regulatory complexes dissociated from the 20S proteasome core complex [Leggett *et al.* 2005].

Extraction and vitrification of 20S proteasome

After the incubation step, a 0.3 µL volume of the cell lysate/Fabs/super-paramagnetic beads mixture was aspirated into the microcapillary of the *cryoWriter* setup at a flow rate of 0.4 µL min^{-1}, and passed through the electromagnetic trap (see Supplementary Information S1). The beads were retained by the magnetic field gradient to form a bead plug. Subsequently, the flow direction was inverted and the particle plug was

washed with 4 µL washing buffer (25 mM HEPES−KOH, pH 7.5, 5 mM $MgCl_2$) at a flow-rate of 3 µL min^{-1}. The aspiration-wash cycle was repeated twice. In all, a total of 0.9 µL cell lysate was loaded into the microcapillary. At the end, the capillary was washed further with 45 µL of washing buffer at a flow-rate of 3 µL min^{-1}.

Before UV cleavage, the sample plug was enclosed between two 6 nL air bubbles that were introduced from the nozzle tip, and were separated by a volume of 25 nL washing buffer containing 1 mg mL^{-1} of tobacco mosaic virus (TMV). See also Supplementary Information 3.6 for more details. TMV was kindly supplied by Ruben Diaz-Avalos, Howard Hughes Medical Institute, USA. The hydrophilicity of the inner surface of the microfluidic capillary retains a thin hydration layer, which allows magnetic beads with loaded samples to remain within the aqueous phase while the air bubbles are introduced. The sample plug was then exposed for 15 min to UV light emitted at a wavelength of 365 nm by a 190 mW UV LED (Thorlabs, # M365L2, Switzerland).

After photo-cleavage, 20 nL of the 25 nL eluate containing the purified protein was primed on a 400-mesh copper grid covered with a holey carbon film (R1.2/1.3, Quantifoil, Germany) that was glow discharged for 45 s in air plasma immediately before use. The cryo-EM grids were prepared as described [Arnold *et al.* 2017], applying *protocol 1*. However, we adjusted the parameters for the sample: the stage temperature was 7 °C above the dew point temperature of the environment, *i.e.*, 10 °C on most days, and the settling time was 50 ms.

Data Acquisition

Cryo-EM image data were collected on a FEI Titan Krios (ThermoFisher Scientific) transmission electron microscope, operated at 300 kV and equipped with a Gatan Quantum-LS imaging energy filter (GIF, 20 eV zero loss energy window; Gatan Inc.). Micrographs were acquired using a K2 Summit direct electron detector (Gatan Inc.) operated in dose fractionation mode (super-resolution 8k, 30 frames, 0.2 s/frames, 6 s total exposure) and controlled by the SerialEM [Mastronarde 2005] software. The physical pixel size was 0.812 Å and the total electron dose was 72 e^- $Å^{-2}$ per recorded image stack (movie). Micrographs were drift-corrected, dose-weighted, and Fourier-cropped to 4k, using MotionCor2 [Zheng *et al.* 2017] via the FOCUS interface [Biyani *et al.* 2017]. Additional data collection parameters are listed in SI C.

Image processing

An initial model for subsequent processing with RELION3 [Zivanov *et al.* 2018] was generated using cryoSPARC v2 (Structura Biotechnology Inc.) [Punjani *et al.* 2017].

Particles were picked in cryoSPARC v2, and then 2D classified. An *ab-initio* model was generated using ≈19 000 particles selected from the best 2D classes, and subsequently refined to 4.1 Å resolution with C2 symmetry imposed.

For RELION3 processing, 55 135 particles were picked with Gautomatch (K. Zhang, www.mrc-lmb.cam.ac.uk/kzhang/) using templates projected from the map obtained using cryoSPARC v2, and low-pass filtered to 20 Å resolution. After 2D classification, 38 848 particles were 3D classified into 4 classes. The best class, containing 16 015 particles was selected for 3D refinement. A generous mask derived from the refined map low-pass filtered to 15 Å and with a soft-edge of 6 voxels was used for postprocessing, yielding a resolution of 4.3 Å. Afterwards, rounds of CTF refinement including defocus refinement per-particle, astigmatism refinement per-micrograph, and beam-tilt refinement per-dataset were iterated with rounds of Bayesian polishing and 3D refinement. A final 3D refinement, using a soft-mask that excluded the flexible Fabs and employed solvent-flattened FSC curves to filter the 3D reference at every iteration, resulted in a map with a final global resolution of 3.5 Å after postprocessing. Image processing parameters are listed in SI C. For more details on resolution estimation please see Supplementary Information S4.

Helical processing of TMV was performed with RELION3 [Zivanov *et al.* 2018] from 481 micrographs of the same data set that contained 20S proteasome, following standard helical refinement and reconstruction procedures [He & Scheres 2017]. The final resolution of the TMV map was 1.9 Å (Supplementary Information S4).

Model building

The model for the native human 20S proteasome was built based on the X-ray structure from Schrader et al. (PDB ID: 5LE5) [Schrader *et al.* 2016]. Chimera [Pettersen *et al.* 2004] was used for the initial rigid-body fitting. The bound Fabs helped to identify the different subunits in the electron density map. For further processing, all heteroatoms were removed. Real space refinement with PHENIX [Adams *et al.* 2010] and manual adjustments in Coot [Emsley *et al.* 2010] were done iteratively to obtain the final model, ending with a cycle of PHENIX real-space refinement. The graphics were generated using Chimera[Pettersen *et al.* 2004] and PyMOL[Schrödinger, LLC 2015].

3.6 Acknowledgments

We thank the workshop of the Biozentrum of the University Basel for technical support, A. Fecteau-LeFebvre, D. Caujolle-Bert and K. Goldie for technical assistance, and A. Engel for discussions (all C-CINA, University of Basel). RELION 3 processing was performed at sciCORE (http://scicore.unibas.ch/) scientific computing center at University of Basel. TMV was kindly provided by R. Diaz-Avalos (now at NanoImaging Services). We thank our former coworker Shirley Müller for critically reading the manuscript. **Funding:** We acknowledge support by the Swiss Nanoscience Institute (project P1401 & ARGOVIA MiPIS) and the Swiss National Science Foundation (projects 200021_162521 and 205320_166164), and the Swiss CTI (project 18272.1). **Author contributions:** C. S. performed microfluidic purification and grid preparation. S. A. and R. R. determined the cryo-EM structures. C. S. integrated the trap setup into the CryoWriter platform with the support of L. R. and P. O.. L. K. assisted with Titan Krios data collection. R. R. and I. M. helped C. S. with model building. H. S. provided support and expertise in cryo-EM. T. B. conceived and coordinated the project. C. S., S. A., H. S., and T. B. wrote the manuscript, with backing from all authors. **Competing interests:** T. B. and H. S. declare the following competing financial interest: The cryoWriter concept is part of patent application PCT/EP2015/065398. **Data and material availability:** Image data are available at the EMPIAR database under EMPIAR-10251. The reconstructed volumes are available at the EMDB under EMDB-4738 (20S proteasome) and EMD-4628 (TMV). The atomic coordinates are available at the PDB under PDB-6R70 (20S proteasome) and PDB-6R7M (TMV).

3.7 Supplementary information

S1 Characteristics of the magnetic trap

The magnetic particle trap consists of two electromagnets arranged with opposite poles facing one another (Figure 3.4). Attached iron tips extend the magnet cores.

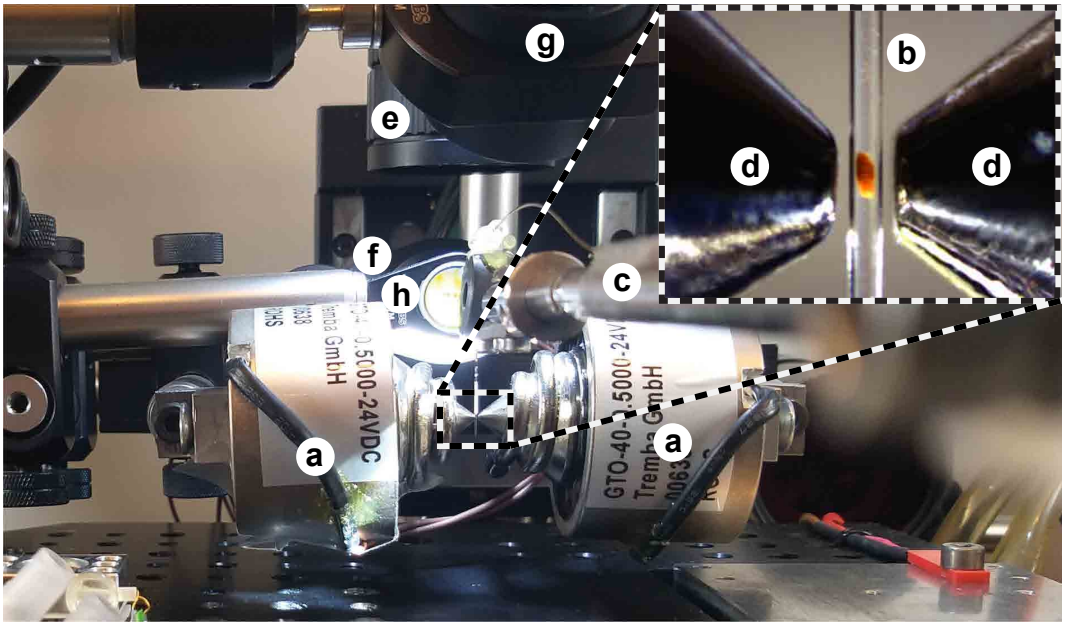

Figure 3.4: Image of the magnetic trap set-up. The opposite poles of two 4.8 W electromagnets **(a)** are facing one another. A microcapillary **(b)**, held with the manipulator arm **(c)**, is placed between the two iron tips **(d)** of the electromagnets. The trapped magnetic plug can be observed with a camera **(e)** via a mirror **(f)**. The photo-cleavable cross-linker can be exposed to UV light using a LED **(g)** emitting light at 365 nm that is deflected by a mirror **(h)**.

This concentrates the magnetic flux to a small area and forms a strong field gradient between the two tips (see Figure 3.5). For magnetic particle trapping, the front part of the microcapillary segment just above the nozzle was placed in this region using a motorized XYZ linear translation stage, and the sample was aspirated. The magnetic force acting on the super-paramagnetic particles immobilized the beads. In experiments, super-paramagnetic beads with sizes from 15 nm to 1000 nm can be trapped and experience a magnetic force F_m acting on a saturated particle according to:

$$F_m = V \cdot M_S \cdot \mu_0 \cdot \nabla H \tag{3.1}$$

where V is the volume of the magnetic particles, M_S the saturation magnetization, μ_0 the magnetic constant, and H the magnetic field strength. The current controls the field applied by the electromagnets. Due to the dependence on the volume (V), higher currents are needed in order to trap smaller particles. When the electromagnets are operated at maximum power, the core and the tips significantly heat up. For this reason, a cooling water system was implemented allowing the tips to be cooled to 4 °C by pumping water through a copper tubing twisted around them. Both, the copper tubing and the iron tips were coated with nickel to reduce corrosion. The magnetic trap is mounted on a motorized stage, allowing it to be moved in the vertical direction, independent of the microcapillary manipulator arm. For sample uptake, the magnetic trap and microcapillary were simultaneously moved down to insert the nozzle tip of the capillary into the sample well.

The parts used to build the magnetic trap are summarized in Table 3.1. Connecting parts were manufactured by the workshop of the Biozentrum, University of Basel, Switzerland. Plans are available upon request. Further cryoWriter parts used for grid preparation are described in [Schmidli *et al.* 2018].

Part Name	**Part Number**	**Distributor**
Electromagnet	GTO-40-0.5000-24VDC	Conrad Electronic AG
Iron magnet tips	-	In-house production
Cooling pump	2449120	Digitec Galaxus AG
Tubing for cooling system	1025U04	Parker Hannifin
Tubing for cooling system	1025U06	Parker Hannifin
Motorized trap stage	M-126.PD2	Dyneos AG
Connector plate (trap-stage)	-	In-house production
Camera (Magnetic Trap)	NetFOculusFO124TC	NET GmbH
Optics (trap camera)	MLM3X-MP	FRAMOS GmbH
Mirror (trap camera)	PF07-03-P01	Thorlabs
UV LED	M365LP1c	Thorlabs
Dielectric Mirror	BB0511-E01	Thorlabs
Syringe pump controller	A3921000093	Cetoni
Syringe pump dosing unit	A3921000095	Cetoni
Liquid handling syringe	HA-80901	BGB Analytik AG
Microcapillary tubing	TSP-150375-D-10	BGB Analytik AG
Liquid handling nozzle	FS360-150-30-N-5-C12	MS Wil GmbH
PressFit Connector	2525LD	BGB Analytik AG

Table 3.1: Parts list of the magnetic trap setup.

Figure 3.5 shows a finite element simulation of the magnetic flux density within the magnetic trap system, which was caluclated with COMSOL Multiphysics. Soft-iron material properties were applied to the magnet cores and tips using a non-linear B-H curve that includes saturation effects. The windings were modelled with coil features.

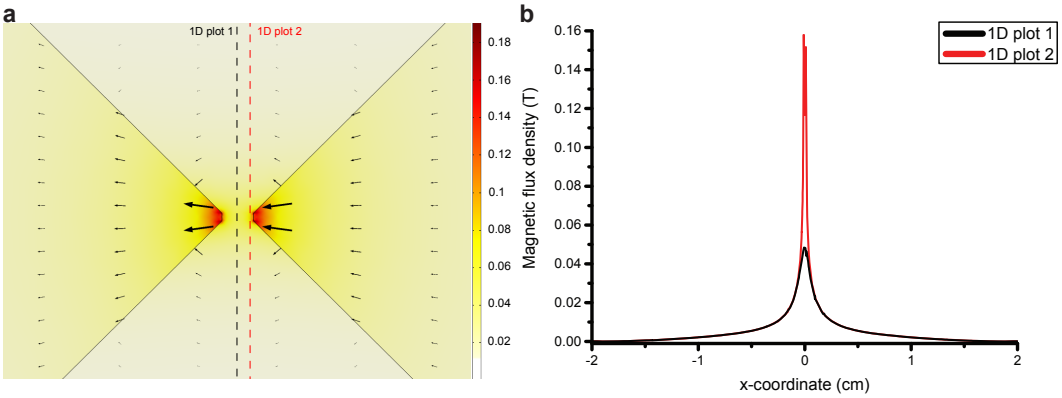

Figure 3.5: Finite element simulation of the magnetic field generated by the electromagnetic trap system. **(a)** 2D plot of the magnetic flux density around the iron tips (black solid lines). The direction of the magnetic fields is shown with black arrows. The size of the arrows is proportional to the field strength. The values in the color scale are given in Tesla (T). **(b)** Extracted 1D plots of the magnetic flux density from the 2D plot in (a) at the positions indicated with dashed lines. The figure shows that between the tips (x=0) the highest field gradients are observed. This leads to a magnetic force F_m pushing magnetic particles towards this region.

S2 Enclosure of sample between air bubbles

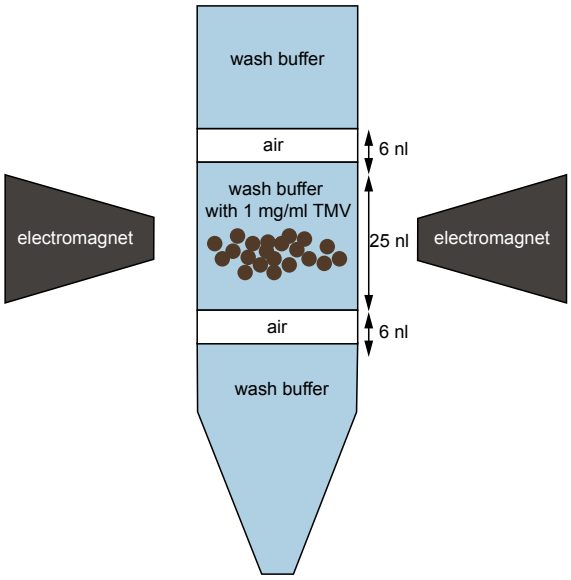

Figure 3.6: Illustration of the magnetic particle-plug enclosed between two 6 nL air bubbles for UV exposure and elution. The air bubbles act as barriers preventing diffusion and Taylor dispersion to keep the protein concentration as high as possible.

S3 Data collection and image processing parameters

The data collection parameters are provided in Table 3.2, and the main image processing parameters used for the 20S proteasome and TMV are given in Tables 3.3 & 3.4.

Data collection	
Voltage	300 kV
Physical pixel size	0.812 Å
Super-resolution pixel size	0.406 Å
GIF zero loss energy window	20 eV
Defocus range	−1.0 µm to −2.2 µm
K2 operating mode	8k super-resolution
Number of frames	30
Second per frame	0.2
Total dose	72 e^{-} $Å^{-2}$
Number of micrographs	523

Table 3.2: Data collection parameters.

Image processing 20S proteasome	
Micrographs	523
Box size	480 pixel
Box size (after down-sampling)	384 pixel
Pixel size (after down-sampling)	1.015 Å
Gautomatch picked particles	55,135
Particles after 2D classification	38,848
Particles for 3D refinement	16,015
Symmetry	C2
Final resolution	3.5 Å
Estimated map sharpening B-factor	$-39.2\ Å^{2}$

Table 3.3: Image processing parameters used for 20S proteasome structure determination with RELION3.

S4 Fourier shell correlation and local resolution histograms

We used the Fourier shell correlation method [Harauz & van Heel 1986] between two independently refined half-maps ('gold standard') [Scheres & Chen 2012] to estimate the resolution of our 3D reconstructions (Figure 3.7a). A threshold of 0.143 on the FSC curve was adopted to define the resolution limit of the reconstruction [Rosenthal &

Image processing TMV	
Micrographs	481
Box size	420 pixel
Number of asymetric units	31
Picked end-to-end coordinated	2,676
Extracted particles	52,806
Initial helical rise	22.03°
Particles after 2D classification	52,806
Particles after 3D refinement	52,776
Symmetry	C1
Final resolution	1.9 Å
Estimated map sharpening B-factor	$-38.9\,\text{Å}^2$

Table 3.4: Image processing parameters used for helical structure determination of TMV with RELION3.

Henderson 2003]. The FSC curves were corrected for artificial correlations introduced by masking [Chen *et al.* 2013]. We found a global resolution of 3.5 Å for the 20S proteasome and of 1.9 Å for the TMV. These estimates correlate well with the features observed in the maps (see Figure 3.3 of the main text for the 20S proteasome and chapter S7 for the TMV). The estimated resolution is further corroborated by the local resolution histograms shown in Figure 3.7b, which display the normalized counts of voxels at each resolution. The resolution for the proteasome varies significantly; for more details, see Chapter S5. The local resolution was assessed based on the half-maps using the method described in [Cardone *et al.* 2013], as implemented in RELION3, with a map sampling of 25 Å (Figure 3.7b).

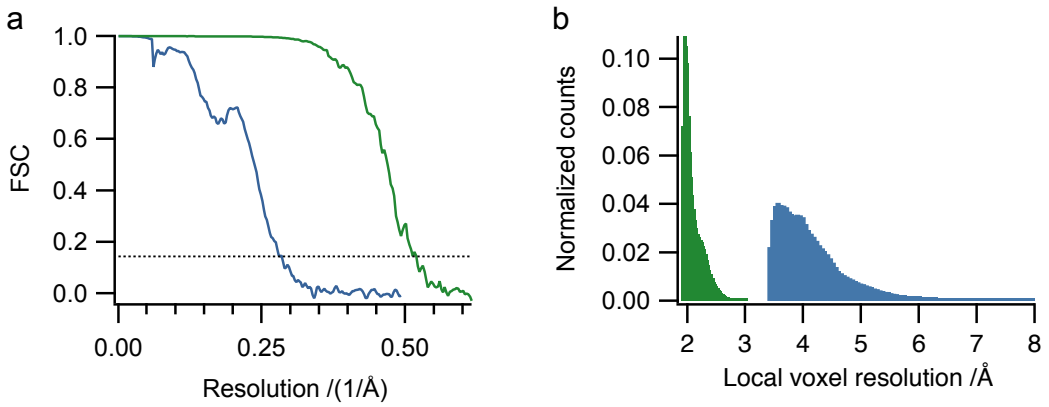

Figure 3.7: Resolution estimation for the 20S proteasome (blue) and TMV (green). (**a**) Fourier shell correlation from the RELION3 refinement. (**b**) Histograms depicting the normalized voxel counts per resolution range.

S5 Local resolution map of the 20S proteasome

Figure 3.8 shows the local resolution calculated for the 20S proteasome using RELION3. Note that the active domains (indicated by red arrowheads in Figure 3.8 are less well resolved than the other domains, and are associated with the catalytic subunits of the β-ring. Interestingly, the resolution of the α-ring around the pseudo-seven-fold axis is quite heterogeneous, whereas the β-ring exhibits lower resolution around subunits $\beta 4$ and $\beta 5$. Since subunits $\beta 4$, $\beta 5$ and $\beta 6$ are the catalytically active elements [da Fonseca & Morris 2015], the lower resolution of subunits $\beta 4$ and $\beta 5$ suggests that these are trapped in various conformations during cryo-EM grid preparation.

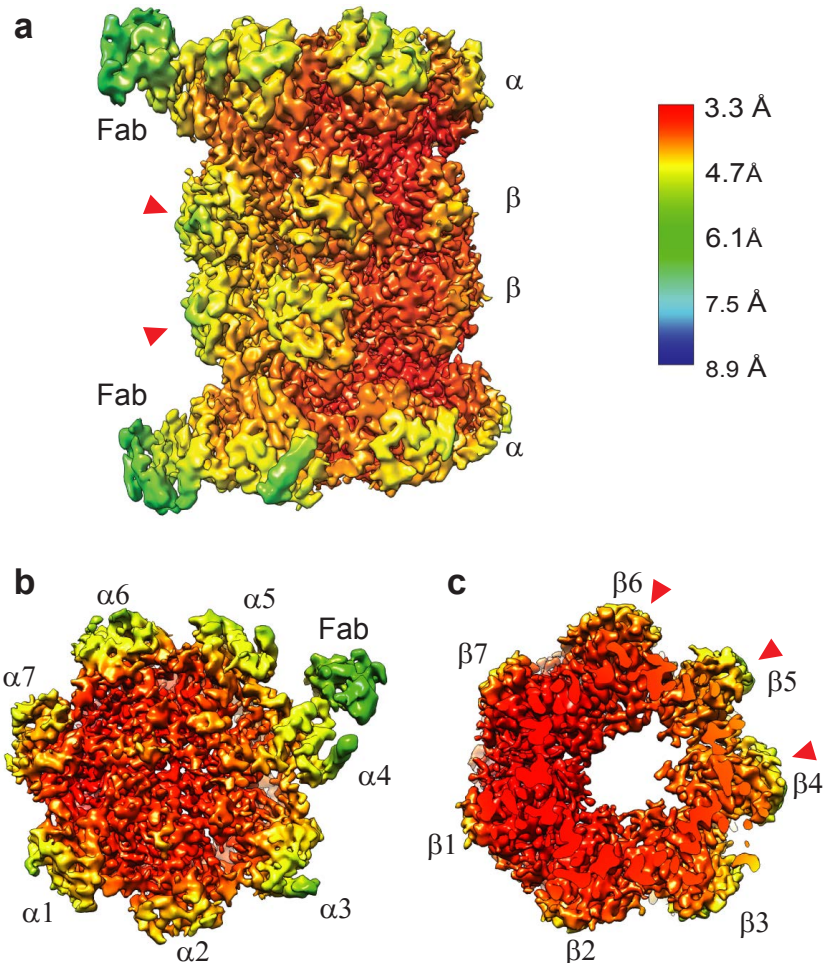

Figure 3.8: Local resolution map for the human 20S proteasome at a global resolution of 3.5 Å. (**a**) Side view with annotated Fabs. (**b**) Local resolution of the α-subunits. (**c**) Local resolution of the β-subunits. The red arrowheads indicate the catalytically active subunits.

S6 Model building results

After initial rigid body fitting, the 20S proteasome and TMV models were refined using PHENIX. The models were assessed by the fit to the experimental density and validated with clashscore, Ramachandran statistics, and good bond/angle lengths as shown in Tables 3.5 & 3.6. Additionally, a random shift (mean 0.3 Å) was introduced to the final models and each model was refined with the same settings against one unfiltered half map (half-map 1). The FSC curves of the models against half-map 1 and the other half map (half-map 2) was then calculated (Figures 3.9 & 3.10). The fact the both curves look very similar indicates that no overfitting took place.

Phenix Real-Space Refinement	
Map CC (around atoms)	0.80

MolProbity[**Davis *et al.* 2007**]	
All-atom clashscore	4.79
Ramachandran favored	96 %
Ramachandran allowed	2.43 %
Ramachandran outliers	0.26 %
Rotamer outliers	0.52 %
Cb deviations	0
RMSD (bonds)	0.008
RMSD (angles)	1.044

Table 3.5: 20S proteasome model validation statistics.

Phenix Real-Space Refinement	
Map CC (around atoms)	0.87

MolProbity[**Davis *et al.* 2007**]	
All-atom clashscore	0.84
Ramachandran favored	97.35 %
Ramachandran allowed	2.65 %
Ramachandran outliers	0 %
Rotamer outliers	0 %
Cb deviations	0
RMSD (bonds)	0.006
RMSD (angles)	0.932

Table 3.6: TMV model validation statistics.

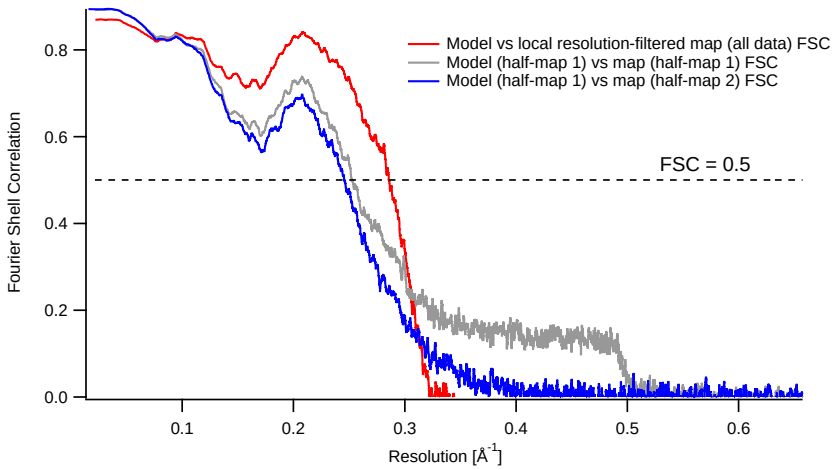

Figure 3.9: FSC curve of the final 20S proteasome model versus the full map (all data), against which the model was refined (red). The full map used to calculate the FSC was resolution filtered. FSC curve of the final 20S proteasome model with randomized coordinates shifts (mean shifts of 0.3 Å) versus the first unfiltered half-map (half-map 1) against which it was refined (grey) and versus the second half-map (half-map 2) against which it was not refined (blue).

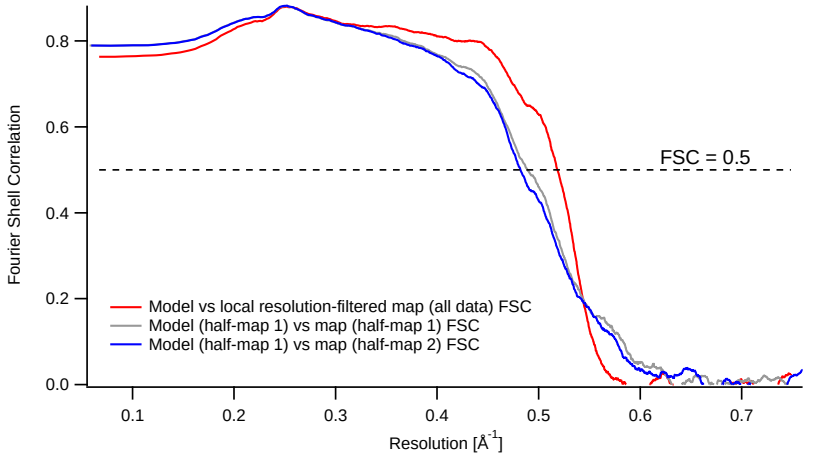

Figure 3.10: FSC curve of the final TMV model versus the full map (all data), against which the model was refined (red). The full map used to calculate the FSC was resolution filtered. FSC curve of the final TMV model with randomized coordinates shifts (mean shifts of 0.3 Å) versus the first unfiltered half-map (half-map 1) against which it was refined (grey) and versus the second half-map (half-map 2) against which it was not refined (blue).

S7 Three-dimensional map of TMV

Fig. 3.11 demonstrates the high quality of the microfluidic grid preparation. We report here the map of TMV at a global resolution of 1.9 Å. Compared to the 20S proteasome, this map has both higher global resolution (see FSC curve in S4, Fig. 3.7a) and less variable local resolution (Fig. 3.7b) due to the higher rigidity of the structure and the helical symmetry averaging imposed on the reconstruction.

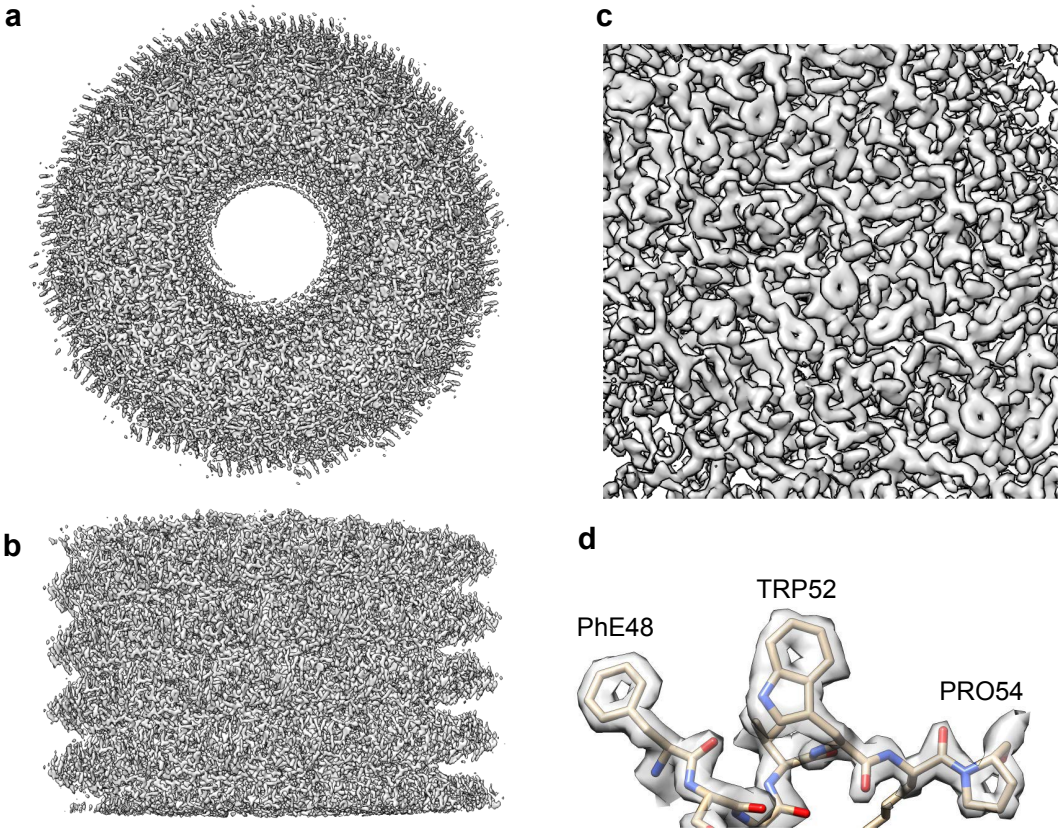

Figure 3.11: 3D reconstruction of TMV at a global resolution of 1.9 Å showing the top view ((**a**) and the side view (**b**) of the electron density map. The zoom-in (**c**) demonstrates the high resolution features of the map. At this resolution it is possible to see the holes of the aromatic rings (**d**).

4 Sample purification for transmission electron microscopy using magnetic nanoparticles

In this section, microfluidic sample purification using 30 nm sized magnetic iron oxide nanoparticles is presented. The small size of nanoparticles offers many advantages as a solid phase support carrier for affinity extraction methods compared to commonly used microspheres (∼1 µm), but on the other hand also makes particle trapping more challenging. We designed and constructed an electromagnetic particle trap allowing the immobilization of magnetic nanoparticles and their cargo by the generation of high magnetic field gradients. Thus, iron oxide particles down to a size of 10 nm could be trapped and employed for protein purification.

My contribution was performing the required simulations to optimize the magnetic trap, manufacturing the trap, carrying out the presented purification experiments and writing this section.

This manuscript has not been published.

Microfluidic purification of Maurer's cleft tethers using magnetic nanoparticles and preparation for transmission electron microscopy

Claudio Schmidli[1,2], Françoise Brand[2,3], Hans-Peter Beck[2,3], Henning Stahlberg[1] and Thomas Braun[1]

1 - Center for Cellular Imaging and NanoAnalytics, Biozentrum, University Basel, Switzerland
2 - Swiss Nanoscience Institute, University of Basel, Switzerland
3 - Swiss Tropical and Public Health Institute, Basel, Switzerland

Contents

Abstract

Biomolecules are vital components within living organisms and play many critical roles. Knowledge about their 3D assembly is crucial for the understanding of biological processes. Using magnetic microspheres in microfluidics enables the extraction of target proteins from minute sample volumes and the analysis of their 3D architecture with transmission electron microscopy (TEM) (see [Schmidli *et al.* 2019] and Chapter 3). Already simple magnetic separators produce magnetic field gradients high enough for the immobilization of ∼1 µm magnetic microparticles within reasonable time. However, extracted biomolecules have to be separated from the attached microspheres after the purification process. Here, we show how ∼30 times smaller iron oxide particles can be applied instead, using our in-house build high field gradient magnetic trap. Thus, there is no need for separation of magnetic particles from bound target molecules anymore. Instead, attached nanoparticles can further be utilized as electron dense markers and can help for protein identification or be used as fiducials for 3D tomogram reconstruction.

For demonstration, we isolated a novel cellular structure involved in Malaria termed Maurer's cleft tethers from <2 µL infected erythrocyte lysate using 30 nm sized magnetic iron oxide particles. Negative stain and cryo-EM grids were directly prepared from the resulting 10 nL of isolated sample by using our recently published grid writing technology [Schmidli *et al.* 2018]. Prepared grids with purified Maurer's cleft tethers allowed a closer inspection of the 3D structure, which has not been investigated before. Further, tilt series on cryo grids were acquired and 3D tomograms reconstructed using the nanoparticles as fiducials. We were able to show that the adjunct of gold fiducials is not needed when using our purification methodology for cryo-electron tomography (cryo-ET).

4.1 Introduction

In the recent years, magnetic particles became extremely popular and were applied in many different areas [Larson *et al.* 2007, Mahon *et al.* 2012, Swain *et al.* 2016] including biomolecule isolation techniques in the field of biosciences and biotechnology [Franzreb *et al.* 2006, Peter *et al.* 2009, Lien *et al.* 2007, Berensmeier 2006]. Conventional biomolecule isolation approaches comprise a variety of chromatography, centrifugation and precipitation procedures [Tan & Yiap 2009]. Among those, especially affinity chromatography is a powerful purification tool whose strength has been shown in many applications [Coelho *et al.* 2012]. However, magnetic separation techniques have several advantages compared to these standard methods designed for the laboratory scale [Safarik & Safarikova 2004]. The comparatively simple procedure usually involving only a few handling steps allows the implementation in one single

reaction vessel without the need of expensive chromatography systems, centrifuges or other equipment. The crude cell lysate containing suspended solid and fouling components can be used directly and common pre-processing steps to remove cellular debris are not required. Further, there is high potential for miniaturization giving rise to microfluidic-based approaches capable of handling sample volumes much smaller than typically used in columns. To solve a protein structure with cryo-EM only 10,000 to a few millions protein particles are required. Such tiny amounts of sample can be provided by miniaturized sample preparation methods. The combination of microfluidics and TEM is a promising approach opening up new opportunities for the analysis of small sample volumes such as e.g. used for diagnosis (biopsies) or single cell analysis. Furthermore, expenditures of costs and time are massively reduced using a purification approach based on magnetic particles.

The size of magnetic particles employed in most biomolecule separation methods is larger than 0.5 µm. This dramatically simplifies particle handling, since the magnetic force acting on the particles depends on the squared particle radius. Simple systems consisting of a single permanent magnet are sufficient for magnetic separation. The particles are pulled down in a pellet within a reasonable time, enabling protein purifications in less than one hour [Giss *et al.* 2014, Schmidli *et al.* 2019]. However, the application of smaller nanoparticles provides considerable benefits. The much higher surface area to volume ratio allows for better accessibility of the antibody functionalized surface and reduces disturbance of the native functions of proteins or protein-protein complexes. Due to the higher diffusion rate of smaller particles also incubation times are minimized. Another advantage is the fact that the magnetic nanoparticles are small enough for further usage as electron dense labels in cryo-EM facilitating the identification and detection of isolated targets. Thus, e.g. regions of interest in protein complexes can be localized. Finally, the magnetic particles can directly be used as fiducials for cryo-electron tomography (cryoET).

Here, we developed a microfluidic particle trap allowing the immobilization of magnetic particles down to a size of 10 nm. This enables the affinity isolation of untagged protein from small sample quantities using antibody functionalized magnetic nanoparticles. The whole protein purification module is implemented in our previously published microfluidic grid preparation system termed cryoWriter [Schmidli *et al.* 2018, Arnold *et al.* 2017, Arnold *et al.* 2016]. Thus, isolated samples can directly be prepared for negative staining or cryo-EM. To demonstrate the usefulness of the method, novel cylindrical structures involved in malarias disease were isolated from trophozoite stage-infected erythrocytes. These cellular structures of not yet clear function and composition were analyzed with negative stain TEM, cryo-TEM and cryo-TEM tomography.

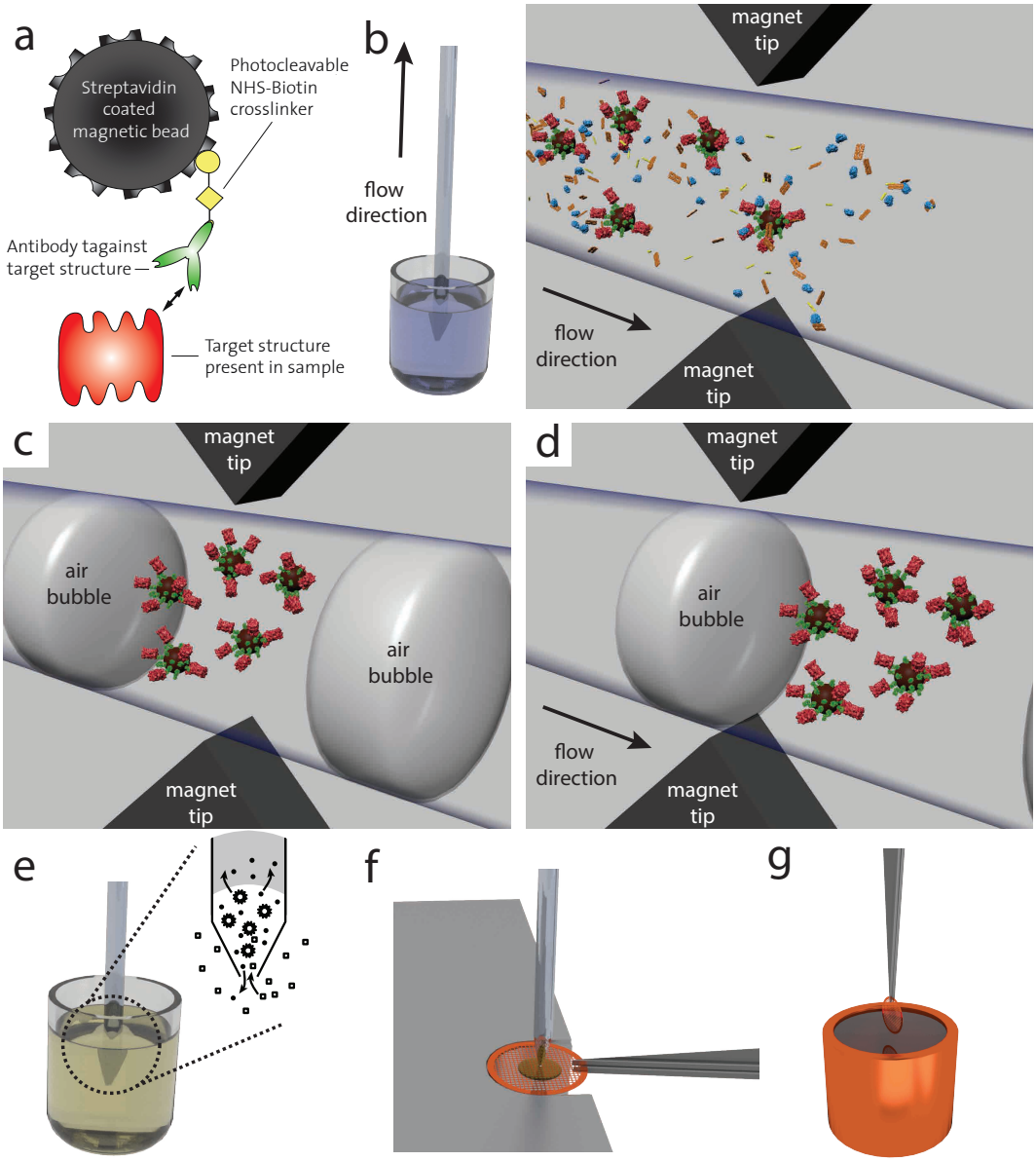

Figure 4.1: Principle of microfluidic protein purification using magnetic nanoparticles. **a)** Illustration of an antibody functionalized nanoparticle. The biotinylated antibody (green) is linked via photo-cleavable crosslinker (yellow) to the streptavidin coated nanoparticle surface (black). This allows recognition and coupling of target structures (red) in biological samples. **b)** After incubation with functionalized nanoparticles the sample is aspirated in the microfluidic system. Nanoparticles with their cargo are immobilize in an electromagnetic trap and thus separated from other constituent parts of the sample. **c)** Finally the isolated nanoparticles are enclosed between two air bubbles, which are introduced from the capillary tip and **d)** eluted with their coupled proteins. Optionally, the photo-labile linkage between the proteins and nanoparticles can be cleaved using an UV LED (not shown). **e)** If needed a sample conditioning step can be performed, **f)** before the sample is deposited on a grid and **g)** in case of cryo-EM vitrified (see Section 1.4).

4.2 Results

The microfluidic sample purification procedure developed to isolate proteins by the use of 30 nm nanoparticles, works as follows see (Figure 4.1). Nanoparticles are functionalized with a specific antibody recognizing the target structures. The particles are then incubated with sample allowing the binding of the antibody to the target epitopes. After incubation, the sample is aspirated in a microcapillary where nanoparticles with their cargo are immobilized by an magnetic field gradient and other components are flushed away. Finally, the magnetic particles and targets are released by switching off the magnetic trap and deposited onto a grid. To increase the final yield of extracted proteins, the magnetic particle plug was enclosed between two 10 nL air bubbles in a volume of 7 nL sample buffer before elution. Thereby, sample dilution caused by diffusion and Taylor dispersion is minimized. Optionally, the photo-labile linkage between the antibody and the nanoparticles can be cleaved by exposing the plug to 365 nm UV light. This alleviates the analysis of the isolated compounds without linked labels.

To demonstrate the usability of the magnetic nanoparticle based affinity purification method, we isolated cellular structures involved in Malaria. In 2010, Esther Pachlatko et al. [Pachlatko *et al.* 2010] showed that during the life cycle of Malaria a protein termed *membrane- associated histidine-rich protein-2* (MAHRP2) is exported to novel tubular structures in the erythrocyte cytoplasm, representing the first protein localizing exclusively there. Further, they hypothesized that the tubes tether organelles known as Maurer's clefts to the erythrocyte cytoplasm, wherefore they are termed Maurer's cleft tethers. So far, the structure and composition of Maurer's cleft tethers is not known. However, more structural knowledge might be helpful for a better understanding of the refurbishing process of the host cell upon the malaria parasite invasion into erythrocytes.

We were able to isolate Maurer's cleft tethers from <2 µL lysate of trophozoite stage infected erythrocytes and deposit the purified sample onto TEM grids with our previously published *grid writing* technology [Schmidli *et al.* 2018]. For negative stain EM, the microcapillary tip containing the purified sample was immersed into negative staining solution. Thereby, a diffusion driven exchange between the heavy metal salts of the staining solution and the salt ions of the sample buffer takes places removing salt ions and introducing stain into the sample buffer. Both, staining and desalting of the sample are crucial for negative stain EM sample preparation [Arnold *et al.* 2016]. After the conditioning step of 12 min a volume of 10 nL of purified protein was deposited onto a glow discharged negative stain TEM grid and slowly air dried on the temperature-controlled stage of the cryoWriter setup. Figure 4.2a & b shows negatively stained isolated tethers, which were cleaved from the bound nanoparticles by UV exposure. The images reveal the variable tether length and

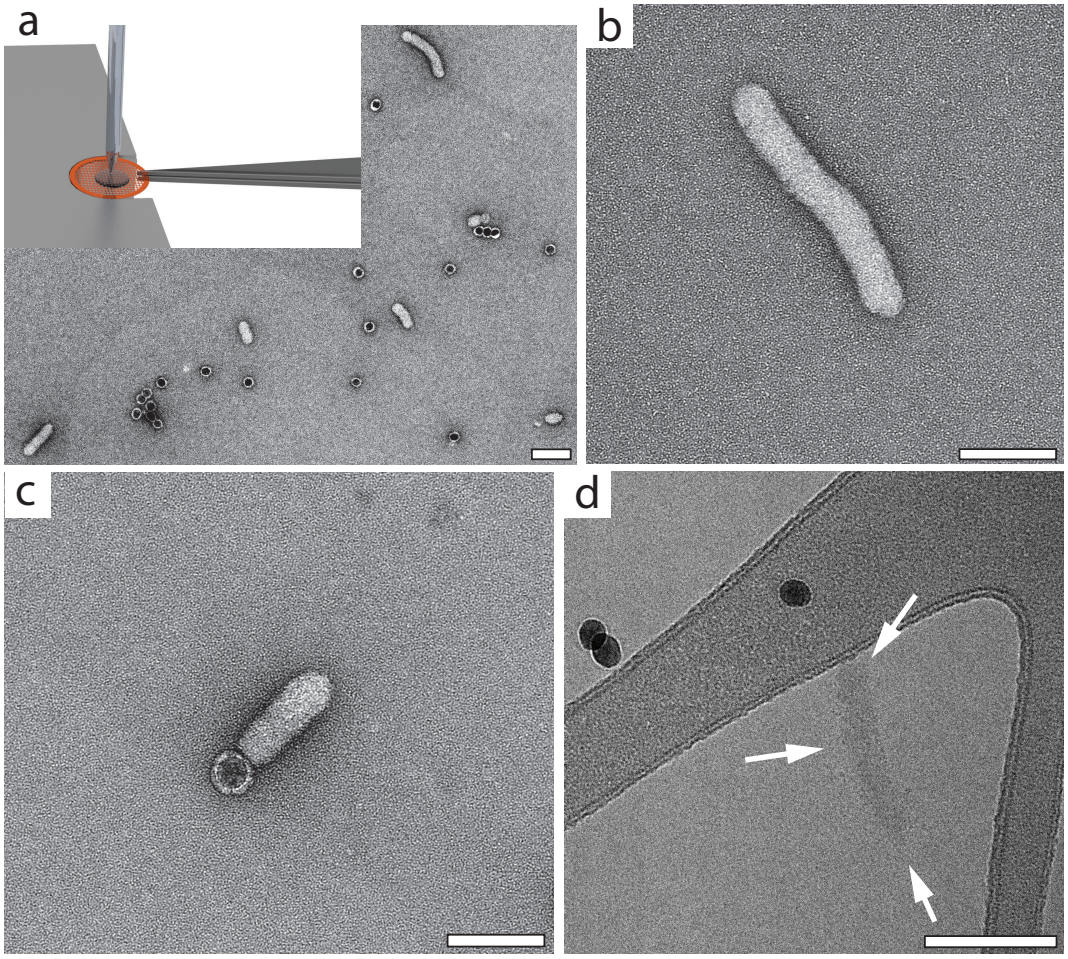

Figure 4.2: TEM images of isolated Maurer's cleft tethers. **a)** Low magnification negative stain image of isolated tethers showing their cylindrical structure and varying length. The nanoparticles were cleaved away from the target structures before elution. Due to the high specificity of the method, an extremely clear background can be observed. The inset illustrates the deposition of the isolated 10 nL sample droplet that was imaged. **b)** High magnification image of an isolated tether. **c)** High magnification image of a tether that was eluted without photo-cleavage of nanoparticles. The bound nanoparticles labels MAHRP2 associated with the Maurer's cleft tether. **d)** Cryo-EM image of an isolated tether where nanoparticles were cleaved away. All scale bars read 100 nm.

the constant diameter of ∼30 nm, leading to the assumption that the structures are arranged in a helical pattern and grow along their longitudinal axis. The recovery of tethers without photo-cleavage where magnetic particles are still bound (Figure 4.2c) confirms the presence of MAHRP2 on the tether surface. Bound particles indicate the location of the isolated target protein and supersede additional labeling steps e.g.

immunogold labeling.

For cryo-EM analysis, isolated and photo-cleaved tethers were deposited onto grids covered with a perforated carbon. By moving the capillary relative to the grid surface during dispensing the droplet spread over a larger area on the grid surface. Subsequently, as much sample as possible was re-aspirated leaving a thin film on the grid which was immediately plunge in liquid ethane for vitrification. Figure 4.2d shows a typical cryo-EM image of a vitrified Maurer's cleft tether. Unfortunately, there are no clear secondary structure features identifiable and the contrast is relatively low. We therefore hypothesize the tethers consist of accumulated lipids associated with certain proteins such as MAHRP2. Since nanoparticles do not interfere with the sample analysis in the electron microscope, they were eluted together with the isolated proteins even when the photo-labile linkage between antibodies and nanoparticles was cleaved before deposition (see Figure 4.2a). This allowed the re-utilization of the nanoparticles as fiducials for the 3D reconstruction of tomograms (see Figure 4.3). Unfortunately, also tomography didn't reveal structural features supporting the assumption of the existence of a lipid composed tether conglomerate. However, the principle of re-using the nanoparticles for cryo-ET image processing works and shows a further application of the nanopartilces besides pulling out specific proteins from crude biological samples.

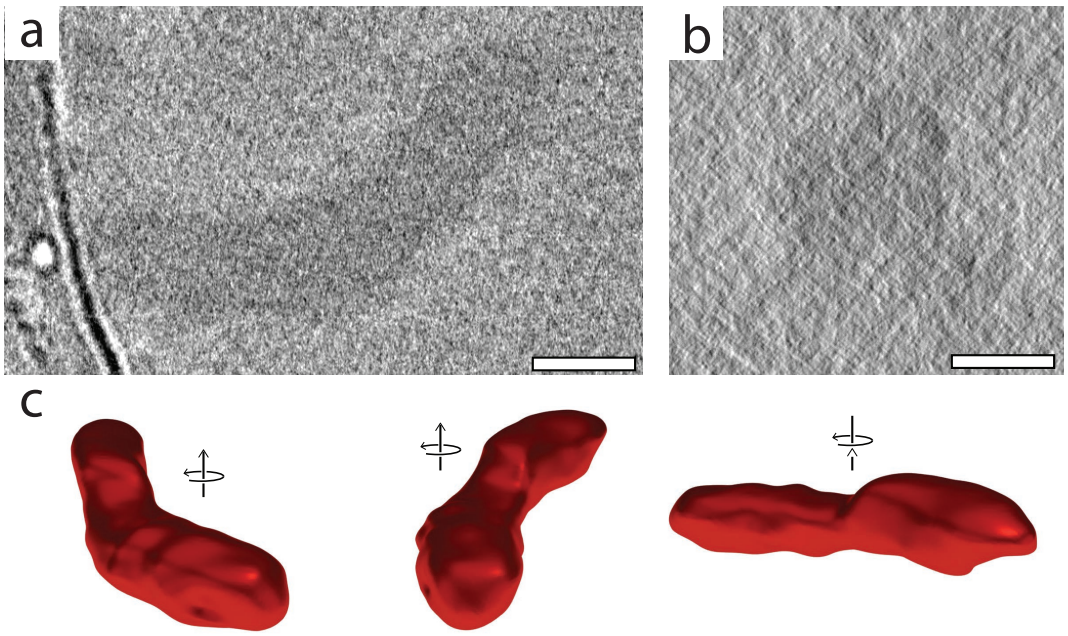

Figure 4.3: Cryo-electron tomography (cryo-ET) of isolated Maurer's cleft tethers. **a)** Longitudinal cross-section and **b)** transverse cross-section through reconstructed 3D tomogram. **c)** 3D model of reconstructed tomogram manually traced with the Amira software. The scale bars read 50 nm.

4.3 Conclusion

Magnetic separation has a high potential for miniaturizing sample purification in cryo-EM. Microfluidics combined with magnetic particles can provide enough protein particles for the analysis in TEM [Giss *et al.* 2014] and the determination of their 3D fold [Schmidli *et al.* 2019]. So far, microspheres were always used for target protein extraction, because of the straightforward immobilization procedures in magnetic separators. However, microspheres have to be separated from isolated protein samples after the purification process due to their large size extension. The micrometer-sized particles otherwise cover up target proteins in the sample and make their analysis impossible. Further, vitrification of samples containing microspheres results in too thick ice, ruling out the possibility of performing cryo-EM studies.

Here, we used ~50x smaller magnetic particles for sample purification and grid preparation. An electromagnetic particle trap was developed allowing the immobilization of particles down to 10 nm in a ∅150 µm microcapillary. The smaller magnetic nanoparticles do not necessary have to be separated from isolated samples and exhibit more beneficial properties. The much higher surface area to volume increases the binding capacity of targets and reduces incubation times for sample

binding. Nanoparticles linked to proteins can be used as electron dense labels for the identification and localization of isolated target structures, making additional labeling steps e.g. immnogold labeling redundant. Finally, tomograms can directly be generated using the magnetic particles as fiducials.

We demonstrated the isolation of Maurer's cleft tethers out of $\sim$2 µL erythrocyte lysate and their subsequent preparation for negative stain and cryo EM. Using the microfluidic grid preparation method combined with 30 nm sized magnetic particles resulted in a considerable yield of purified targets. In addition, 3D tomograms of the structures were generated. These experiments, show the first affinity purification of a biological sample for TEM using magnetic nanoparticles.

4.4 Material and methods

Preparation of infected erythrocyte lysate

Cell lysate was prepared according to the experimental procedures section in the paper of Pachlatko et al. [Pachlatko *et al.* 2010]. Briefly, erythrocytes were infected with wild type *P. falciparum 3D7* parasites that were cultured at 5 % haematocit with RPMI medium containing 0.5 % Albumax. For the synchronization of the parasites 5 % sorbitol was used. Infected cells from a 30 ml culture were then then hypotonically lysed on ice for 5 min with 6.5 mL 5 mM Na_2HPO_4. To reduce degradation of proteins complete proteasome inhibitor cocktail from Roche was added to the buffer. Consecutive centrifugation steps at 5000 g, 38 000 g and 80 000 g were performed and pellets from each fraction were collected. For protein fishing experiments, the 80 000 g pellet was used.

Generation of the MAHRP2 rabbit polyclonal antibody

The antibody used for the affinity extraction experiments was generated according to the paper of Pachlatko et al. [Pachlatko *et al.* 2010]. In short, recombinantly expressed MAHRP2 fused to a GST tag was injected into New Zealand white rabbits to provoke an immune reaction. After 13 d, 20 mL antiserum was collected and purified using a HiTrap NHS-activated column which was coupled to MAHRP2-GST. The loaded column was then washed with 50 mL PBS and antibodies were finally eluted with 0.1 M glycine, pH 2.5 and stored at 4 °C.

Functionalization of magnetic nanoparticles with MAHRP2 antibodies

30 nm magnetic nanoparticles with a streptavidin coating were purchased from (Ocean Nanotech, # SHS-30-01, USA). In order to conjugate antibodies to the nanoparticle surface, the streptavidin biotin interaction was used. Thus, antibodies had to be biotinylated first.

Biotinylation of antibodies: The buffer of 12 µL MAHRP2 antibody (0.6 mg mL^{-1}) was changed to PBS (PBS, pH 7.4, 150 mM NaCl, 1.5 mM KH_2PO_4, 8.1 mM Na_2HPO_4, 2.6 mM KCl; Sigma, # D8537, Switzerland) using a desalting column (Thermo Fisher Scientific, # 87764, Switzerland). Then a 10x molar excess of photo-labile NHS-biotin crosslinker (Fisher Scientific, # NC1042-383, USA) was added and incubated for 30 min at room temperature. Excess crosslinker was removed using a desalting column (Thermo Fisher Scientific, # 87764, Switzerland), which was equilibrated with PBS to obtain biotinylated antibody at a concentration of 0.23 mg mL^{-1}.

Coupling of antibody to nanoparticles: 0.8 µL of biotinylated antibody was added to 6 µL of magentic nanoparticles (Ocean Nanotech, # SHS-30-01, USA) and incubated 2 h at room temperature. The functionalized nanoparticles were then stored at 4 °C.

Microfluidic protein purification and grid preparation setup

The microfluidic protein purification and grid preparation setup is described in [Schmidli *et al.* 2018, Schmidli *et al.* 2019].

Extraction of Maurer's Cleft tethers

A 1:10 dilution of the functionalized nanoparticles was made with PBS (PBS, pH 7.4, 150 mM NaCl, 1.5 mM KH_2PO_4, 8.1 mM Na_2HPO_4, 2.6 mM KCl; Sigma, # D8537, Switzerland). 1 µL from this solution was added to 10 µL of the prepared erythrocyte lysate and incubated on ice for 45 min. After incubation, a volume of 0.4 µL was aspirated at a flow rate of 0.1 µL min^{-1} and passed through the electromagnetic trap. The electromagnetic trap was operated at maximum power to immobilize as much nanoparticles as possible. In order to avoid heating up of the trap system it was cooled with the implemented cooling circuit down to 4 °C. The aspiration-wash cycle was repeated twice for a total sample loading of 1.2 µL. Subsequently, the capillary was flushed with 5 µL of PBS (PBS, pH 7.4, 150 mM NaCl, 1.5 mM KH_2PO_4, 8.1 mM Na_2HPO_4, 2.6 mM KCl; Sigma, # D8537, Switzerland) at a flow rate of 0.5 µL min^{-1}. After the washing step two 7 nL air bubbles were introduced from the nozzle tip to enclose the nanoparticle plug in 10 nL PBS (PBS, pH 7.4, 150 mM NaCl, 1.5 mM KH_2PO_4, 8.1 mM Na_2HPO_4, 2.6 mM KCl; Sigma, # D8537, Switzerland). The hydrophilicity of the inner surface of the microfluidic capillary retains a thin hydration layer, which allows magnetic beads with loaded samples to remain within the aqueous phase while the air bubbles are introduced. The nanoparticle plug was then dissolved by applying a Degaussing process, which removes remaining magnetism in the particle trap. Depending on the experiment the nanoparticle plug was exposed to UV light with a LED (Thorlabs, # M365L2, Switzerland) to cleave the photo-labile crosslinker. Finally, the purified sample was pumped (0.1 µL min^{-1}) to the microcapillary tip.

EM grid preparation

Negative staining: Negative staining was done based on the protocol shown in [Schmidli *et al.* 2018]. In brief, a conditioning step was performed by immersing the microcapillary tip into a reservoir with 100 µL tungsten based negative staining solution (Nanoprobes , NanoW 2 % , USA). Driven by diffusion the stain gets into the capillary tip and salt ions of the sample move out of the sample in the staining reservoir. After a conditioning time of 12 min the sample was deposited on an EM grid (400 mesh Cu grid, covered by a carbon-coated parlodion film) that was treated 20 s with an air plasma. The grid was cooled with the temperature-controlled stage of our setup to 7 °C above the dew point allowing gentle evaporation of the sample buffer.
Cryo-electron microscopy: Cryo EM grids were prepared as described in [Schmidli *et al.* 2018] with the difference that 300 mesh Cu Lacey carbon grids (Agar Scientific Ltd. , # AGS166-3, UK) were used. Basically, 10 nL of purified sample was deposited on a glow discharged Lacey carbon grid kept 7 °C above the dew point while moving the capillary relative to the grid surface. As much sample as possible was re-aspirated leaving a thin film that was vitrified in liquid ethane. The whole procedure was performed automatically using a macro script of our cryoWriter setup.

Electron microscopy and image processing

Negative stain imaging was performed on a 120 kV FEI Tecnai 12 microscope equipped with a TVIPS F416 CMOS camera. Cryo-EM images were collected with a 200 kV FEI Talos on a FEI Ceta 16M Pixel CMOS camera. Dual axis tilt series were acquired using the SerialEM software [Mastronarde 2005]. Images were recorded at a pixel size of 1.61 Å at 3° intervals over a tilt range of ±60°. IMOD [Kremer *et al.* 1996] was used for the 3D reconstruction of tomograms from tilt series. The tether structures were traced by hand to create 3D models with the Amira® software (Visage Imaging Inc.). Images of the final 3D models were rendered with Blender (www.blender.org).

4.5 Supplementary materials

Analysis of the crude erythrocyte lysate

Crude lysate of infected erythrocytes was analyzed by conventional negative staining. Using standard protocols no Maurer's cleft tethers could be observed in the electron microscope. Few tethers could be found on grids that were not glow discharged incubating 4 µL sample for a long time of 8 min on the grid (Figure 4.4). The images show also other constituent parts of the erythrocyte lysate.

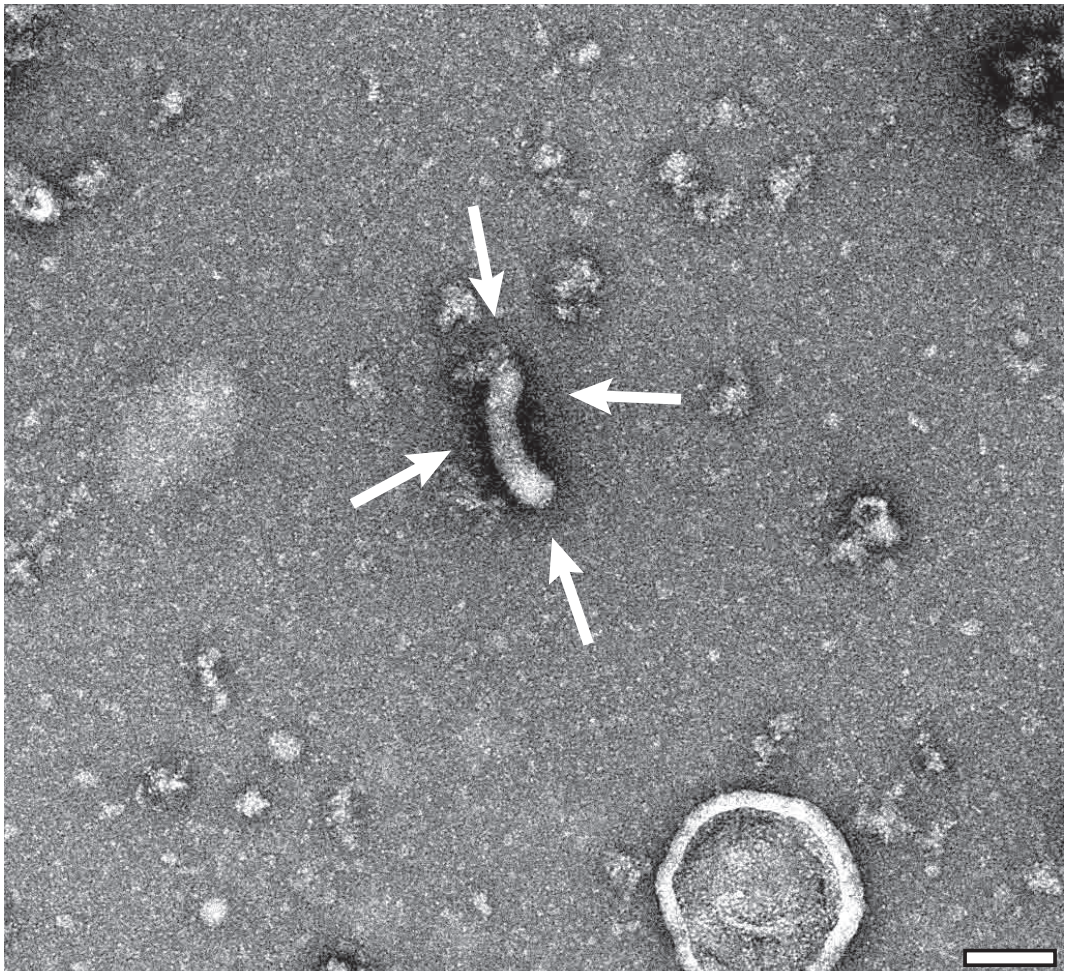

Figure 4.4: Conventional negative stain imaging of erythrocytes lysate containing Maurer's cleft tethers. 4 µL sample droplets were incubated for 8 min on negative stain grids before blotting, which allowed discovering tethers (labeled with white arrows) after intensively screening the grid. The scale bar reads 100 nm.

Multiple biotinylated antibodies

Ideally, antibodies are mono-biotinylated for the attachment to the streptavidin coated magnetic particle surface. Multiple biotinylated antibodies can lead to crosslinking of nanoparticles and the formation of large aggregates as shown in Figure 4.5. Biotinylation via NHS-biotin compounds is a stochastic process, where a certain amount of antibodies are biotinylated over time. We obtained best results by incubating the antibodies for 1 h with 10x molar excess of NHS-biotin crosslinker. We estimate this leads in average to 1-2 biotins per antibody.

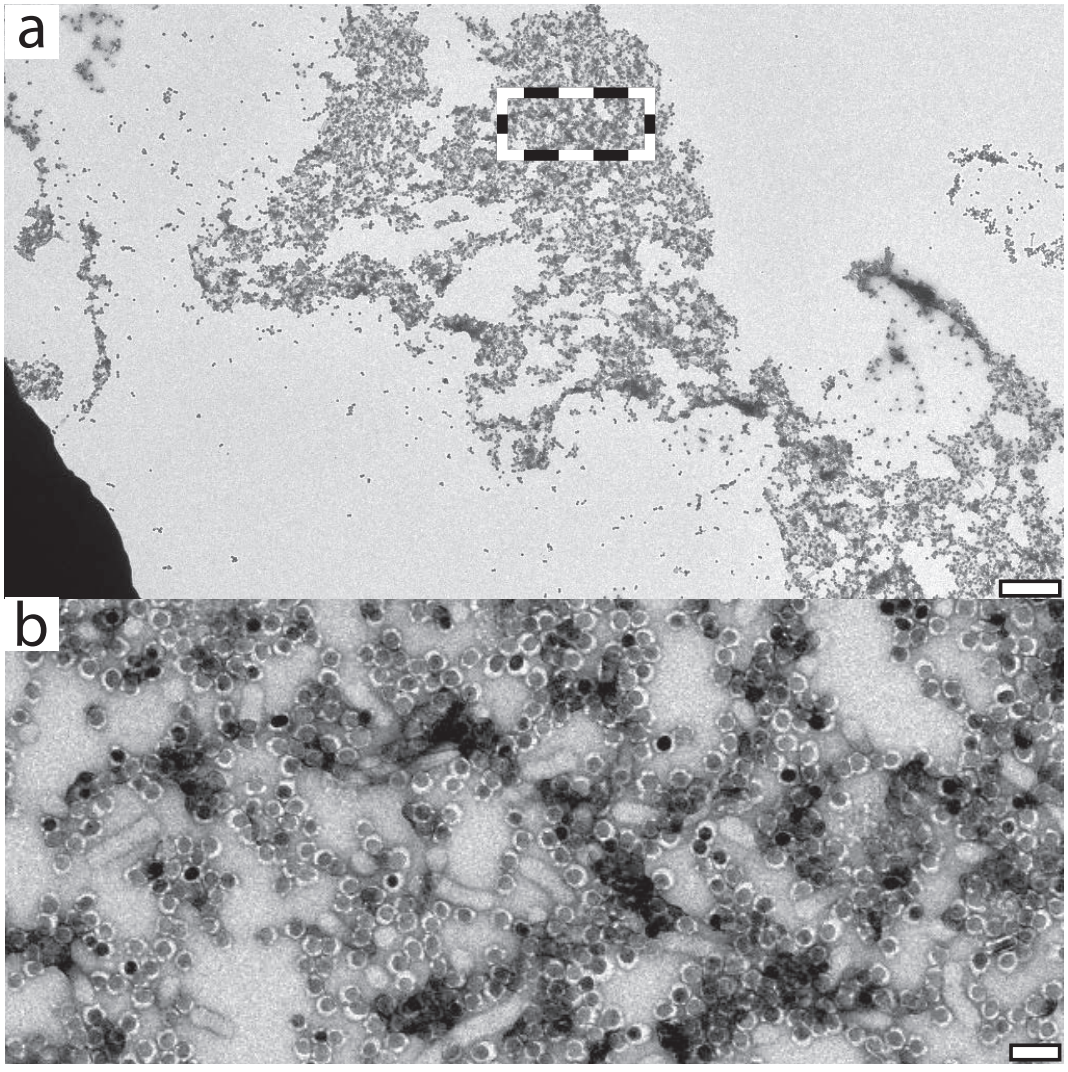

Figure 4.5: a) Low magnification and **b)** high magnification image of clustered nanoparticles and tethers due to excess antibody biotinylation. The scale bars read a) 1 µm and b) 100 nm.

Incubation of sample with antibodies before adding nanoparticles

Instead of linking the antibodies to the nanoparticles they can also be incubated first with the sample and the streptavidin coated nanoparticles can be added later. However, with this approach aggregation of Maurer's cleft tethers (see Figure 4.6) was observed. When using antibody functionalized nanoparticles this was not the case.

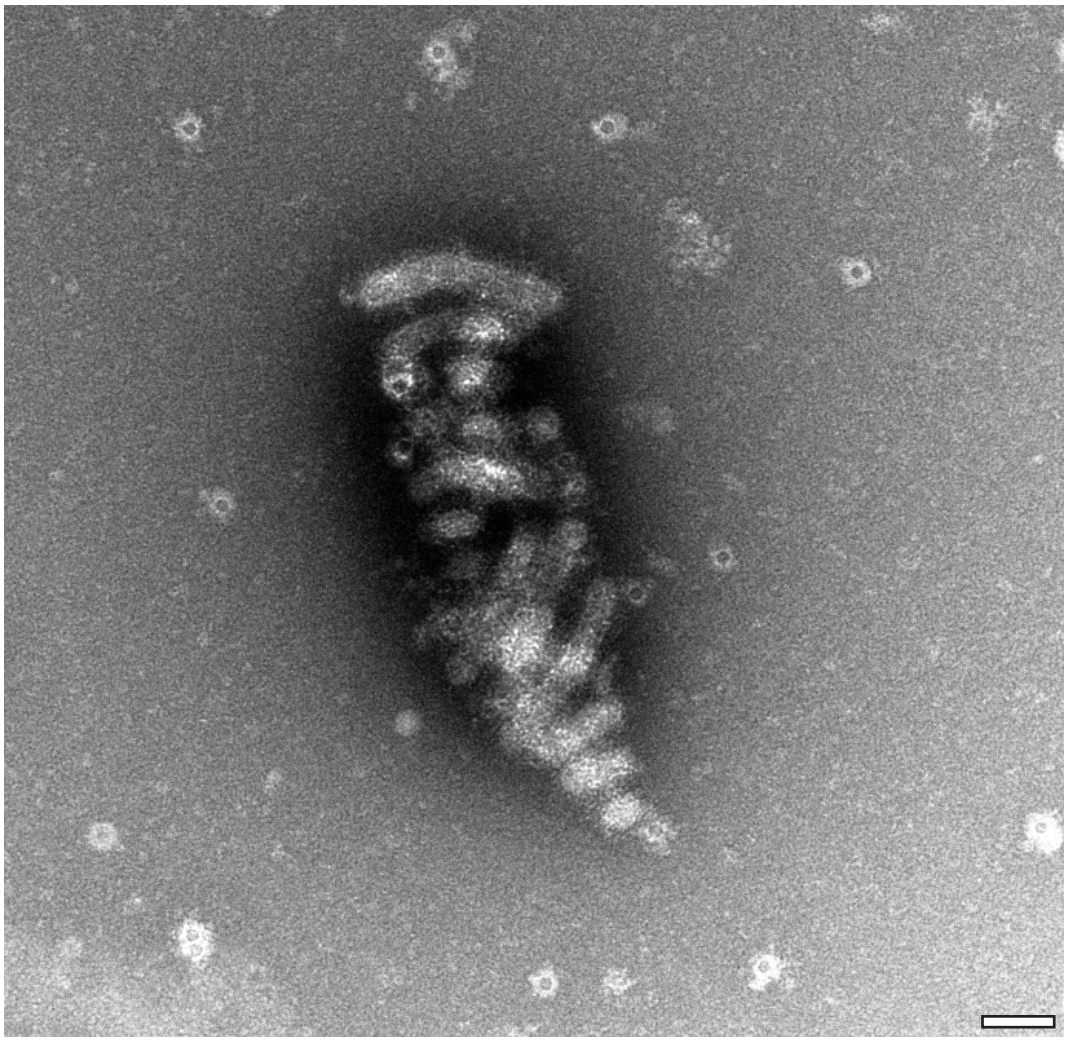

Figure 4.6: Incubation of antibodies with sample before adding magnetic nanoparticles. When incubating MAHRP2 antbodies with infected erythrocyte lysate followed by the addition of strepavidin coated nanoparticles, clustering of the tethers was observed. Interestingly, this is not the case when the antibodies were linked first to the magnetic nanoparticles and then added to the sample. The scale bar reads 100 nm.

Over-labeling of target structures

Some samples such as Maurer's cleft tethers have a large surface area presenting many target epitopes where an antibody can bind. The addition of high amounts of antibody-functionalized nanoparticles can lead to the decoration of the whole surface (see Figure 4.7). "Over-labeling" can become a problem, hampering the analysis of isolated targets because regions of interest are covered. The amount of coupled nanoparticles has to be carefully adjusted in order to get satisfactory results.

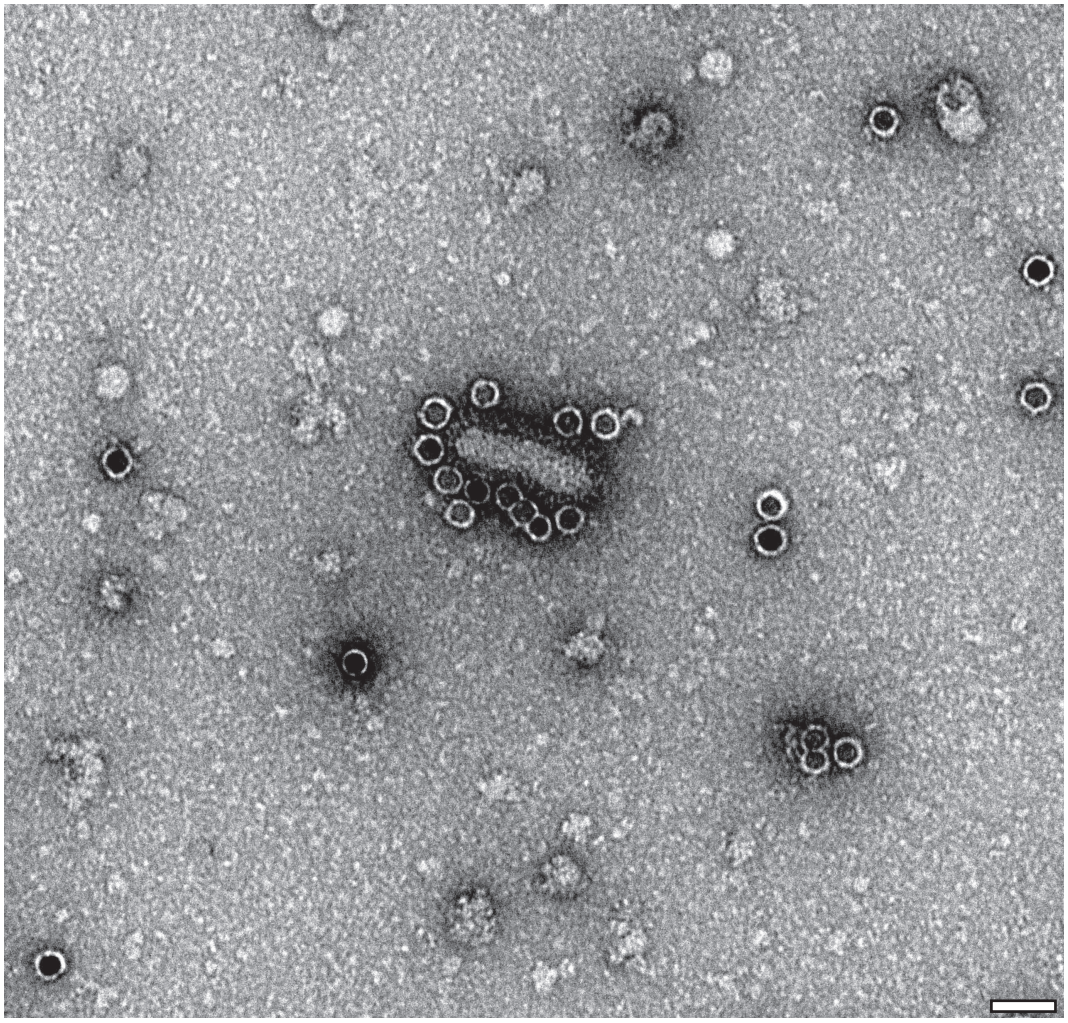

Figure 4.7: Over-labeling of Maurer's cleft tethers by adding high amounts of antibody functionalized magnetic nanoparticles. MAHRP2 seems to be present all over the tether surface. Adding high amounts of magnetic nanoparticles results in the decoration of the whole tether surface with particles. Labeling with too many nanoparticles makes the analysis in TEM difficult.

4.6 Acknowledgments

We thank the workshop of the Biozentrum for their support. Lubomir Kovacik for the assistance on the microscope. Stefan Arnold and Luca Rima for the technical assistance on developing of the electromagnetic trap. The project was supported by the Swiss Nanoscience Institute (projects P1401 & ARGOVIA MiPIS). Thomas Braun and Henning Stahlberg declare the following competing financial interest: The cryoWriter concept is part of patent application PCT/EP2015/065398.

5 Microfluidic affinity purification of tagged proteins for transmission electron microscopy

In this section, microfluidic protein isolation using the affinity interaction of nitrilotriacetic acid (NTA)/Ni_2^+ chelates with His-tagged targets is presented. In collaboration with a group at the University of Applied Sciences Northwestern Switzerland (FHNW) a novel NTA crosslinker was synthesized and coupled to magnetic particles. The usability of the NTA-particles is demonstrated by the re-isolation of His-tagged Ferritin from spiked cell lysate.

My contribution was testing the cross-linker, forming the Ni-NTA complexes, establishing the protein isolation protocols, performing the presented purification experiments and writing this section.

The content of this section are results of the ARGOVIA MiPIS project.

Isolation of His-tagged Ferritin from spiked cell lysate with NTA-functionalized magnetic beads

Claudio Schmidli[1,2], Daniel Bopp[3], Maianne Hürzeler[3], Henning Stahlberg[1] and Thomas Braun[1]

1 - Center for Cellular Imaging and NanoAnalytics, Biozentrum, University Basel, Switzerland
2 - Swiss Nanoscience Institute, University of Basel, Switzerland
3 - School of Life Sciences, Muttenz, Switzerland

Contents

5.1 Introduction

During the early 70's recombinant DNA technology (rDNA) was developed on *Escherichia coli* (E.coli) [Marston 1986] moving biology from an exclusively analytical science to a synthetic one. After the synthesis of functional products cloned in bacterial plasmids, the potential of the rDNA technique was soon realized. Samples of proteins rarely occurring in living cells could suddenly be generated in high amounts and the effort for purification was dramatically reduced using fusion proteins and affinity tags [Brewer *et al.* 1991, Sassenfeld 1990, Malhotra 2009]. As a consequence, the majority of solved protein structures are nowadays derived from recombinant expressed proteins. The expression of recombinant protein in E.coli or mammalian cells with attached affinity tags is one of the most popular methods for protein production and purification. Affinity tags are short artificial amino acid sequences usually grafted either to the N- or C-terminus of an expressed target by appending a complementary DNA (cDNA) piece to the polypeptide encoding sequence. Thus, affinity columns with specific matrices can be used for the purification increasing the yield and solubility of isolated target proteins. The most frequently used affinity tag is the hexahistidine tag (His_6-tag), which enables protein isolation via immobilized metal affinity chromatography (IMAC) [Lichty *et al.* 2005]. The IMAC resin binds to the His-tag of proteins in near-neutral buffer conditions due to the interaction between the negatively charged His-tag and the transition metal ions (Ni_2^+,CO_2^+,Cu_2^+,Zn_2^+) immobilized on the column matrix [Porath *et al.* 1975]. Hochuli et al. [Hochuli *et al.* 1987] developed a method where Ni_2^+ is linked to nitrilotriacetic acid (NTA) providing an inexpensive matrix with high affinity for adjacent histidine residues. Disassociation of bound recombinant protein is permitted by an imidazole gradient (20 to 200 mM) [Janknecht *et al.* 1991, Hefti *et al.* 2001], changes in pH or metal chelation. The column matrix can be re-used and withstands multiple regeneration cycles under stringent conditions. Due to the simple and cost effective purification procedure providing protein in the multimilligram scale, His_6-tag is the by far the most common fusion partner used in structural studies. The small size of His_6-tag does generally not interfere with the protein structure. However, the required elution approached based on buffer changes may result in protein aggregates [Hefti *et al.* 2001] and are not optimal for cryo-EM. Often dialysis has to be performed after the purification procedure to change to an appropriate buffer. Further, chemical elution has the drawback of releasing unspecific bound proteins, particular prominent in microfluidic systems.

In this section, microfluidic protein purification of recombinant expressed proteins by the His_6-tag is demonstrated. In collaboration with a group at the University of Applied Sciences Northwestern Switzerland (FHNW) a crosslinker featuring a NTA moiety on one side and an amine reactive ester group on the other side was synthesized and coupled to magnetic particles. The NTA functionalized magnetic

particles were then used to isolated His_6-Ferritin from Ferritin spiked cell lysate. Besides offering the possibility of purifying minimal amounts of protein, a main advantage of this method is the gentle photo-elution technique which makes changes in buffer conditions redundant and keeps proteins in physiological buffer conditions. By performing first proof-of-concept experiments, we show the high potential of the method and lay the foundations for more complex protein purification experiments in future.

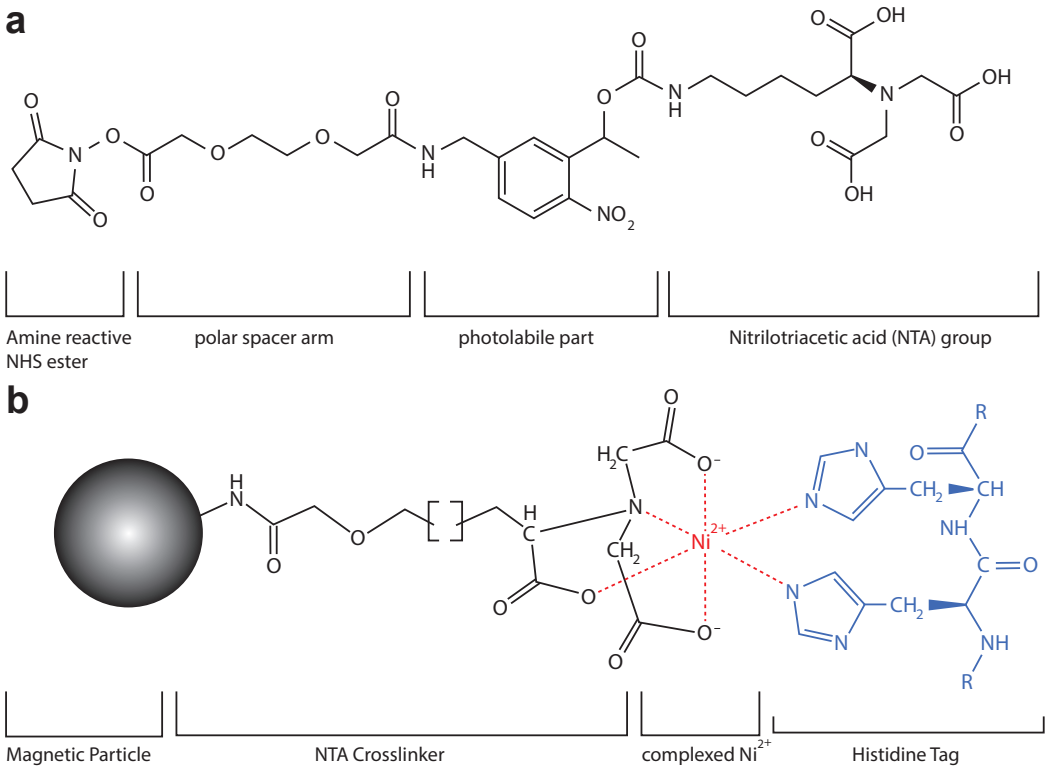

Figure 5.1: Illustration of the novel NTA-crosslinker and how it links a magnetic particle to a histidine group via Ni^{2+} chelation. **(a)** The crosslinker consists of four functional parts: (i) A NHS ester group reacting with amines present on the magnetic particle surface to form a covalent bond, (ii) a polar spacer arm increasing the solubility and lowering steric hindrance of the NTA group, (iii) a photo-cleavable part which is used for elution of isolated proteins and (iv) a NTA group featuring high affinity to His-tagged proteins. **(b)** Illustration of the crosslinker attached to a magnetic particle via the amine reactive ester group. The NTA group on the other site has a high affinity to Ni^{2+} (red), which coordinates with histidine tagged proteins (blue).

5.2 Results

We manufactured superparamagnetic nanoparticles with a photo-cleavable NTA coating (see Figure 5.1). The NTA moiety present on the nanoparticle surface chelates Ni^{2+} ions, which can bind His-tagged proteins from recombinant expression. For coupling the NTA groups to the magnetic particles, a photo-labile crosslinker was synthesized in collaboration with FHNW (see Figure 5.1). The crosslinker consists of four functional parts: (i) An amine reactive NHS ester group allowing the linkage of the crosslinker to the amine functionalized magnetic nanoparticles, (ii) a polar spacer arm increasing the crosslinker solubility and lowering steric hindrance of the NTA group, (iii) a photo-labile part used for cleavage of the crosslinker and (iv) a NTA group that can bind His-tagged proteins.

50 mg of crosslinker was synthesized in a multi-stage procedure and the final product was validated with NMR. The photo-decomposition of the photo-labile part was tested by irradiation with UV light for several minutes. A change of the solvent color from transparent to an intensive orange indicated degradation of the photo-reactive core. Following NMR measurements confirmed successful cleavage, which was also observed when exposing the crosslinker to sunlight for several days. An ideal storage place is therefore protected from light and should also be in a water free environment avoiding hydrolysis of the ester groups. Amine functionalized magnetic particles were prepared by incubating commercial amine coated microspheres with the NTA-crosslinker. After incubation, unbound excess crosslinker was removed using magnetic separation. Final incubation of the magnetic particles with $NiCl_2$ solution resulted in the chelate complex between Ni^{2+} and NTA.

To show the usability of the NTA-beads for microfluidic protein purification, His-tagged, recombinant Soybean Ferritin-2 was mixed with HEK293 lysate resulting in a heterogeneous sample containing 2 µM Ferritin (see Figure 5.2a). This mixture was used to re-isolate Ferritin particles followed by subsequent grid preparation for negative stain EM. Therefore, 50 µg of functionalized magnetic particles were added to the Ferritin spiked cell lysate and incubated for 15 min on ice. After incubation, the total sample volume of 10 µL was aspirated in a 150 µm microcapillary and passed through a magnetic trap where magnetic particles with the bound Ferritin targets were immobilized. The capillary was then rinsed with buffer to remove HEK293 lysate components. Isolated Ferritin was separated from magnetic particles by UV cleavage and 4 µL Ferritin eluate were deposited on a glow discharged negative stain grid. Conventional negative staining was done manually resulting in grids with isolated Ferritin at high concentration and purity (see Figure 5.2b). The fairly clean background demonstrates the specificity of the method and the high particle number how protein are up-concentrated through the isolation process.

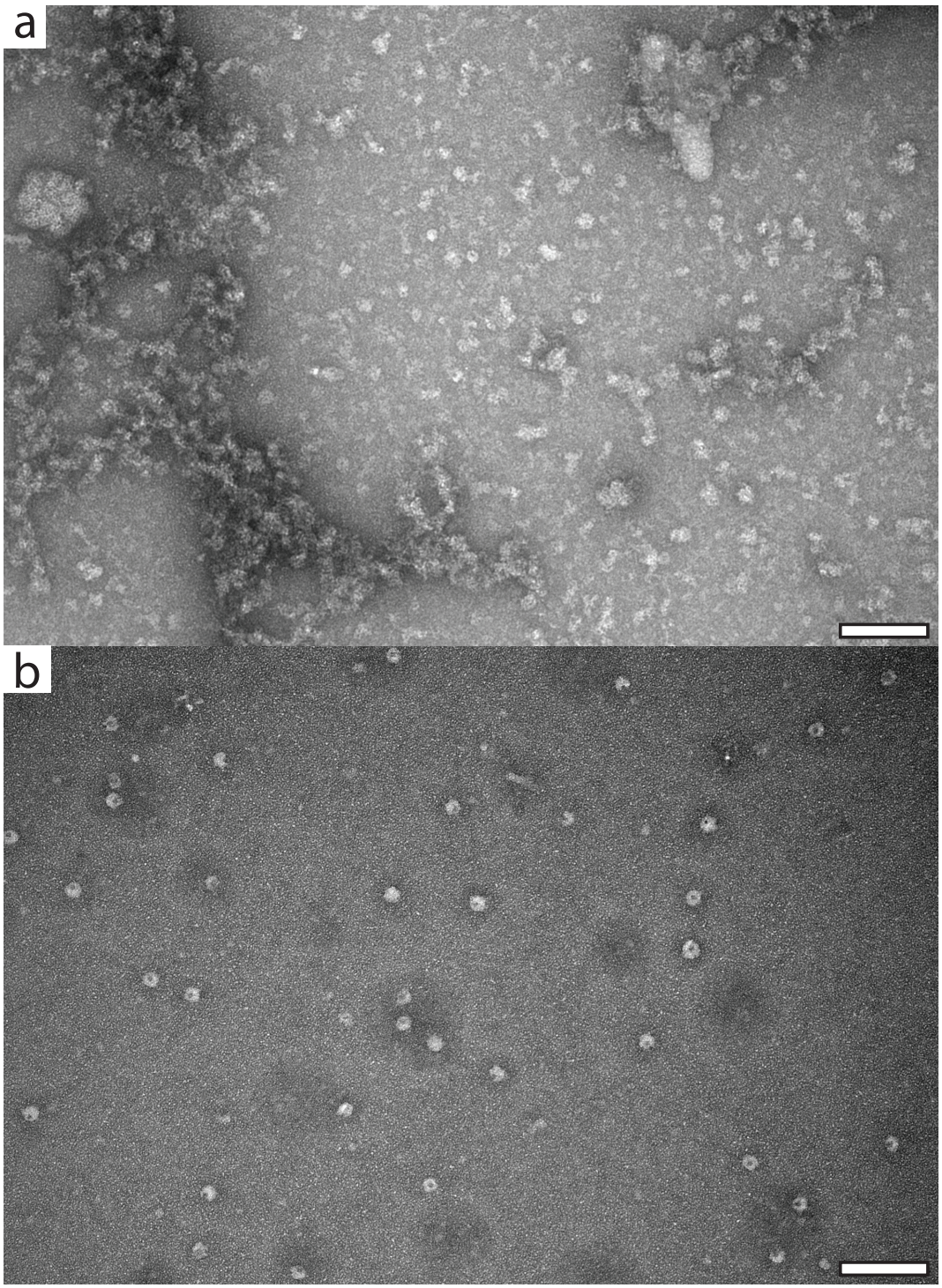

Figure 5.2: TEM images of the Ferritin sample before and after purification. **a)** HEK293 cell lysate spiked with His-tagged Ferritin (2 uM) from Soybean. **b)** Negatively stained Ferritin that was isolated out of the HEK293 lysate.

5.3 Conclusion

The overwhelming majority of biomolecules analyzed in cryo-TEM studies are recombinantly derived proteins. Most of these proteins are expressed as fusion constructs to facilitate subsequent protein purification in affinity columns or to increase protein yields, solubility, and even folding of target partners [Waugh 2005, Smyth *et al.* 2003]. Among all the different fusion partners being used nowadays, the His_6-tag is the most common one. Due to its utility in nickel affinity chromatography it allows simple and cost effective protein purification on a large scale [Bucher *et al.* 2002]. We were able to manufacture NTA functionalized microspheres for microfluidic protein isolation. This allowed us to supplement our antibody based protein purification methodology with an alternative affinity interaction approach. The application of NTA functionalized beads enables purification of His-tagged proteins without the need of antibodies, which are often not available for a given target. Thereby, we were able to significantly reduce incubation times for binding proteins to the solid phase and avoided crosslinking between proteins that may occur with full antibodies. Finally, the preparation of beads coupled to specific primary antibodies is not needed anymore.

5.4 Acknowledgments

I thank Maianne Hürzeler and Daniel Bopp from FHNW in Muttenz for the synthesis of the NTA-crosslinker and the pleasant collaboration. Thomas Braun for the coordination and the Swiss Nanoscience Institute for funding the project(P1401 & ARGOVIA MiPIS).

5.5 Material and Methods

Synthesis of the NTA-crosslinker

Manufacturing of the NTA-crosslinker was done by a multiple stage synthesis as described in [Bopp 2018].

Coupling of the NTA-crosslinker to magnetic beads

1 mg crosslinker was dissolved in anhydrous DMF (Sigma-Aldrich, #227056, Switzerland) and 30 µL magnetic beads (Thermo Fisher Scientific, #14307D, Switzerland) featuring amine groups on the surface were added. After 1 h incubation at room

temperature with constant mixing using an overhead shaker, the magnetic particles were washed 4x with 200 µL PBS using a permanent magnet. Finally, the particles were dissolved in 200 µL PBS.

Complexation with Ni^{2+}

For Ni^{2+} complexation of the NTA-beads, 0.05 M $NiCl_2$ was added to the bead solution and incubated overnight in an overhead shaker at 4 °C. Finally, the magnetic particles were washed 4x in 50 µL PBS using a permanent magnet and suspended in 10 µL PBS.

Test sample

For testing the protein purification methodology 0.2 µM Soybean Ferritin (abcam, #ab225968, Switzerland) was added to HEK293 lysate (83 Mio cells/ml). HEK 293 cells were prepared according to [Arnold *et al.* 2016] and lysed with a dounce homogenizer by applying 100 strokes. After lysis, proteasome inhibitor cocktail was added (Sigma-Aldrich, #11697498001, Switzerland). The lysate was aliquoted and stored at −20 °C in the fridge. For protein fishing experiments, aliquots were dawn on ice and Soybean Ferritin was added.

Protein purification

For protein purification experiments 3 µL of prepared NTA-beads were mixed with 10 µL spiked lysate and incubated 15 min. To reduce unspecific binding 35 mM imidazole was added. Then the solution was aspirated in a 150 µm microcapillary at 2 µL min^{-1} and passed through the magnetic trap where magnetic particles with attached target proteins were immobilized. Then the flow direction was inverted and the plug was washed with 300 µL wash buffer (20 mM NaH_2PO_4,0.5 mM NaCl, pH 7). For elution the plug was exposed to 365 nm UV light (1150 mW) for 15 min. Finally, the cleaved target proteins were dispensed on a glow discharged negative stain grid (400 mesh Cu, covered by a carbon-coated parlodion film) and negatively stained using a conventional protocol described in [Giss *et al.* 2014].

6 Conclusion and Outlook

Cryo-EM massively improved in recent years, leading to a virtual explosion of published TEM protein structures. These advances can be attributed to improved detectors, instrumentation, and software. However, sample preparation methods lack behind and did not change a lot since their invention 30 years ago. Classical approaches involve a problematic paper blotting step and require several micrograms of protein, despite only 10'000 to a few million protein particles are needed to solve a high-resolution structure. Thus, tremendous amounts of overexpressed proteins have to be purified, from which the largest portion is lost during specimen preparation.

The results presented in this thesis show that microfluidics enables the purification and preparation of endogenous proteins for structure determination by TEM, offering an attractive alternative to typical protein isolation strategies. Often, the natural expression level of proteins is too low; therefore, the target proteins are produced in overexpression systems. However, several pitfalls can hamper recombinant production such as low solubility or toxicity to the host cell. Furthermore, vast amounts of biological starting material are required, and several time-consuming chromatography steps involving cycles of target binding and washing have to be applied. For each step, retention of the biological activity and chemical integrity has to be ensured. In summary, the classical approach is time-consuming and labor-intensive, and only a small fraction of the protein can be finally used for the structural analysis.

The presented microfluidic protein purification method allows protein isolation in a single purification step within only a few hours. In contrast to standard purification approaches, the *cryoWriter* setup does not rely on expensive protein production systems, chromatography columns or centrifuges. Isolated targets can be vitrified in a swift manner reducing potential damage during sample preparation, which is especially important for unstable proteins such as membrane proteins. The elution by photo-cleavage is more specific than competitive elution approaches and does not release unspecifically bound proteins; therefore acting similar to a second 'purification step.' Due to the high affinity provided by specific antibodies, the method allows the purification of endogenous proteins from minimal amounts of cell lysate without overexpression. Thus, much less biological starting material is required, facilitating the use e.g., for diagnostics in amyloid diseases, where only biopsies of a minimal amount of analytes can be taken. The ultimate test for the *cryoWriter* system would be to solve the structure of a protein from the single-cell lysate. Theoretically, the amount of some highly expressed proteins is enough to perform a cryo-EM single-particle analysis, e.g., the proteasome 20S is reported to be expressed in the µM range. Assuming a volume of ≈6 µL for a eukaryotic cell, we expect 3 600 000 copies of the protein complexes in a single cell. If only 1 % of these particles could be imaged, one should be able to obtain a high-resolution map of the protein. In the

case of the proteasome 20S it will be of interest if structural changes between cells in different states can be seen, e.g., after triggering by a heat-shock, and if one can draw any conclusions about the ligands and the regulatory subunits. The single-cell lysis module could be used to open and aspirate eukaryotic HeLa cells in a volume of ≈3 nL into the apex of the microcapillary (a dilution of ≈500 ×). Subsequently, the cell lysate is directly mixed with a 3 nL Fab fragment solution, and after a short incubation, with streptavidin-coated superparamagnetic particles (volume: 14 nL) resulting in a total volume of 20 nL, or a dilution factor of ≈3500 ×. Therefore, for high-affinity monoclonal antibodies, we are comfortably above typical antibody dissociation constants of K_D, where recently a median value for the $K_D = 66$ pM ($n = 1450$) was reported [Landry *et al.* 2015]. Using high antibody concentrations, which can be performed at reasonable costs, further stabilizes antigen-Fab binding.

Another goal is performing quantitative studies using the *cryoWriter* setup. Since the method allows preparing grids in a lossless manner, the visual investigation of the proteome of individual cells becomes feasible. As shown by [Syntychaki *et al.* 2019], the expression levels of proteins in single cells can be analyzed and compared to each other using *differential visual proteomics*. We envisage the method as a tool for the untargeted profiling of the structural changes in the proteome of single-cells as a response to a disturbing force.

Further, the quality of prepared grids could be improved. The presented instrument and methods bypass paper blotting steps entirely. However, the aggressive air-water interface (AWI) can inherently not be avoided. Therefore, a conditioning module to dope the system with detergent molecules covering the air-water interface could be used. Through the injection of low-molecular-weight substances in the gas stream subsequently, a thin layer at the AWI is formed, which eventually protects sensitive proteins. Additionally, this might influence the orientation of the protein particles in the ice and might help in cases where 2D classes of specific orientations are missing.

7 Acknowledgments

The work presented here would not have been possible without the help of many others. First of all I express gratitude to my advisors Thomas Braun and Henning Stahlberg. They paced great confidence in me and gave me the opportunity to work on a very interesting project with fantastic people. For co-refereeing my thesis, I greatly appreciate Andreas Engel. Further, I thank the whole Braun team, Luca Rima, Paolo Oliva, Stefan Albiez, Rosmarie Sütterlin, Andrej Bieri, Cedric Leu, Fabian Heule, Andri Fränkl and Anastasia Syntychaki for an excellent teamwork and a pleasant atmosphere in the lab. Especially I thank Luca Rima and Paolo Oliva who helped me a lot with their technical know-how and Rosmarie Sütterlin for taking care of our cells. I would like to acknowledge Karen Bergmann and Claudia Wirth for solving administrative tasks connected with my PhD. I thank Ariane Fecteau-LeFebvre, Daniel Caujolle-Bert and Kenneth Goldie for maintaining the microscopes. Further, I thank Lubomir Kovacik for the excellent support on the Titan during data collection sessions and Stefan Albiez and Ricardo Righetto for processing the acquired images. It was the skills and expertise of this guys that yielded to the published high-resolution protein structures. I very much appreciated the work of Raymond Strittmatter and his team from the mechanical workshop of the Biozentrum at the University of Basel. They advised me with technical questions and provided a lot important parts for the cryoWriter setup. I also express my gratitude to the director of the Swiss Nanoscience Institute Prof. Christian Schönenberger, the coordinator Dr. Andreas Baumgartner and the whole team for offering an excellent PhD program with many great educational and social events. I thank all members of C-CINA for a friendly working environment, many discussions and their help in many different situations. Finally, I'm very thankful to my family and close friends who supported and accompanied me during my studies. This thesis would not be the same without you. Thanks a lot!

References

[Adams *et al.* 2010] Paul D. Adams, Pavel V. Afonine, Gábor Bunkóczi, Vincent B. Chen, Ian W. Davis, Nathaniel Echols, Jeffrey J. Headd, Li-Wei Hung, Gary J. Kapral, Ralf W. Grosse-Kunstleve, Airlie J. McCoy, Nigel W. Moriarty, Robert Oeffner, Randy J. Read, David C. Richardson, Jane S. Richardson, Thomas C. Terwilliger and Peter H. Zwart. *PHENIX: a comprehensive Python-based system for macromolecular structure solution.* Acta Crystallographica Section D Biological Crystallography, vol. 66, no. 2, pages 213–221, jan 2010. (Cited on page 56.)

[Arnold *et al.* 2016] Stefan A. Arnold, Stefan Albiez, Nadia Opara, Mohamed Chami, Claudio Schmidli, Andrej Bieri, Celestino Padeste, Henning Stahlberg and Thomas Braun. *Total Sample Conditioning and Preparation of Nanoliter Volumes for Electron Microscopy.* ACS Nano, vol. 10, no. 5, pages 4981–4988, apr 2016. (Cited on pages 7, 24, 25, 33, 35, 36, 38, 42, 43, 47, 52, 69, 71 and 91.)

[Arnold *et al.* 2017] Stefan A. Arnold, Stefan Albiez, Andrej Bieri, Anastasia Syntychaki, Ricardo Adaixo, Robert A. McLeod, Kenneth N. Goldie, Henning Stahlberg and Thomas Braun. *Blotting-free and lossless cryo-electron microscopy grid preparation from nanoliter-sized protein samples and single-cell extracts.* Journal of Structural Biology, vol. 197, no. 3, pages 220–226, mar 2017. (Cited on pages 24, 35, 40, 42, 47, 50, 52, 55 and 69.)

[Arnold *et al.* 2018] Stefan A. Arnold, Shirley A. Müller, Claudio Schmidli, Anastasia Syntychaki, Luca Rima, Mohamed Chami, Henning Stahlberg, Kenneth N. Goldie and Thomas Braun. *Miniaturizing EM Sample Preparation: Opportunities, Challenges, and "Visual Proteomics".* PROTEOMICS, vol. 18, no. 5-6, page 1700176, mar 2018. (Cited on page 47.)

[Baker & Rubinstein 2010] Lindsay A Baker and John L Rubinstein. *Radiation damage in electron cryomicroscopy.* Methods in enzymology, vol. 481, pages 371–388, 2010. (Cited on page 23.)

[Barnard *et al.* 2009] D Barnard, Z Lu, TR Shaikh, A Yassin, H Mohamed, R Agrawal, T-M Lu and T Wagenknecht. *Time Resolved Cryo-Electron Microscopy Of Ribosome Assembly using Microfluidic Mixing.* Microscopy and Microanalysis, vol. 15, no. S2, pages 942–943, jul 2009. (Cited on page 6.)

[Baumeister & Seredynski 1976] W. Baumeister and J. Seredynski. *Preparation of performed films with predeterminable hole size distributions.* Micron (1969), vol. 7, no. 1, pages 49–54, jan 1976. (Cited on page 3.)

[Bedanta & Kleemann 2008] Subhankar Bedanta and Wolfgang Kleemann. *Supermagnetism.* Journal of Physics D: Applied Physics, vol. 42, no. 1, page 013001, dec 2008. (Cited on page 10.)

[Berensmeier 2006] Sonja Berensmeier. *Magnetic particles for the separation and purification of nucleic acids.* Applied Microbiology and Biotechnology, vol. 73, no. 3, pages 495–504, oct 2006. (Cited on page 68.)

[Berriman & Unwin 1994] John Berriman and Nigel Unwin. *Analysis of transient structures by cryo-microscopy combined with rapid mixing of spray droplets.* Ultramicroscopy, vol. 56, no. 4, pages 241–252, dec 1994. (Cited on page 6.)

[Bhardwaj *et al.* 2009] Rajneesh Bhardwaj, Xiaohua Fang and Daniel Attinger. *Pattern formation during the evaporation of a colloidal nanoliter drop: a numerical and experimental study.* New Journal of Physics, vol. 11, no. 7, page 075020, jul 2009. (Cited on page 47.)

[Biyani *et al.* 2017] Nikhil Biyani, Ricardo D. Righetto, Robert McLeod, Daniel Caujolle-Bert, Daniel Castano-Diez, Kenneth N. Goldie and Henning Stahlberg. *Focus: The interface between data collection and data processing in cryo-EM.* Journal of Structural Biology, vol. 198, no. 2, pages 124–133, may 2017. (Cited on page 55.)

[Bopp 2018] Daniel Bopp. Synthese eines photolabilen linkers für die proteinreinigung. Master's thesis, University of Applied Sciences Northwestern Switzerland (FHNW), 2018. (Cited on page 90.)

[BRENNER & HORNE 1959] S BRENNER and R W HORNE. *A negative staining method for high resolution electron microscopy of viruses.* Biochimica et biophysica acta, vol. 34, pages 103–110, July 1959. (Cited on page 23.)

[Brewer *et al.* 1991] S J Brewer, B L Haymore, T P Hopp and H M Sassenfeld. *Engineering proteins to enable their isolation in a biologically active form.* Bioprocess technology, vol. 12, pages 239–266, 1991. (Cited on page 86.)

[Brullot *et al.* 2012] W. Brullot, N.K. Reddy, J. Wouters, V.K. Valev, B. Goderis, J. Vermant and T. Verbiest. *Versatile ferrofluids based on polyethylene glycol coated iron oxide nanoparticles.* Journal of Magnetism and Magnetic Materials, vol. 324, no. 11, pages 1919–1925, jun 2012. (Cited on page 10.)

[Bucher *et al.* 2002] Matthew H Bucher, Artem G Evdokimov and David S Waugh. *Differential effects of short affinity tags on the crystallization of Pyrococcus furiosus maltodextrin-binding protein.* Acta crystallographica. Section D, Biological crystallography, vol. 58, pages 392–397, March 2002. (Cited on page 90.)

[Campbell *et al.* 2012] Melody G. Campbell, Anchi Cheng, Axel F. Brilot, Arne Moeller, Dmitry Lyumkis, David Veesler, Junhua Pan, Stephen C. Harrison, Clinton S. Potter, Bridget Carragher and Nikolaus Grigorieff. *Movies of Ice-Embedded Particles Enhance Resolution in Electron Cryo-Microscopy.* Structure, vol. 20, no. 11, pages 1823–1828, nov 2012. (Cited on page 23.)

[Campbell *et al.* 2015] Melody G Campbell, David Veesler, Anchi Cheng, Clinton S Potter and Bridget Carragher. 2.8 Å *resolution reconstruction of the Thermoplasma acidophilum 20S proteasome using cryo-electron microscopy.* eLife, vol. 4, mar 2015. (Cited on page 2.)

[Cardone *et al.* 2013] Giovanni Cardone, J. Bernard Heymann and Alasdair C. Steven. *One number does not fit all: Mapping local variations in resolution in cryo-EM reconstructions.* Journal of Structural Biology, vol. 184, no. 2, pages 226–236, nov 2013. (Cited on page 62.)

[Carlo & Harris 2011] Sacha De Carlo and J. Robin Harris. *Negative staining and cryo-negative staining of macromolecules and viruses for TEM.* Micron, vol. 42, no. 2, pages 117–131, feb 2011. (Cited on page 23.)

[Castro-Hartmann *et al.* 2013] Pablo Castro-Hartmann, Gerard Heck, Jose M. Eltit, Paul Fawcett and Montserrat Samsó. *The ArrayGrid: A methodology for applying multiple samples to a single TEM specimen grid.* Ultramicroscopy, vol. 135, pages 105–112, dec 2013. (Cited on page 7.)

[chen Bai *et al.* 2015] Xiao chen Bai, Greg McMullan and Sjors H.W Scheres. *How cryo-EM is revolutionizing structural biology.* Trends Biochem. Sci., vol. 40, no. 1, pages 49–57, jan 2015. (Cited on page 22.)

[Chen *et al.* 2013] Shaoxia Chen, Greg McMullan, Abdul R. Faruqi, Garib N. Murshudov, Judith M. Short, Sjors H.W. Scheres and Richard Henderson. *High-resolution noise substitution to measure overfitting and validate resolution in 3D structure determination by single particle electron cryomicroscopy.* Ultramicroscopy, vol. 135, pages 24–35, dec 2013. (Cited on page 62.)

[Cheng *et al.* 2015] Yifan Cheng, Nikolaus Grigorieff, Pawel A. Penczek and Thomas Walz. *A Primer to Single-Particle Cryo-Electron Microscopy.* Cell, vol. 161, no. 3, pages 438–449, apr 2015. (Cited on page 23.)

[Cheng 2018] Yifan Cheng. *Single-particle cryo-EM—How did it get here and where will it go.* Science, vol. 361, no. 6405, pages 876–880, aug 2018. (Cited on page 46.)

[Chester *et al.* 2007] David W. Chester, James F. Klemic, Eric Stern, Fred J. Sigworth and Kathryn G. Klemic. *Holey carbon micro-arrays for transmission*

electron microscopy: A microcontact printing approach. Ultramicroscopy, vol. 107, no. 8, pages 685–691, aug 2007. (Cited on page 3.)

[Coelho *et al.* 2012] Luana C. B. B. Coelho, Andra F. S. Santos, Thiago H., Maria T. S. Correia and Patrcia M. G. Paiv. *Protein Purification by Affinity Chromatography.* In Protein Purification. InTech, jan 2012. (Cited on page 68.)

[Crewe *et al.* 1968] A. V. Crewe, D. N. Eggenberger, J. Wall and L. M. Welter. *Electron Gun Using a Field Emission Source.* Review of Scientific Instruments, vol. 39, no. 4, pages 576–583, apr 1968. (Cited on page 23.)

[Cromm & Crews 2017] Philipp M. Cromm and Craig M. Crews. *The Proteasome in Modern Drug Discovery: Second Life of a Highly Valuable Drug Target.* ACS Central Science, vol. 3, no. 8, pages 830–838, aug 2017. (Cited on page 47.)

[da Fonseca & Morris 2015] Paula C.A. da Fonseca and Edward P. Morris. *Cryo-EM reveals the conformation of a substrate analogue in the human 20S proteasome core.* Nature Communications, vol. 6, no. 1, jul 2015. (Cited on pages 50, 52 and 63.)

[Dandey *et al.* 2018] Venkata P. Dandey, Hui Wei, Zhening Zhang, Yong Zi Tan, Priyamvada Acharya, Edward T. Eng, William J. Rice, Peter A. Kahn, Clinton S. Potter and Bridget Carragher. *Spotiton: New features and applications.* Journal of Structural Biology, vol. 202, no. 2, pages 161–169, may 2018. (Cited on page 52.)

[Davis *et al.* 2007] I. W. Davis, A. Leaver-Fay, V. B. Chen, J. N. Block, G. J. Kapral, X. Wang, L. W. Murray, W. B. Arendall, J. Snoeyink, J. S. Richardson and D. C. Richardson. *MolProbity: all-atom contacts and structure validation for proteins and nucleic acids.* Nucleic Acids Research, vol. 35, no. Web Server, pages W375–W383, may 2007. (Cited on page 64.)

[Derrick 1973] K S Derrick. *Quantitative assay for plant viruses using serologically specific electron microscopy.* Virology, vol. 56, pages 652–653, December 1973. (Cited on page 52.)

[Dubochet *et al.* 1987] Jacques Dubochet, Marc Adrian, Jiin-Ju Chang, Jean Lepault and Alasdair W. McDowall. *Cryoelectron Microscopy of Vitrified Specimens.* In Cryotechniques in Biological Electron Microscopy, pages 114–131. Springer Berlin Heidelberg, 1987. (Cited on page 3.)

[Dubochet *et al.* 1988] J Dubochet, M Adrian, J J Chang, J C Homo, J Lepault, A W McDowall and P Schultz. *Cryo-electron microscopy of vitrified specimens.* Quarterly reviews of biophysics, vol. 21, pages 129–228, May 1988. (Cited on pages 22, 46 and 47.)

[Emsley *et al.* 2010] P. Emsley, B. Lohkamp, W. G. Scott and K. Cowtan. *Features and development ofCoot.* Acta Crystallographica Section D Biological Crystallography, vol. 66, no. 4, pages 486–501, mar 2010. (Cited on page 56.)

[Engel 2009] Andreas Engel. Single molecule spectroscopy in chemistry, physics and biology, volume 96. Springer Berlin Heidelberg, Berlin, Heidelberg, 2009. (Cited on page 24.)

[Feng *et al.* 2017] Xiangsong Feng, Ziao Fu, Sandip Kaledhonkar, Yuan Jia, Binita Shah, Amy Jin, Zheng Liu, Ming Sun, Bo Chen, Robert A. Grassucci, Yukun Ren, Hongyuan Jiang, Joachim Frank and Qiao Lin. *A Fast and Effective Microfluidic Spraying-Plunging Method for High-Resolution Single-Particle Cryo-EM.* Structure, vol. 25, no. 4, pages 663–670.e3, apr 2017. (Cited on page 52.)

[Frank 1975] J Frank. *Averaging of low exposure electron micrographs of non-periodic objects.* Ultramicroscopy, vol. 1, pages 159–162, December 1975. (Cited on page 46.)

[Franzreb *et al.* 2006] Matthias Franzreb, Martin Siemann-Herzberg, Timothy J. Hobley and Owen R. T. Thomas. *Protein purification using magnetic adsorbent particles.* Applied Microbiology and Biotechnology, vol. 70, no. 5, pages 505–516, feb 2006. (Cited on page 68.)

[Furlani & Sahoo 2006] E P Furlani and Y Sahoo. *Analytical model for the magnetic field and force in a magnetophoretic microsystem.* Journal of Physics D: Applied Physics, vol. 39, no. 9, pages 1724–1732, apr 2006. (Cited on page 15.)

[Gerber *et al.* 1983] R. Gerber, M. Takayasu and F. Friedlaender. *Generalization of HGMS theory: The capture of ultra-fine particles.* IEEE Transactions on Magnetics, vol. 19, no. 5, pages 2115–2117, sep 1983. (Cited on page 14.)

[Giss *et al.* 2013] Dominic Giss, Simon Kemmerling, Venkata P. Dandey, Henning Stahlberg and Thomas Braun. *Microfluidics to isolate untagged proteins from cell extracts for visual analysis by electron microscopy.* In 17th International Conference on Miniaturized Systems for Chemistry and Life Sciences, 2013. (Cited on page 49.)

[Giss *et al.* 2014] Dominic Giss, Simon Kemmerling, Venkata Dandey, Henning Stahlberg and Thomas Braun. *Exploring the Interactome: Microfluidic Isolation of Proteins and Interacting Partners for Quantitative Analysis by Electron Microscopy.* Analytical Chemistry, vol. 86, no. 10, pages 4680–4687, apr 2014. (Cited on pages 10, 44, 47, 49, 69, 74 and 91.)

[Glaeser & Han 2016] Robert M. Glaeser and Bong-Gyoon Han. *Opinion: hazards*

faced by macromolecules when confined to thin aqueous films. Biophysics Reports, vol. 3, no. 1-3, pages 1–7, jul 2016. (Cited on page 47.)

[Glaeser 2016] Robert M Glaeser. *How good can cryo-EM become?* Nature Methods, vol. 13, no. 1, pages 28–32, jan 2016. (Cited on pages 24 and 47.)

[Grigorieff 2007] Nikolaus Grigorieff. *FREALIGN: High-resolution refinement of single particle structures.* Journal of Structural Biology, vol. 157, no. 1, pages 117–125, jan 2007. (Cited on page 23.)

[Harauz & van Heel 1986] George Harauz and Marin van Heel. *Exact filters for general geometry three dimensional reconstruction.* Optik, vol. 78, no. 4, pages 146–156, 1986. (Cited on page 61.)

[He & Scheres 2017] Shaoda He and Sjors H.W. Scheres. *Helical reconstruction in RELION.* Journal of Structural Biology, vol. 198, no. 3, pages 163–176, jun 2017. (Cited on page 56.)

[Heel & Frank 1981] Marin Van Heel and Joachim Frank. *Use of multivariate statistics in analysing the images of biological macromolecules.* Ultramicroscopy, vol. 6, no. 2, pages 187–194, jan 1981. (Cited on page 46.)

[Hefti *et al.* 2001] M H Hefti, C J Van Vugt-Van der Toorn, R Dixon and J Vervoort. *A novel purification method for histidine-tagged proteins containing a thrombin cleavage site.* Analytical biochemistry, vol. 295, pages 180–185, August 2001. (Cited on page 86.)

[Hellmich *et al.* 2005] Wibke Hellmich, Jan Regtmeier, Thanh Tu Duong, Robert Ros, Dario Anselmetti and Alexandra Ros. *Poly(oxyethylene) Based Surface Coatings for Poly(dimethylsiloxane) Microchannels.* Langmuir, vol. 21, no. 16, pages 7551–7557, aug 2005. (Cited on page 17.)

[Heuberger *et al.* 2005] M Heuberger, T Drobek and N D Spencer. *Interaction forces and morphology of a protein-resistant poly(ethylene glycol) layer.* Biophysical journal, vol. 88, pages 495–504, January 2005. (Cited on page 17.)

[Hochuli *et al.* 1987] E. Hochuli, H. Döbeli and A. Schacher. *New metal chelate adsorbent selective for proteins and peptides containing neighbouring histidine residues.* Journal of Chromatography A, vol. 411, pages 177–184, jan 1987. (Cited on page 86.)

[Jain *et al.* 2012] Tilak Jain, Patrick Sheehan, John Crum, Bridget Carragher and Clinton S. Potter. *Spotiton: A prototype for an integrated inkjet dispense and vitrification system for cryo-TEM.* Journal of Structural Biology, vol. 179, no. 1, pages 68–75, jul 2012. (Cited on page 6.)

[Janknecht *et al.* 1991] R Janknecht, G de Martynoff, J Lou, R A Hipskind, A Nordheim and H G Stunnenberg. *Rapid and efficient purification of native histidine-tagged protein expressed by recombinant vaccinia virus.* Proceedings of the National Academy of Sciences of the United States of America, vol. 88, pages 8972–8976, October 1991. (Cited on page 86.)

[Ji *et al.* 2007] Xiaojun Ji, Ruping Shao, Andrew M. Elliott, R. Jason Stafford, Emilio Esparza-Coss, James A. Bankson, Gan Liang, Zhi-Ping Luo, Keeseong Park, John T. Markert and Chun Li. *Bifunctional Gold Nanoshells with a Superparamagnetic Iron Oxide-Silica Core Suitable for Both MR Imaging and Photothermal Therapy.* The Journal of Physical Chemistry C, vol. 111, no. 17, pages 6245–6251, may 2007. (Cited on page 10.)

[Kelly *et al.* 2008] Deborah F. Kelly, Priyanka D. Abeyrathne, Danijela Dukovski and Thomas Walz. *The Affinity Grid: A Pre-fabricated EM Grid for Monolayer Purification.* Journal of Molecular Biology, vol. 382, no. 2, pages 423–433, oct 2008. (Cited on page 52.)

[Kemmerling *et al.* 2012] Simon Kemmerling, Jörg Ziegler, Gabriel Schweighauser, Stefan A. Arnold, Dominic Giss, Shirley A. Müller, Philippe Ringler, Kenneth N. Goldie, Nils Goedecke, Andreas Hierlemann, Henning Stahlberg, Andreas Engel and Thomas Braun. *Connecting* µ*-fluidics to electron microscopy.* Journal of Structural Biology, vol. 177, no. 1, pages 128–134, jan 2012. (Cited on pages 24, 36 and 47.)

[Kemmerling *et al.* 2013] Simon Kemmerling, Stefan A. Arnold, Benjamin A. Bircher, Nora Sauter, Carlos Escobedo, Gregor Dernick, Andreas Hierlemann, Henning Stahlberg and Thomas Braun. *Single-cell lysis for visual analysis by electron microscopy.* Journal of Structural Biology, vol. 183, no. 3, pages 467–473, sep 2013. (Cited on pages 24, 33, 35, 40, 42 and 52.)

[Kleckner & Foster 2011] Ian R. Kleckner and Mark P. Foster. *An introduction to NMR-based approaches for measuring protein dynamics.* Biochimica et Biophysica Acta (BBA) - Proteins and Proteomics, vol. 1814, no. 8, pages 942–968, aug 2011. (Cited on page 2.)

[Kremer *et al.* 1996] James R. Kremer, David N. Mastronarde and J.Richard McIntosh. *Computer Visualization of Three-Dimensional Image Data Using IMOD.* Journal of Structural Biology, vol. 116, no. 1, pages 71–76, jan 1996. (Cited on page 78.)

[Kuhlbrandt 2014] W. Kuhlbrandt. *The Resolution Revolution.* Science, vol. 343, no. 6178, pages 1443–1444, mar 2014. (Cited on pages 2, 22 and 46.)

[Landry *et al.* 2015] J P Landry, Yaohuang Ke, Guo-Liang Yu and X D Zhu. *Measuring affinity constants of 1450 monoclonal antibodies to peptide targets with a microarray-based label-free assay platform.* Journal of immunological methods, vol. 417, pages 86–96, February 2015. (Cited on page 94.)

[Larson *et al.* 2007] Timothy A Larson, James Bankson, Jesse Aaron and Konstantin Sokolov. *Hybrid plasmonic magnetic nanoparticles as molecular specific agents for MRI/optical imaging and photothermal therapy of cancer cells.* Nanotechnology, vol. 18, no. 32, page 325101, jul 2007. (Cited on pages 10 and 68.)

[Leggett *et al.* 2005] David S. Leggett, Michael H. Glickman and Daniel Finley. *Purification of Proteasomes, Proteasome Subcomplexes, and Proteasome-Associated Proteins From Budding Yeast.* In Ubiquitin-Proteasome Protocols, pages 057–070. Humana Press, 2005. (Cited on page 54.)

[Lepault *et al.* 1983] J Lepault, F P Booy and J Dubochet. *Electron microscopy of frozen biological suspensions.* Journal of microscopy, vol. 129, pages 89–102, January 1983. (Cited on page 22.)

[Li *et al.* 2013a] Xueming Li, Paul Mooney, Shawn Zheng, Christopher R Booth, Michael B Braunfeld, Sander Gubbens, David A Agard and Yifan Cheng. *Electron counting and beam-induced motion correction enable near-atomic-resolution single-particle cryo-EM.* Nature Methods, vol. 10, no. 6, pages 584–590, may 2013. (Cited on page 23.)

[Li *et al.* 2013b] Xueming Li, Paul Mooney, Shawn Zheng, Christopher R Booth, Michael B Braunfeld, Sander Gubbens, David A Agard and Yifan Cheng. *Electron counting and beam-induced motion correction enable near-atomic-resolution single-particle cryo-EM.* Nature methods, vol. 10, pages 584–590, June 2013. (Cited on page 23.)

[Lichty *et al.* 2005] Jordan J Lichty, Joshua L Malecki, Heather D Agnew, Daniel J Michelson-Horowitz and Song Tan. *Comparison of affinity tags for protein purification.* Protein expression and purification, vol. 41, pages 98–105, May 2005. (Cited on page 86.)

[Lien *et al.* 2007] Kang-Yi Lien, Jr-Lung Lin, Cheng-Yu Liu, Huan-Yao Lei and Gwo-Bin Lee. *Purification and enrichment of virus samples utilizing magnetic beads on a microfluidic system.* Lab on a Chip, vol. 7, no. 7, page 868, 2007. (Cited on page 68.)

[Lin *et al.* 1992] Z. Lin, L. E. Scriven and H. T. Davis. *Cryogenic electron microscopy of rodlike or wormlike micelles in aqueous solutions of nonionic surfactant*

hexaethylene glycol monohexadecyl ether. Langmuir, vol. 8, no. 9, pages 2200–2205, sep 1992. (Cited on page 4.)

[Lu *et al.* 2009] Zonghuan Lu, Tanvir R. Shaikh, David Barnard, Xing Meng, Hisham Mohamed, Aymen Yassin, Carmen A. Mannella, Rajendra K. Agrawal, Toh-Ming Lu and Terence Wagenknecht. *Monolithic microfluidic mixing–spraying devices for time-resolved cryo-electron microscopy.* Journal of Structural Biology, vol. 168, no. 3, pages 388–395, dec 2009. (Cited on page 6.)

[Mahon *et al.* 2012] Eugene Mahon, Anna Salvati, Francesca Baldelli Bombelli, Iseult Lynch and Kenneth A. Dawson. *Designing the nanoparticle–biomolecule interface for "targeting and therapeutic delivery".* Journal of Controlled Release, vol. 161, no. 2, pages 164–174, jul 2012. (Cited on pages 10 and 68.)

[Malhotra 2009] Arun Malhotra. *Tagging for protein expression.* Methods in enzymology, vol. 463, pages 239–258, 2009. (Cited on page 86.)

[Markwick *et al.* 2008] Phineus R. L. Markwick, Thérèse Malliavin and Michael Nilges. *Structural Biology by NMR: Structure, Dynamics, and Interactions.* PLoS Computational Biology, vol. 4, no. 9, page e1000168, sep 2008. (Cited on page 2.)

[Marston 1986] F A Marston. *The purification of eukaryotic polypeptides synthesized in Escherichia coli.* Biochemical Journal, vol. 240, no. 1, pages 1–12, nov 1986. (Cited on page 86.)

[Mastronarde 2005] David N. Mastronarde. *Automated electron microscope tomography using robust prediction of specimen movements.* Journal of Structural Biology, vol. 152, no. 1, pages 36–51, oct 2005. (Cited on pages 55 and 78.)

[McLeod *et al.* 2017] Robert A. McLeod, Julia Kowal, Philippe Ringler and Henning Stahlberg. *Robust image alignment for cryogenic transmission electron microscopy.* Journal of Structural Biology, vol. 197, no. 3, pages 279–293, mar 2017. (Cited on page 23.)

[McPherson & Gavira 2013] Alexander McPherson and Jose A. Gavira. *Introduction to protein crystallization.* Acta Crystallographica Section F Structural Biology Communications, vol. 70, no. 1, pages 2–20, dec 2013. (Cited on page 1.)

[Milazzo *et al.* 2011] Anna-Clare Milazzo, Anchi Cheng, Arne Moeller, Dmitry Lyumkis, Erica Jacovetty, James Polukas, Mark H. Ellisman, Nguyen-Huu Xuong, Bridget Carragher and Clinton S. Potter. *Initial evaluation of a direct detection device detector for single particle cryo-electron microscopy.* Journal of Structural Biology, vol. 176, no. 3, pages 404–408, dec 2011. (Cited on page 23.)

[Morris & da Fonseca 2017] Edward P. Morris and Paula C. A. da Fonseca. *High-resolution cryo-EM proteasome structures in drug development.* Acta Crystallographica Section D Structural Biology, vol. 73, no. 6, pages 522–533, may 2017. (Cited on page 52.)

[Mulligan *et al.* 2015] Sėan K. Mulligan, Jeffrey A. Speir, Ivan Razinkov, Anchi Cheng, John Crum, Tilak Jain, Erika Duggan, Er Liu, John P. Nolan, Bridget Carragher and Clinton S. Potter. *Multiplexed TEM Specimen Preparation and Analysis of Plasmonic Nanoparticles.* Microscopy and Microanalysis, vol. 21, no. 04, pages 1017–1025, jul 2015. (Cited on page 7.)

[Na *et al.* 2011] Hyon Bin Na, Goutam Palui, Jens T. Rosenberg, Xin Ji, Samuel C. Grant and Hedi Mattoussi. *Multidentate Catechol-Based Polyethylene Glycol Oligomers Provide Enhanced Stability and Biocompatibility to Iron Oxide Nanoparticles.* ACS Nano, vol. 6, no. 1, pages 389–399, dec 2011. (Cited on page 10.)

[Noble *et al.* 2018] Alex J. Noble, Hui Wei, Venkata P. Dandey, Zhening Zhang, Yong Zi Tan, Clinton S. Potter and Bridget Carragher. *Reducing effects of particle adsorption to the air–water interface in cryo-EM.* Nature Methods, vol. 15, no. 10, pages 793–795, sep 2018. (Cited on page 52.)

[Pachlatko *et al.* 2010] Esther Pachlatko, Sebastian Rusch, Anouk Müller, Andrew Hemphill, Leann Tilley, Eric Hanssen and Hans-Peter Beck. *MAHRP2, an exported protein of Plasmodium falciparum, is an essential component of Maurer's cleft tethers.* Molecular Microbiology, vol. 77, no. 5, pages 1136–1152, aug 2010. (Cited on pages 71 and 76.)

[Padmakar *et al.* 1999] A. S. Padmakar, Kajari Kargupta and Ashutosh Sharma. *Instability and dewetting of evaporating thin water films on partially and completely wettable substrates.* The Journal of Chemical Physics, vol. 110, no. 3, pages 1735–1744, jan 1999. (Cited on page 50.)

[Parmar *et al.* 2018] Mayuriben Parmar, Shaun Rawson, Charlotte A. Scarff, Adrian Goldman, Timothy R. Dafforn, Stephen P. Muench and Vincent L.G. Postis. *Using a SMALP platform to determine a sub-nm single particle cryo-EM membrane protein structure.* Biochimica et Biophysica Acta (BBA) - Biomembranes, vol. 1860, no. 2, pages 378–383, feb 2018. (Cited on page 4.)

[Peter *et al.* 2009] Jochen F. Peter, Angela M. Otto and Bernhard Wolf. *Magnetic particles as Powerful Purification Tool for High Sensitive Mass Spectrometric Screening Procedures.* PROTEOMICS, dec 2009. (Cited on page 68.)

[Petri-Fink *et al.* 2008] Alke Petri-Fink, Benedikt Steitz, Andrija Finka, Jatuporn

Salaklang and Heinrich Hofmann. *Effect of cell media on polymer coated superparamagnetic iron oxide nanoparticles (SPIONs): Colloidal stability, cytotoxicity, and cellular uptake studies.* European Journal of Pharmaceutics and Biopharmaceutics, vol. 68, no. 1, pages 129–137, jan 2008. (Cited on page 10.)

[Pettersen *et al.* 2004] Eric F. Pettersen, Thomas D. Goddard, Conrad C. Huang, Gregory S. Couch, Daniel M. Greenblatt, Elaine C. Meng and Thomas E. Ferrin. *UCSF Chimera?A visualization system for exploratory research and analysis.* Journal of Computational Chemistry, vol. 25, no. 13, pages 1605–1612, 2004. (Cited on page 56.)

[Porath *et al.* 1975] J Porath, J Carlsson, I Olsson and G Belfrage. *Metal chelate affinity chromatography, a new approach to protein fractionation.* Nature, vol. 258, pages 598–599, December 1975. (Cited on page 86.)

[Punjani *et al.* 2017] Ali Punjani, John L Rubinstein, David J Fleet and Marcus A Brubaker. *cryoSPARC: algorithms for rapid unsupervised cryo-EM structure determination.* Nature Methods, vol. 14, no. 3, pages 290–296, feb 2017. (Cited on pages 50 and 55.)

[Ramakrishnan *et al.* 2014] Chandrasekhar Ramakrishnan, Andrej Bieri, Nora Sauter, Sophie Roizard, Philippe Ringler, Shirley A Müller, Kenneth N Goldie, Kaloyan Enimanev, Henning Stahlberg, Bernd Rinn and Thomas Braun. *openBEB: open biological experiment browser for correlative measurements.* BMC Bioinformatics, vol. 15, no. 1, page 84, 2014. (Cited on pages 7 and 24.)

[Razinkov *et al.* 2016] Ivan Razinkov, Venkata P. Dandey, Hui Wei, Zhening Zhang, David Melnekoff, William J. Rice, Christoph Wigge, Clinton S. Potter and Bridget Carragher. *A new method for vitrifying samples for cryoEM.* Journal of Structural Biology, vol. 195, no. 2, pages 190–198, aug 2016. (Cited on page 52.)

[Ripstein & Rubinstein 2016] Z.A. Ripstein and J.L. Rubinstein. *Processing of Cryo-EM Movie Data.* In Methods in Enzymology, pages 103–124. Elsevier, 2016. (Cited on page 23.)

[Rosenthal & Henderson 2003] Peter B. Rosenthal and Richard Henderson. *Optimal Determination of Particle Orientation, Absolute Hand, and Contrast Loss in Single-particle Electron Cryomicroscopy.* Journal of Molecular Biology, vol. 333, no. 4, pages 721–745, oct 2003. (Cited on page 62.)

[Ruskin *et al.* 2013] Rachel S. Ruskin, Zhiheng Yu and Nikolaus Grigorieff. *Quantita-*

tive characterization of electron detectors for transmission electron microscopy. Journal of Structural Biology, vol. 184, no. 3, pages 385–393, dec 2013. (Cited on page 23.)

[Safarik & Safarikova 2004] Ivo Safarik and Mirka Safarikova. *Magnetic techniques for the isolation and purification of proteins and peptides.* BioMagnetic Research and Technology, vol. 2, no. 1, page 7, 2004. (Cited on page 68.)

[Sassenfeld 1990] H M Sassenfeld. *Engineering proteins for purification.* Trends in biotechnology, vol. 8, pages 88–93, April 1990. (Cited on page 86.)

[Scheres & Chen 2012] Sjors H W Scheres and Shaoxia Chen. *Prevention of overfitting in cryo-EM structure determination.* Nature Methods, vol. 9, no. 9, pages 853–854, jul 2012. (Cited on page 61.)

[Scheres 2012] Sjors H.W. Scheres. *RELION: Implementation of a Bayesian approach to cryo-EM structure determination.* Journal of Structural Biology, vol. 180, no. 3, pages 519–530, dec 2012. (Cited on page 23.)

[Schmidli *et al.* 2018] Claudio Schmidli, Luca Rima, Stefan A. Arnold, Thomas Stohler, Anastasia Syntychaki, Andrej Bieri, Stefan Albiez, Kenneth N. Goldie, Mohamed Chami, Henning Stahlberg and Thomas Braun. *Miniaturized Sample Preparation for Transmission Electron Microscopy.* Journal of Visualized Experiments, no. 137, jul 2018. (Cited on pages 47, 50, 59, 68, 69, 71, 77 and 78.)

[Schmidli *et al.* 2019] Claudio Schmidli, Stefan Albiez, Luca Rima, Ricardo Righetto, Inayatulla Mohammed, Paolo Oliva, Lubomir Kovacik, Henning Stahlberg and Thomas Braun. *Microfluidic protein isolation and sample preparation for high-resolution cryo-EM.* Proceedings of the National Academy of Sciences, page 201907214, jul 2019. (Cited on pages 68, 69, 74 and 77.)

[Schrader *et al.* 2016] Jil Schrader, Fabian Henneberg, Ricardo A. Mata, Kai Tittmann, Thomas R. Schneider, Holger Stark, Gleb Bourenkov and Ashwin Chari. *The inhibition mechanism of human 20Sproteasomes enables next-generation inhibitor design.* Science, vol. 353, no. 6299, pages 594–598, aug 2016. (Cited on pages 50 and 56.)

[Schrödinger, LLC 2015] Schrödinger, LLC. The PyMOL molecular graphics system, version 1.8. November 2015. (Cited on page 56.)

[Smyth *et al.* 2003] Douglas R Smyth, Marek K Mrozkiewicz, William J McGrath, Pawel Listwan and Bostjan Kobe. *Crystal structures of fusion proteins with large-affinity tags.* Protein science : a publication of the Protein Society, vol. 12, pages 1313–1322, July 2003. (Cited on page 90.)

[Squires & Quake 2005] Todd M. Squires and Stephen R. Quake. *Microfluidics: Fluid physics at the nanoliter scale.* Reviews of Modern Physics, vol. 77, no. 3, pages 977–1026, oct 2005. (Cited on page 49.)

[Stark & Chari 2015] Holger Stark and Ashwin Chari. *Sample preparation of biological macromolecular assemblies for the determination of high-resolution structures by cryo-electron microscopy.* Microscopy, vol. 65, no. 1, pages 23–34, dec 2015. (Cited on page 47.)

[Swain *et al.* 2016] Suryakanta Swain, Prafulla Kumar Sahu, Sarwar Beg and Sitty Manohar Babu. *Nanoparticles for Cancer Targeting: Current and Future Directions.* Current drug delivery, vol. 13, pages 1290–1302, 2016. (Cited on pages 10 and 68.)

[Syntychaki *et al.* 2019] Anastasia Syntychaki, Luca Rima, Claudio Schmidli, Thomas Stohler, Andrej Bieri, Rosmarie Sütterlin, Henning Stahlberg, Daniel Castaño-Díez and Thomas Braun. *"Differential Visual Proteomics": Enabling the Proteome-Wide Comparison of Protein Structures of Single-Cells.* Journal of Proteome Research, aug 2019. (Cited on page 94.)

[Tan & Yiap 2009] Siun Chee Tan and Beow Chin Yiap. *DNA, RNA, and Protein Extraction: The Past and The Present.* Journal of Biomedicine and Biotechnology, vol. 2009, pages 1–10, 2009. (Cited on page 68.)

[Taylor & Glaeser 1976] Kenneth A. Taylor and Robert M. Glaeser. *Electron microscopy of frozen hydrated biological specimens.* Journal of Ultrastructure Research, vol. 55, no. 3, pages 448–456, jun 1976. (Cited on page 47.)

[Thompson *et al.* 2016] Rebecca F. Thompson, Matt Walker, C. Alistair Siebert, Stephen P. Muench and Neil A. Ranson. *An introduction to sample preparation and imaging by cryo-electron microscopy for structural biology.* Methods, vol. 100, pages 3–15, may 2016. (Cited on page 47.)

[Veesler *et al.* 2013] David Veesler, Melody G. Campbell, Anchi Cheng, Chi yu Fu, Zachary Murez, John E. Johnson, Clinton S. Potter and Bridget Carragher. *Maximizing the potential of electron cryomicroscopy data collected using direct detectors.* Journal of Structural Biology, vol. 184, no. 2, pages 193–202, nov 2013. (Cited on page 23.)

[Walker *et al.* 1994] M. Walker, H. White, B. Belknap and J. Trinick. *Electron cryomicroscopy of acto-myosin-S1 during steady-state ATP hydrolysis.* Biophysical Journal, vol. 66, no. 5, pages 1563–1572, may 1994. (Cited on page 4.)

[Walker *et al.* 1999] M. Walker, X.-Z. Zhang, W. Jiang, J. Trinick and H. D. White.

Observation of transient disorder during myosin subfragment-1 binding to actin by stopped-flow fluorescence and millisecond time resolution electron cryomicroscopy: Evidence that the start of the crossbridge power stroke in muscle has variable geometry. Proceedings of the National Academy of Sciences, vol. 96, no. 2, pages 465–470, jan 1999. (Cited on page 6.)

[Waugh 2005] David S Waugh. *Making the most of affinity tags.* Trends in biotechnology, vol. 23, pages 316–320, June 2005. (Cited on page 90.)

[White *et al.* 2003] H D White, K Thirumurugan, M L Walker and J Trinick. *A second generation apparatus for time-resolved electron cryo-microscopy using stepper motors and electrospray.* Journal of structural biology, vol. 144, pages 246–252, 2003. (Cited on page 6.)

[Wlodawer *et al.* 2007] Alexander Wlodawer, Wladek Minor, Zbigniew Dauter and Mariusz Jaskolski. *Protein crystallography for non-crystallographers, or how to get the best (but not more) from published macromolecular structures.* FEBS Journal, vol. 275, no. 1, pages 1–21, nov 2007. (Cited on page 1.)

[Wu *et al.* 2015] Shenping Wu, Jean-Paul Armache and Yifan Cheng. *Single-particle cryo-EM data acquisition by using direct electron detection camera.* Microscopy, vol. 65, no. 1, pages 35–41, nov 2015. (Cited on page 2.)

[Yu *et al.* 2016] Guimei Yu, Kunpeng Li and Wen Jiang. *Antibody-based affinity cryo-EM grid.* Methods, vol. 100, pages 16–24, may 2016. (Cited on page 52.)

[Zemlin 1994] F. Zemlin. *Expected contribution of the field-emission gun to high-resolution transmission electron microscopy.* Micron, vol. 25, no. 3, pages 223–226, jan 1994. (Cited on page 23.)

[Zheng *et al.* 2017] Shawn Q Zheng, Eugene Palovcak, Jean-Paul Armache, Kliment A Verba, Yifan Cheng and David A Agard. *MotionCor2: anisotropic correction of beam-induced motion for improved cryo-electron microscopy.* Nature Methods, vol. 14, no. 4, pages 331–332, feb 2017. (Cited on page 55.)

[Zivanov *et al.* 2018] Jasenko Zivanov, Takanori Nakane, Björn O Forsberg, Dari Kimanius, Wim JH Hagen, Erik Lindahl and Sjors HW Scheres. *New tools for automated high-resolution cryo-EM structure determination in RELION-3.* eLife, vol. 7, nov 2018. (Cited on pages 50, 55 and 56.)

List of Figures

List of Tables

CURRICULUM VITAE

Personal Data

Place and Date of Birth:	Liestal, 03.05.1990
Nationality:	Swiss
Address:	Steinenring 3, 4051 Basel, CH
Phone:	+ 41 61 387 32 13
email:	claudio.schmidli@unibas.ch

Education

2015-2019	**PhD** in Nanosciences Faculty of Science, University of Basel, Switzerland
2013-2015	**Master of Science** in Nanosciences, Major in Physics Faculty of Science, University of Basel, Switzerland
2010-2013	**Bachelor of Science** in Nanosciences Faculty of Science, University of Basel, Switzerland
2006-2009	**Secondary school,** Major in biology and chemistry Gymnasium Münchenstein, Switzerland

Publication list

Peer-reviewed and published articles

Schmidli, C., Rima, L., Arnold, S. A., Stohler, T.,Syntychaki A., Bieri, A., Albiez, S., Goldie, K. N., Chami, M., Stahlberg H., Braun, T. 2018. **Miniaturized sample preparation for transmission electron microscopy.** JoVE, e57310

Schmidli, C., Albiez, S., Rima, L., Righetto, R., Mohammed, I., Oliva, P., Kovacik, L., Stahlberg, H., Braun, T. 2019. **Microfluidic protein isolation and sample preparation for high-resolution cryo-EM** PNAS, 116 (30) 15007-15012

Arnold, S. A., Müller, S. A., Schmidli, C, Chami, M., Stahlberg, H., Goldie K. N., Stahlberg, H., Braun, T., 2018. **Miniaturizing EM Sample Preparation: Opportunities, Challenges, and "Visual Proteomics."**
Proteomics 18 (5-6), 1700176

Arnold, S. A., Albiez, S., Opara, N., Chami, M., Schmidli, C., Bieri, A., Padeste, C., Stahlberg, H., Braun, T. 2016. **Total sample conditioning and preparation of nanoliter volumes for electron microscopy.** ACS Nano 10, 981–4988

Syntychaki, A., Rima, L., Schmidli, C., Stohler, T., Bieri, A., Sütterlin R., Stahlberg, H., Castano-Diez, D., Braun, T. 2019. **'Differential visual proteomics': Enabling the proteome-wide comparison of protein structures of single-cells.** Journal of Proteome Research, XXXXXX-XXX

Published Data

Schmidli, C., *et al.* **Endogeneous native human 20S proteasome with bound Fabs isolated from less than** 1 L **cell lysate.**
The Electron Microscopy Data Bank. http://www.ebi.ac.uk/pdbe/entry/emdb/EMD-4738.
Deposited 28 March 2019.

Schmidli, C., *et al.* **Cryo-EM structure of Tobacco Mossaic Virus from microfluidic grid preparation.** The Electron Microscopy Data Bank.
http://www.ebi.ac.uk/pdbe/entry/emdb/EMD-4628. Deposited 22 February 2019.

Schmidli, C., *et al.* **Endogeneous native human 20S proteasome.** Protein Data Bank.
http://www.rcsb.org/structure/6R70. Deposited 28 March 2019.

Schmidli, C., *et al.* **Tobacco Mosaic Virus (TMV)**. Protein Data Bank.
http://www.rcsb.org/structure/6R7M. Deposited 29 March 2019.

Schmidli, C., *et al.* **CryoWriter:** 3.5 Å **structure of human 20S proteasome with bound Fabs from microfluidic protein isolation, and** 1.9 Å **TMV structure.** Electron Microscopy Public Image Archive.
https://www.ebi.ac.uk/pdbe/emdb/empiar/entry/10251.
Deposited 21 February 2019.